IN VIVO QUANTIFICATION OF HEAVY METALS IN BONE AND TOENAIL USING X-RAY FLUORESCENCE (XRF)

by

Xinxin Zhang

A Dissertation

Submitted to the Faculty of Purdue University

In Partial Fulfillment of the Requirements for the degree of

Doctor of Philosophy

School of Health Sciences

West Lafayette, Indiana

August 2020

THE PURDUE UNIVERSITY GRADUATE SCHOOL
STATEMENT OF COMMITTEE APPROVAL

Dr. Linda H Nie
School of Health Sciences, Purdue University

Dr. Keith M Stantz
School of Health Sciences, Purdue University

Dr. Wei Zheng
School of Health Sciences, Purdue University

Dr. Marc G Weisskopf
School of Public Health, Harvard T.H. Chan

Approved by:
Dr. Aaron Bowman

For my husband Yichen, son Jason, parents, and the time spent in West Lafayette.

你的话是我脚前的灯，是我路上的光。

ACKNOWLEDGMENTS

I would like to express my deepest gratitude to my mentor Dr. Linda Nie. The completion of this work would not have been possible without her continuous guidance, support, and encouragement. She was always willing to dedicate as much time as she could to discuss and share her advice with me and to help me in any way she could to accomplish my goals. I will always be grateful for her passion and dedication as a scientist, as well as her patience and humility as a mentor.

I would like to extend my sincere gratitude to my other committee members Dr. Keith Stantz, Dr. Marc Weiskopf, and Dr. Wei Zheng, for their patient teaching, insightful guidance, and sincere help in directing my research and career path. Completion of this work was made possible through their continuous supports.

I would like to pay my special regards to Dr. Aaron Specht, Dr. Jennifer Weuve, and Dr. Ellen Wells for their strong supports, thoughtful suggestions, and positive collaborations.

I would also like to thank all my fellow lab members: Mychaela Coyne, Dr. Mindy Joo, Dr. Michael Abel, Dr. Yingzi Liu, Colby Neumann, Sana Tabbassum, Dr. Farshard Mostafaei, Alexis Webb and Patrick Byrne, for their advice and support, for all the fun we have had throughout my graduate study at Purdue, and for helping me to fill in the liquid nitrogen whenever there was a need.

Lastly, I am extremely grateful to my husband, Yichen, for his love, caring, and support, to my parents for their love and prayers, and to my son, Jason, for holding me with his little hands.

TABLE OF CONTENTS

LIST OF TABLES

LIST OF FIGURES

ABSTRACT

Background and Objective: Pb is a well-known toxic metal that can accumulate in bones over time and still threatening large populations nowadays, even those who are environmentally exposed to it. Strontium (Sr) is a metal directly related to bone health and has been used in the treatment of osteoporosis disease as a supplement. Manganese (Mn) is an essential nutrient in the body, yet excessive Mn is toxic and affecting many organ systems. Another toxic metal, mercury (Hg), has been poising different populations primarily through seafood consumptions, especially inducing neurological disorders in infants and fetuses. Even though significant associations between the above metal exposures and health outcomes have been recognized over the decades, the current technologies are limited in assessing cumulative long-term exposures *in vivo* to evaluate such associations further. Bone and toenail are appropriate biomarkers to reflect long-term exposure due to the longer half-life of these metals in them than in the traditional biomarkers. Therefore, this work evaluated the usefulness of portable x-ray fluorescence (XRF) technology on *in vivo* quantification of Pb and Sr in bone, and Mn and Hg in toenail.

Materials and Methods: The portable XRF device was calibrated by using the Pb- and Sr-doped bone-equivalent phantoms, and Mn- and Hg-doped nail-equivalent phantoms, correspondingly in different projects. Seventy-six adults (38-95 years of age, 63 ± 11 years) from Indiana, USA, were recruited to participate in this study. For the *in vivo* bone measurements, each participant was measured at the mid-tibia bone using the portable XRF and K-shell XRF system (KXRF). We estimated the correlation between the bone Pb concentration measured by both devices to evaluate the use of the portable XRF in the bones. Using the portable XRF, the bone Sr exposure of the study population were simultaneously assessed with the bone Pb exposures. Besides, we analyzed the mid-tibia bone Sr data of a Chinese population, which were measured with the same portable XRF device by our research group. We also examined the extent to which the detection limit (DL) of the portable XRF was influenced by scan time and overlying soft tissue thickness for both Pb and Sr.

For the exposure assessment of Mn and Hg in toenails, we first established system calibrations and determined the DL with phantoms. In order to validate the portable XRF in a population study, the recruited participants were measured at the big toenail by the device, and their toenail clippings were analyzed by the inductively coupled plasma spectrometry (ICP-MS).

Besides, we analyzed the toenail data of an occupationally-exposed population, collected by our collaborators in Boston. A portable XRF device with the same model as ours was used in that study.

Results: The uncertainty of *in vivo* individual bone measurement increased with higher soft tissue thickness overlying bone, and reduced with extending measurement time. With thickness ranging from 2 to 6 mm, the uncertainty of a 3-minute *in vivo* measurement ranged from 1.8 to 6.3 μg/g (ppm) for bone Pb and from 1.3 to 2.3 ppm for bone Sr. Bone Pb measurements via portable XRF and KXRF were highly correlated: R=0.48 for all participants, and R=0.73 among participants with soft tissue thickness < 6 mm (72% of the sample). A trend of different bone Sr concentrations was observed across the races and sexes.

The DL of the portable XRF with 3-minute toenail measurements was 3.59 ppm for Mn and 0.58 ppm for Hg. The portable XRF and ICP-MS measurements were highly correlated in the occupational populations for both Mn (R = 0.59) and Hg (R = 0.75). A positive correlation (R = 0.34) was found for toenail Mn measurements in the environmentally-exposed population, while a non-significant correlation was observed for toenail Hg due to the extremely low-level of Hg (Mean = 0.1 ppm) in the study population.

Discussion and Conclusion: The portable XRF could be a valuable tool for non-invasive *in vivo* quantifications of bone Pb and Sr, especially for people with thinner soft tissue; and of toenail Mn and Hg, especially for people with moderate- to high-level exposures.

CHAPTER 1. INTRODUCTION

1.1 Pb and Sr Toxicity

Lead (Pb) is one of the most popular metals used in a wide variety of industries over the centuries. In fact, it is the cause of the first recorded occupational disease [1]. Currently, in the USA, the majority of Pb is produced from secondary refining of scrap metal, especially from manufacturing the Pb-acid batteries used in the automotive and mining industry across the nation [1]. Occupational exposures can be a result of the workplace environment, including battery manufacturing, smelting, and other production activities involved in Pb refining. One of the primary causes of occupational Pb exposure is the inhalation of Pb-contained dust and fumes produced during industrial processes. Other possible sources of occupational exposure can be the ingestion of Pb via contaminated hands or surfaces and dermal absorption when the skin contacts with Pb. However, the amount of dermal absorption is much less than that of the inhalation and ingestion [2]. Environmental exposure to Pb also remains a significant issue to public health. Leaded gasoline is still used in some developing countries endangering people to high-level of environmental Pb exposure. Older adults have had more time to accumulate Pb in bone than younger adults, and in the United States, many older adults who are alive today were exposed to a substantial amount of Pb before the ban of leaded gasoline. In addition to gasoline, Pb that persists in pipes and paints in some old buildings can contaminate the drinking water and release Pb dust, causing high exposure to both adults and children. Hazardous waste sites, such as lead superfund sites, can also be a threat to the nearby residents by releasing Pb contamination to soil, drinking water, and air. Furthermore, the report from a recent test on baby foods with a wide variety of brands revealed that over 94% of the studied baby food contained Pb, putting infants under the risk of Pb exposure [3].

Upon intake, Pb combines with the red blood cells, is distributed throughout the body following blood circulation, and excretes mainly via urine and feces. The gastrointestinal absorption of ingested Pb is 40-50% in children, which is much higher than 3-10% in adults [4-6]. The majority of Pb is located within the bone in the human body. In adults, the bone reflects approximately 94% of the total body Pb burden, whereas it is 73% in children [7]. It has been recognized widely that Pb poisoning can cause cardiovascular disease and mortality [8, 9]. Recent

studies found that cardiovascular disease and its mortality rate were even associated with low-level environmental Pb exposure [10-12]. Pb is also known as a neurotoxicant that can induce various neurological disorders. Low-level or cumulative Pb exposure is associated with cognitive impairment in both children [13, 14] and adults [15-17].

Strontium (Sr) is a standard element in food, water, and air. Among them, food and drinking water are the primary sources of Sr exposure for humans, and the average daily Sr intake is approximately 2 to 4 mg [18, 19]. The concentration of Sr varies in different types of food. For example, vegetables, grain, and seafood contain more Sr than meats [20], and cereal and vegetables are the dominant sources of Sr exposure from a person's regular diet [21]. Therefore, the amount of Sr intake through diet might be related to dietary habits in different geographic areas. Sr is closely related to calcium (Ca), and shares similar chemical and physical characteristics with it. Relatively speaking, 99% of the total body Sr burden is uniformly deposited in bone [20] and gradually replaces approximately 0.03% to 0.05% of the Ca increasing with age [22]. Sr also shares similarities with Ca in biological process, including being transported in the blood via serum, competing with Ca in the gastrointestinal absorption, renal reabsorption, and storage in bones [23-25].

Since Sr is a bone-seeking element, it has been used to treat bone diseases over the decades. *In vitro* studies have shown that Sr could stimulate osteoblast function and inhibit osteoclast function [26-28]. A study among Sr-salt treated cynomolgus monkeys has shown that the amount of administered Sr was heterogeneously deposited in bones. Newly formed bones had higher Sr levels than old bones, and trabecular bones had more Sr accumulation than cortical bones [29]. These could be explained by the different Sr absorption process and the turnover of different bones [24]. Moreover, a study using rats found that the uptake of Sr reached a plateau level with the administration of high-dose Sr, and this was likely due to the saturation of Sr absorption in the gastrointestinal tract [24, 30].

Low-dose of strontium ranelate is used as an alternative supplement to treat osteoporosis disease in some European countries and Australia, yet, the FDA did not approve it for sale in the USA. A few *in vivo* studies and clinical trials have shown that the use of low-dose of strontium ranelate can lead to bone formation, reducing the fracture incidences caused by osteoporosis [20, 31, 32], especially in the treatment for postmenopausal women [33-35]. Increased risks of myocardial infarction, however, have been investigated [36, 37], and the recent reassessment of

the benefit-risk balance for strontium ranelate by the European Medicines Agency (EMA) suggested its use in patients with severe osteoporosis but without cardiovascular contraindications [38, 39].

On the other hand, excessive intake of Sr could disturb Ca metabolism [20, 40]. Studies with rats had shown a decrease of Ca level in both the bone and serum when high-dose of Sr was administrated. In addition, various bone abnormalities in structure and mineralization were observed in the rats [40, 41]. Similar results were found in a long-term study among children living in villages in Turkey. For the studied children, their nutrition was mainly based on the grain cereals planted in the Sr contaminated soils. It was found that the Sr concentration in the soils was significantly associated with the prevalence of childhood rickets [42]. Moreover, protein and Ca deficient-diet might increase the incorporation of Sr into the bone and increase adverse effects induced by the overexposure of Sr [19, 43, 44].

1.2 Biomarkers of Pb and Sr Exposure

Blood is the most commonly used biomarker for Pb exposure assessment, and the half-life of Pb in the blood varies in age, which is approximately 20 to 30 days for adults [45, 46] and can be as low as seven days for children [47]. Moreover, Pb in the blood reflects less than 2% of the total body Pb burden because most of it will eventually be deposited in the skeleton. Therefore, blood is a useful biomarker to measure acute Pb exposure and evaluate short-term biological responses. Unlike blood, the measurement sensitivity of Pb in urine and plasma is not good enough to assess very low-level of Pb exposures. A recent study found that plasma and urine had much less effect of discriminating Pb levels than the blood between individuals who had Pb exposures under regular environmental levels. However, a better result of using both plasma and urine was observed in Pb workers, and the variability of urine density or creatine had a smaller influence on samples of the workers than the general population [48]. A study among the environmentally exposed reproductive-age women in Mexico City, Mexico, found a significant positive correlation between the Pb concentrations in blood and plasma [49]. Besides, another population-based cohort study among the Chinese populations found that maternal serum Pb level during pregnancy was associated with the risk of preterm birth [50]. Therefore, urine and plasma could still be useful biomarkers but for those who have Pb exposure above regular environmental levels. Non-invasive biomarkers such as hair and nail could be used to measure Pb exposure in high-level exposed

populations [51, 52] but have their limitations in low-level exposed populations [52, 53]. Unlike the above traditional biomarkers, bone is a more advantageous biomarker to reflect the total body burden of Pb since over 90% of Pb is deposited in bones. Moreover, the long half-life of Pb in bone makes it a useful biomarker to assess long-term cumulative exposures.

Similar to Pb, Sr levels could also be quantified in traditional biomarkers such as blood, urine, serum [54-57], and hair [58-60] via standard approaches such as inductively coupled plasma spectrometry (ICP-MS). Nevertheless, over 99% of Sr exposure is deposited in bones, making bone is the most appropriate biomarker to reflect total body Sr burden. The biopsy is a traditional approach to measure Sr levels in bone; however, the painful procedure to patients made it generally avoided and has been only used in a few studies to evaluate the treatment efficacy of osteoporosis disease [61, 62]. A recently developed technology, dual-energy X-ray absorptiometry (DXA), is the current gold standard method to measure bone mineral density (BMD) and diagnose osteoporosis. A few studies have used it to evaluate the effectiveness of Sr ranelate in osteoporosis treatment by estimating the Sr ratio in the bone. This ratio was defined as the ratio of the percentage overestimation of BMD to the molar percentage of strontium [63, 64]. Since the DXA can only roughly measure Sr levels in terms of molar percentage ratio instead of an absolute value, it is challenging to compare and validate the bone Sr results from DXA with other techniques and biomarkers.

As Pb accumulation is preferentially at sites of most active calcification, it is unequally distributed in different bone sites [65]. The same assumption applied to Sr because of the similarity between Sr and Pb. Cortical bone is a preferable biomarker than trabecular bone for long-term Pb or Sr exposure due to its slow bone turnover, especially for adults [2]. A study with cadaver bones showed that after body growth ceased, Pb accumulated more in cortical bones than trabecular bones, whereas the accumulation of Pb was more in trabecular bones during adolescence, but then ceased and even declined throughout life [65]. According to the same study, no considerable difference was observed in the Pb levels measured at many positions along the diaphyseal length of the tibia bone, and no difference was observed in the right and left tibia bone from the same individual. It is also a fact that higher Pb or Sr levels were measured on the surface of tibia bone than the core bone [66, 67].

1.3 Mn and Hg Toxicity

As an essential nutrient in the body, manganese (Mn) is typically found in food and drinking waters. It acts as a co-factor for various enzymes that are important for many functions, including healthy development, immune response, and blood clotting [68, 69]. An adequate daily intake (ADI) level for Mn is 2.3 mg for men and 1.8 mg for women, set by the Food and Nutrition Board (FNB) of the Institute of Medicine (IOM) [70]. Excessive intake and overexposure to Mn, however, can be toxic to many organ systems, including cardiovascular disorders [71], liver and kidney disease [72], and neurological disorders [73, 74]. For general populations, the dominating pathway of excessive Mn intake is the ingestion of contaminated food and drinking water. Industry activities, including welding, smelting, and ferroalloy production, can generate dust and fumes that contain high levels of Mn. Inhalation of these fumes in the workplace environment is the primary route of Mn overexposure for occupational populations [75]. Upon Mn inhalation, it interacts with the red blood cells and is distributed into all of the organs of the body. The primary excretion pathway of Mn is through feces, but a small amount can be excreted through urine and sweat. As the main target organ of Mn toxicity, brain tissue is expected to have a slower Mn elimination rate than the liver and kidney [68]. Among occupational populations, *in vivo* magnetic resonance imaging (MRI) showed that globus pallidus had higher levels of Mn accumulation than other brain structures [76]. The Mn-induced neurological disorder known as manganism can be permanent, and the syndromes resemble Parkinson's disease, including tremors, difficulty walking, and facial muscle spasms [75, 77-80].

Unlike Mn, mercury (Hg) is a non-essential but toxic element. The chemical forms of Hg vary in different exposure routes with their respective metabolism and toxicity in the bodies. Elemental Hg (Hg^0) is a form of Hg in the atmosphere and absorbed mainly by the inhalation of mercury vapor. Workers involving the use of Hg, including mining, smelting, and Chlor-alkali production, are under the risk of Hg overexposures. And dental amalgams filling is a major source for non-occupational populations being exposed to Hg^0 [81]. Hg^0 is highly cumulated in the brain and kidney, inducing related health effects [82]. Inorganic Hg compounds (IHg) are formed when Hg combines with elements such as oxygen, sulfur, or chlorine, and they are generally in solid states. Similar to Hg^0, the ingestion of IHg ions from the dental amalgams fillings is the primary exposure route for IHg, and the kidney is the main target of its accumulation. Cosmetic products containing IHg, such as skin lightening cream, can also induce dermal absorption of IHg [83]. IHg

is not lipid-soluble; hence, they typically cannot transport across the placenta or brain to cause effects in fetus or induce neurotoxicity [82]. Both forms of Hg can be excreted through urine and feces. When Hg combines with carbon, organic Hg is formed. In the environment, IHg can be methylated by microorganisms to methylmercury (MeHg), which is the most common organic Hg compound [81].

Fish and other seafood in the diet are the most dominant sources of MeHg exposure for general populations. Upon intake, MeHg binds to hemoglobin in the red blood cells and is carried throughout the body. The brain is the dominant target of MeHg toxicity, and MeHg-induced neurological disorders have been shown in both humans and animals [84, 85]. Moreover, MeHg can penetrate the placental barrier and affect developing fetuses in the uterus [86-88]. The high affinity of MeHg to fetal hemoglobin leads to a higher level of MeHg in cord blood than maternal blood, and the MeHg levels in cord blood are highly related to the maternal fish consumption [89-91]. Furthermore, total Hg in breast milk has been shown to associate with maternal fish consumption positively [92, 93] but not with the number of amalgam fillings after a few months of lactation [94]. The positive correlation between Hg in breast milk and MeHg in the infant has indicated a possible postnatal exposure risk to infants via breast milk [95].

1.4 Biomarkers of Mn and Hg Exposure

Blood and urine are the most common biomarkers for biomonitoring; however, their use in Mn exposure assessment is questionable. A study among occupational populations found that Mn in blood was related to the intensity of external exposure, but given a high variability, making it not suitable for individual biological monitoring [96]. Later on, another study suggested that the complex and limited associations between blood Mn and external exposure could depend upon exposure attributes and the latency of blood measurement relative to exposure [97]. No association was observed in urine Mn [96, 97], plasma Mn [97], and external Mn exposure among the occupationally exposed adults. This could be explained by the short half-life of Mn in blood and urine. For example, the half-life of Mn in the blood is less than two hours [98]. A recent study among environmentally exposed children from drinking water found that the Mn in water or Mn intake was weakly correlated to the saliva supernatant, while no correlation was found with the whole saliva [99]. The large variation in saliva Mn made it not a recommended biomarker for exposure assessment [68, 100]. Bone can be a useful biomarker to assess past and cumulative Mn

exposure since the half-life of Mn in human bone is approximately eight years [101]. A recent study among the occupational population found that bone Mn was significantly correlated with external Mn exposure and years of employment [102]. The detection system used in that study, *in vivo* neutron activation analysis (IVNAA), is a novel and valuable technology developed in our lab group. However, the requirement of the expensive equipment and highly trained operator limited its use to a few research groups.

Unlike Mn, blood and urine can be useful biomarkers for Hg exposure assessment. Since different forms of Hg are varied in metabolism and toxicity, their exposure can be reflected by different biomarkers. For example, urine is a suitable biomarker to assess inorganic Hg exposure because most of them are excreted through urine [103]. Total Hg in red blood cells is typically used to reflect the methylmercury (MeHg) exposure, while total Hg in plasma reflects the inorganic Hg [104]. Moreover, cord blood has been used as a biomarker for prenatal MeHg exposure [105, 106]. As a non-invasive biomarker, scalp hair typically reflects the MeHg exposure and has been used in many studies [107-110]. However, external contaminations created challenges to differentiate the endogenous hair Hg from the external Hg contamination on hairs. A study evaluated different washing reagents to remove the external contaminations of hair samples before measurements, and the contamination issue remained. Hence it was suggested that scalp hair was not a suitable biomarker for an occupationally exposed population like mercury miners due to considerable external contaminations [111].

There is a growing interest in using the nail as a biomarker to assess Mn and Hg exposures. A recent study used toenail clippings to biomonitoring the Mn exposure among welders and found that toenail could reflect the Mn exposure of 7 to 12 months [112], indicating that toenail is a valid biomarker for cumulative Mn exposure assessment. Another study observed a significant correlation between toenail Mn and Mn in drinking water, as well as toenail Mn and Mn intake among low-level exposed children [99]. The same study found that the toenail Mn was significantly correlated with the fingernail and hair Mn. In an autopsy study [113], the total Hg concentration in toenails was significantly correlated with the MeHg in blood and occipital lobe cortex, indicating that toenail Hg could be a suitable biomarker for MeHg exposure. In addition, MeHg levels in toenail were highly correlated with fish consumption [114, 115], and with MeHg levels in hair and blood [115] among the general populations. Toenail could also be used for prenatal MeHg exposure. A study among healthy Japanese pregnant women found that at

parturition, MeHg levels in the maternal toenail clippings were significantly correlated with the MeHg levels in the cord blood and the maternal hair [91]. Moreover, the MeHg in toenail clippings at early pregnancy reflected the maternal Hg exposure about five months retroactively, indicating a cumulative Hg exposure assessment in the toenail. Therefore, the toenail is an advantageous biomarker to measure cumulative Mn and Hg exposure, and it is typically less susceptible to external contamination than fingernails and scalp hairs.

For the *in vivo* portable XRF measurements, we measure at the center of great toenail instead of nail clippings. The great toenail growth rate is about 2 mm per month, with an average length of 2 cm [116]. Therefore, the *in vivo* toenail and nail clippings can reflect different exposure window, which may slightly vary in individuals due to different nail length and growth rate.

1.5 X-ray Fluorescence Technology

The principle of XRF technology, in general, is to quantify the concentration of elements in a sample via radiation. Once photons are produced from a radioactive source or x-ray tube, they will interact with the sample atom, generating photons of different energies that will then be detected and used for analytical purposes. The photoelectric effect rather than Compton and Rayleigh effects is the predominant interaction of low-energy photons with matter. During this effect, incident photons can eject an inner shell electron when the incident energy is higher than the binding energy of the electron. An electron from the outer shell then de-excites into the inner shell and releases energy in the form of characteristic x-rays that are detected by the systems. The energy of characteristic x-rays is determined by the energy difference between the two orbitals and specific to an individual element. In the measured spectrum from a sample, the characteristic x-ray of each presented element is shown as a Gaussian peak, and the net counts of each Gaussian peak correlate to the amount of element in a positive linear relationship. Therefore, we can use phantoms of known concentrations of a particular element to establish a calibration line with the net counts of the peak and determine the unknown concentration of the element from the measured counts.

The K-shell x-ray fluorescence technique (KXRF) was firstly used in 1976 to measure *in vivo* Pb concentration in bone via the detection of Pb K-shell characteristic x-rays by Ahlgren *et al.*[117]. Back then, the KXRF used a ^{57}Co as the radioactive source that emitting γ-rays of 122 keV, a Ge (Li) semiconductor as the detector, and a measurement angle of 90^{o}. Later on,

Somervaille *et al.* have improved the system by using a ^{109}Cd source instead of ^{57}Co to maximize Pb K x-ray signals and a detection angle of 180^{o} to minimize backgrounds from the Compton scatterings [118]. Moreover, the signal normalization method, via the coherent scatterings generated from the bone mineral, was developed to eliminate the uncertainty induced by the geometry of irradiation and detection. The system design then has been further improved by using a larger size (51 mm x 20 mm) high-purified germanium (HpGe) detector surrounding a point source to replace the annular source surrounding a small detector (16 mm x 7mm) by Gordon *et al.* [119, 120]. This conventional KXRF system is used in most of the labs now. Beyond that, Nie *et al.* have completed the latest system optimization, which is consisted of four HpGe detectors with a dimension of 16 mm in diameter and 10 mm in thickness. This cloverleaf KXRF system has a sensitivity 2 to 3 times better than a conventional one-unit KXRF system with bone Pb measurement capability [121] and was used in work presented in this dissertation.

In a cloverleaf ^{109}Cd based KXRF system, a ^{109}Cd source is mounted in front of the detectors, emitting gamma-ray with 88.035 keV energy to irradiate the bone or bone-equivalent phantoms. In response, Pb atoms in the bone emit Pb K-shell-characteristic x-rays with the energy of 74.97 keV ($K_{\alpha 1}$), 72.80 keV ($K_{\alpha 2}$), and 84.94 keV ($K_{\beta 1}$). The system consists of four HpGe detectors, four feedback resistance pre-amplifiers, four digital signal analyzers (DSA-1000), and a Genie 2k spectroscopy software for data collection. A non-linear least-squares fitting program is used to analyze the measured Pb K_{α} and K_{β} peaks and calculate the respective uncertainties [122, 123]. The Pb K_{α} and K_{β} signals collected from each detector are analyzed independently and normalized to the coherent scattering signals generated from the bone mineral. Hence, the bone Pb concentration of an individual *in vivo* measurement is presented in a unit of μg/g (ppm) bone mineral. The bone Pb concentration is computed as an average of the K_{α} and K_{β} signals from all the four detectors, with the concentrations weighed by uncertainty according to the inverse variance weighting method [124]. Each *in vivo* measurement requires 30 minutes and induces a whole-body effective radiation dose of approximately 0.26 μSv for adults and 10 μSv for children with the use of a 135mCi ^{109}Cd source [125].

The KXRF technique has become a standard approach to quantify cumulative Pb concentration in bone *in vivo* [126-128] and investigate the associated health effects such as hypertension, cognitive impairment, and Parkinson's disease [8, 15, 129-131]. These findings, however, are limited to the research groups who possess the technology because of the

sophisticated system set-up and operational requirements. Moreover, study participants must visit a central research facility to undergo long KXRF measurements making it difficult to be applied in a large-scale population.

Close to the development history of KXRF systems, an L-shell XRF system (LXRF) was firstly used to measure Pb levels in tibia bone by Wielopolski *et al.* in 1983, via the detection of Pb L-shell characteristic x-rays [132]. This system consisted of a ^{125}I source and a lithium-drifted silicon detector (Si(Li)). Later on, the polarized x-ray radiation was adopted to simulate the Pb L x-rays and improved the system detection limit [133, 134]. The LXRF was further upgraded by using an x-ray tube source with a secondary target for *in vivo* bone Pb measurements [124, 135, 136]. In our research group, we have adapted and validated a portable LXRF system to quantify Pb concentration in the bone. The portable XRF device was developed by Niton (later became Thermo Niton) Inc. and initially designed for detecting elements in environmental media such as rock, soil, and paint. Modifications were made to this device by our research group for its use in the *in vivo* measurements. This customized portable XRF device (Thermo Niton XL3t, Billerica, MA) has a power output of 2 watts, an x-ray tube with an energy span up to 50 kV, a silver anode, and a silicon PIN diode (Si PIN) detector with an 8 mm^2 area and 1-mm thickness [126, 137-141]. In a feasibility study [137], the detection limit for this device was 8.4 ppm at 2 mm soft tissue overlying the bone, which was much better than the detection limit of 57 ppm at the same soft tissue thickness, obtained from previous LXRF systems [124].

An upgraded portable XRF with advances in the base instrumentation was, later on, developed by the manufacturer (Figure 1). To further improve the system sensitivity, we adapted this new portable XRF system (Thermo Niton XL3t GOLDD+, Billerica, MA) with optimized instrumental parameters for the *in vivo* application. The XL3t GOLDD+ model has a more compact and optimized geometry than the previous model XL3t. It uses a thermoelectric- cooled silicon drift detector of 25 mm^2 area instead of the Si PIN detector with 8 mm^2 area. More importantly, it has different device settings available via special software and hardware, including voltage, current, and filter combinations, for users to choose and optimize the sensitivity for different *in vivo* measurement purposes other than bone Pb. In a feasibility study [126], this new portable XRF system was validated using goat bones with known Pb concentrations determined by ICP-MS, and a significant correlation between the measurements was obtained (R = 0.98). Besides, human cadaver bones with intact soft tissue attached to them were used to simulate the *in vivo* situation,

and an excellent reproducibility and a significant correlation were found between the measurements from both the portable XRF and the KXRF system.

Compared to KXRF systems, the portable XRF measures bone Pb or Sr concentrations in μg/g dry bone and is an easier-to-use technique that can non-invasively quantify bone Pb concentrations *in vivo* in a few minutes [126, 140, 142]. Thus, this device can be more practical for use in large-scale epidemiologic studies and especially useful among populations whose participation may be limited by physical mobility or proximity to a KXRF system. Nevertheless, like other LXRF systems, the primary issue of the portable XRF technique for bone measurement is the signal attenuation induced by soft tissues overlying the bone. A consequence of the low energy of the Pb L x-rays, as opposed to the high energy of the K x-rays, is that fewer Pb L x-ray signals are detected as the soft tissue thickness increases. Therefore, the system detection limit is associated with soft tissue thickness, and better sensitivity can result in participants who have thinner soft tissue. This fact also applies to bone Sr measurements since the energy of Sr K-rays is close to the energy of Pb L x-rays.

The availability of different device settings allows the portable XRF device not only to be used in bone Pb quantification but also in measuring many other elements in different biomarkers. Applications of the new portable XRF system have been expanded recently in a variety of study purposes, including Pb quantification in children, adults, and condor bones [127, 140, 143] and multiple trace elements quantifications in nail clipping samples [144-147]. In the projects described in this dissertation, this new portable XRF system has been evaluated, for the first time, for *in vivo* Pb and Sr quantification in bone, and Mn and Hg quantification in toenail in a population study.

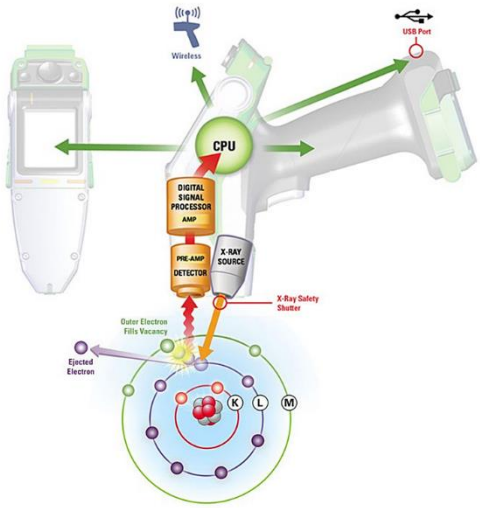

Figure 1. Schematic diagram of a portable XRF system [148].

1.6 Specific Aims

The overall objective of this doctoral work is to evaluate the use of the new portable XRF technology for *in vivo* Pb and Sr exposure assessment in bone with a population study and to develop, validate, and evaluate the device for *in vivo* Mn and Hg quantification in toenails. Four specific aims were accomplished to achieve this objective:

Aim 1: *Evaluate the portable XRF for in vivo bone Pb quantification.* We recruited adults of the general population in Indiana, USA, to participate in the study. Both the portable XRF and KXRF systems were used to measure Pb concentration in their mid-tibia bone. We compared the estimates of bone Pb concentrations from both measurements and determined the correlation. In addition, we evaluated the detection limit of the portable XRF with different soft tissue thickness overlying bone and extended measurement time and compared it to the detection limit of the KXRF system. Finally, we tested the associations of bone Pb concentration with age and age with soft tissue thickness overlying bone. Manuscript of this work is under internal review.

Aim 2: *In vivo Sr exposure assessment in bone among adults with different demographic characteristics using the portable XRF*. We quantified bone Sr concentration in two different populations: one is the American adult population that was the same as that for the bone Pb project, and the other one is a Chinese adult population, whose mid-tibia bone were measured with the same portable device by our research group in China. We evaluated the detection limit of the

portable XRF in different measurement time and compared the bone Sr estimates of participants with different sexes and races. Manuscript of this work is under internal review.

Aim 3: *Investigate the feasibility of portable XRF for in vivo toenail Mn and Hg quantification.* We made different sets of Mn- and Hg- doped nail phantoms and optimized the device settings. Methods for spectral analysis and system calibration were developed. Furthermore, we evaluated the effects of nail thickness and soft tissue thickness underneath nails on the system calibration and determined the detection limits for both Mn and Hg measurements. The radiation dose induced by the portable XRF was also evaluated. This work was published in Biomarkers by Zhang *et al.* in 2018 [142].

Aim 4: *Validate the portable XRF for in vivo toenail Mn and Hg quantification within a population study*. The same recruited participants for the bone measurements were also measured on their big toenails using the portable XRF for the Mn and Hg exposure assessment. The portable XRF measurement was followed by a collection of their nail clippings samples, which were analyzed by the ICP-MS approach. We compared the results from both the portable XRF and ICP-MS measurements and determined their correlation for both Mn and Hg. Besides, we repeated the data analysis for an occupational population that was recruited and measured by our collaborators in Boston. The portable XRF device with the same system design as ours was used for the occupational population, and the same measurement procedures were followed. The manuscript for parts of this work was submitted, and another manuscript is in preparation.

1.7 Significance

This section summarizes the importance and impact of identifying a proper biomarker for the exposure to Pb, Sr, Mn, and Hg. For a more detailed description, refer to the introduction section in each chapter.

The toxic effects of Pb are related to almost every organ system in the body. Even at the lower exposure levels typical today, there are well-documented health effects, including neurodegenerative disease [129, 149], cardiovascular disease [8], and even mortality [12]. Sr is a ubiquitous element in food and drinking water, and diet is the primary source for general populations to be Sr exposed. Low-doses of Sr ranelate has been used as an effective treatment for osteoporosis disease in some European countries [32, 150]; nevertheless, excessive doses of Sr

could disturb Ca metabolism [40, 151] and cause possible bone-related health issues such as childhood rickets [19, 42].

Unlike Pb and Sr, Mn is an essential nutrient in the body. Excessive intake and overexposure to Mn, however, can be toxic to many organ systems [68], including cardiovascular disorders [71], liver and kidney diseases [72], and, most importantly, neurological disorders [73, 74]. Hg-induced health effects are related to the different Hg chemical forms. Methylmercury (MeHg) that can be ingested through seafood consumption is one of the most common chemical forms in environmental exposure. The MeHg-induced neurotoxic effects are more threatening to infants and even fetus who can suffer from developmental brain dysfunction and early sensorimotor dysfunction [152, 153].

Since there are significant associations between metal exposure and adverse health effects, identifying a useful biomarker for metal exposure becomes critical in a better understanding of these associations. Bone is the more advantageous biomarker to assess past and cumulative exposure to bone-seeking metals such as Pb and Sr because they have much longer half-lives in bone compared to other traditional biomarkers such as blood and urine [45, 154]. In addition, over 90% of total body Pb and over 99% of the total body Sr is deposited in bone, making it a more appropriate biomarker to reflect the total body burden of these metals. The ^{109}Cd based KXRF technique has been successfully used to quantify bone Pb concentration for over two decades [15, 16, 121]. However, because of the operational requirements for the KXRF system, including a sophisticated device setup, licenses for the radioactive source, and well-trained researchers to operate the data acquisition and analysis, only a few research groups possess the technology. In addition, the measurement time is half to one hour, and participants have to travel to the appointed site for measurement; these conditions limit the use of the KXRF system in larger-scale population study and clinical applications.

As an advantageous biomarker, the nail can reflect cumulative exposures of Mn and Hg from a few months to a year. Toenail, in particular, is less susceptible to external contamination than fingernail and hair. Standard approaches for Mn and Hg assessment in nail samples include inductively coupled plasma mass spectrometry (ICP-MS), atomic absorption spectrophotometry (AAS), and cold vapor atomic fluorescence spectroscopy (CVAS). However, they are typically time and cost consuming analytical methods. Moreover, the collection of nail clippings samples is

required in such methods, which might be challenging for some populations who have low nail growing or not feeling comfortable to cut nails.

In this work, we proposed to explore and validate the portable XRF technique to non-invasively quantify Pb and Sr in bone, and Mn and Hg in toenail in human *in vivo*. This work is significant because the portable XRF device overcomes the disadvantages of the state-of-the-art approaches, KXRF and ICP-MS: 1. Cost- and time-effective. It requires only a few minutes of measurement time, and the operational requirement is less complicated; 2. Easy to use. It can be brought onto work sites, allowing more participants to be measured; 3. *In vivo* measurement. No collection of nails clippings is required; 4. Multi-metals assessment. It can simultaneously quantify multiple metals with one measurement on bone or nail. Once the development and validation of the portable XRF are complete, it will provide a valuable tool for accurate exposure assessment of these metals in large-scale populations and greatly expand the research on metals in humans to vulnerable populations such as the elderly and children. Moreover, the portable XRF system can be extended to other elements such as selenium, arsenic, and uranium. In conclusion, essential advances in assessing the health effects of exposures to pollutant mixtures, including the early diagnosis of metal intoxication, could be expected with the portable XRF technique.

1.8 Structure of This Dissertation

The structure of this dissertation is organized as this: Chapter 1 presents an introduction and background information; Chapter 2 focuses on the evaluation of the portable XRF for bone Pb measurements among a US population; Chapter 3 addresses the application of portable XRF in bone Sr measurements among adults with different sexes and races and population study results; Chapter 4 focuses on the methodology development of the portable XRF for toenail Mn and Hg measurements [142]; Chapter 5 focuses on the validation of the portable XRF for *in vivo* toenail Mn and Hg measurements in a population study; Chapter 6 presents an overall summary and future directions of this study.

CHAPTER 2. EVALUATION OF A PORTABLE XRF DEVICE FOR IN VIVO QUANTIFICATION OF LEAD IN BONE AMONG A US POPULATION

2.1 Introduction

Lead (Pb) exposure has declined dramatically over the last several decades due to the regulatory actions prompted by numerous scientific findings that Pb is related to many adverse health outcomes [155-157]. However, even at lower exposure levels still typical today, there are well-documented health effects [12, 13, 158, 159]. Pb remains one of the most common chemical toxicants in the environment and is second, following arsenic, on the substance priority list of the Agency for Toxic Substances and Disease Registry [160]. Pb exposure is still a significant public concern for many populations, especially some vulnerable populations, including older adults, children, and occupational workers [12, 159, 161]. Blood Pb is a commonly used biomarker of Pb exposure. However, the half-life of Pb in the blood is relatively short, approximately 35 days for adults and as low as 7 days for children [162, 163]. By contrast, Pb in bone has a longer half-life of years to decades [154], rendering it a more appropriate biomarker of cumulative Pb exposure, especially for populations with long-term Pb exposure or exposure that occurred mostly in the past.

K-shell x-ray fluorescence (KXRF) technology has been used to measure bone Pb *in vivo* and to investigate the adverse health effects of cumulative exposure [8, 15, 121, 129, 164]. However, the system's size, long measurement time, and other operational requirements limit such studies to only a few research groups who possess the technology. Furthermore, study participants must visit a central research facility to undergo KXRF measurements, making it impossible to use this technology in field studies. The portable XRF approach developed in our group employs an easy-to-use device that can non-invasively quantify metal concentrations *in vivo* in a few minutes [126, 140, 142]. Thus, this device is more practical for use in large-scale epidemiologic studies and in field settings. The portable device may be especially useful among vulnerable and underrepresented populations, whose participation may be limited by physical mobility or proximity to a KXRF system. This study compares the use of portable XRF for bone Pb measurements *in vivo* in adults of the general population against the cloverleaf KXRF bone Pb measurement.

This chapter uses a new methodology of spectral analysis and establishes system calibration for bone Pb. It demonstrates the detection limit (DL) of portable XRF and its comparison to the KXRF with different scan times and overlying soft tissue thicknesses. Furthermore, it shows the associations of bone Pb concentrations with age and age with soft tissue thickness.

2.2 Material and Methods

2.2.1 Study Population

We recruited seventy-six adults from the community-dwelling population in northwestern Indiana, to participate in this study. Data from five participants were excluded from the analysis. Three of those participants had a very thick layer of soft tissue overlying their tibia bone, resulting in unacceptable high uncertainty and unrealistically negative bone Pb concentrations. External Pb contamination on the portable XRF device interfered with the measurements of the other two excluded participants. We eliminated this contamination in subsequent scans by cleaning the surface of the portable XRF. Forty-one participants (22 women and 19 men; ages 43-83 years) were recruited from the vicinity around West Lafayette, Indiana (USA), among whom 1 was previously occupationally exposed to Pb. Nineteen participants (10 women and 9 men; ages 38-95 years) were recruited from East Chicago, Indiana (USA), in partnership with a community group concerned about Pb contamination in the area. East Chicago is the site of intense industrial activity over the past century, including refining Pb ore and recovering Pb from scrap metal and batteries. The East Chicago-based US Smelter and Lead Refinery Pb superfund site was added to the National Priorities List in 2009. All these participants were residents in the operable unit 1 site, a 322-acre residential area in the Pb superfund site. To cover a broader range of bone Pb concentrations, we recruited eleven participants (2 women and 9 men; ages 45-87 years) with potential moderate to high historical Pb exposure from the vicinity around Muncie, Indiana (USA), among whom 9 were occupationally exposed to Pb at some time point of their life.

The Institutional Review Board of Purdue University, Boston University, and Harvard University approved this study. All participants provided their informed consent forms before undergoing the study procedures.

2.2.2 XRF Systems and In Vivo Measurement

The portable XRF used in this study was described in Chapter 1. The device setting consisted of a voltage of 50 kVp, a current of 40 μA, and a silver (Ag) and iron (Fe) combination filer, which was optimized for *in vivo* bone Pb measurement providing the best DL [126]. For portable XRF measurement, the participant sat on a chair with one leg straightened and resting on a chair in front. Before the measurement, we cleaned the participant's mid-tibia area with alcohol swabs to eliminate any extraneous contamination. The portable XRF device was placed in contact with the participant's skin right above the target area (Figure 2). We performed a 3-minute measurement with the portable XRF on participants from West Lafayette and East Chicago. To determine the extent to which a longer scan time would reduce the detection limit of the device, we extended the measurement to 5 minutes for Muncie participants. The induced whole-body effective radiation dose from the 3-minute scan was about 2.4 μSv [127, 141], which increased to approximately 4.0 μSv with the 5-minute scan. By contrast, the dose for a standard anteroposterior chest x-ray is 100 μSv, and one day of natural cosmic radiation is equivalent to 10 μSv.

Figure 2. *In vivo* bone measurement with the portable XRF system.

The cloverleaf ^{109}Cd based KXRF system was also described in Chapter 1, and the system set up followed what was used in previous studies [121, 126, 127, 165]. For the KXRF measurement, the same mid-tibial spot was cleaned and measured. We immobilized the sitting

participant's target leg by securing it to the chair leg with Velcro straps and then positioned it about 1-2 mm away from the ^{109}Cd source. The bone was measured with the KXRF system for 30 minutes (Figure 3). The Muncie participants were measured with a new 135 mCi ^{109}Cd source, which had higher activity than the one used for the West Lafayette and East Chicago participants. Thus, a lower uncertainty of the bone Pb concentration measured by the KXRF has resulted in the Muncie participants.

Figure 3. *In vivo* bone measurement with the KXRF system.

2.2.3 Spectral Analyses

In response to irradiation, Pb atoms in the bone generate Pb L-shell-characteristic x-rays with energies of 10.55 keV (L_α) and 12.61 keV (L_β) with the portable XRF. However, only the L_β peak was used for estimating bone Pb concentration because of the lower background level under the Pb peak region. We used peak fitting with least-squares algorithms to extract the net counts of Pb L_β. We fit a Gaussian distribution to the Pb L_β peak and used an exponential function to fit the background. The bone Pb concentration was measured in μg/g dry bone by the portable XRF [140].

In response to the KXRF system, Pb atoms in the bone emit Pb K-shell-characteristic x-rays with energies of 74.97 keV ($K_{\alpha 1}$), 72.80 keV ($K_{\alpha 2}$), and 84.94 keV ($K_{\beta 1}$). An in-house peak fitting program was used to calculate bone Pb concentration and its uncertainty separately with each detector [122, 123]. The Pb K_α and K_β signals were analyzed independently and normalized to the generated coherent peak signal, and the bone Pb concentration obtained from an individual measurement has a unit of μg/g bone mineral. The bone Pb concentration was computed as an average of the K_α and K_β signals from all four detectors, with the concentrations weighed by uncertainty according to the inverse variance weighting method [124].

2.2.4 Calibration of the XRF Systems

We calibrated the portable XRF system using a 100 μg/g (ppm) plaster of Paris Pb-doped bone-equivalent phantom. A consequence of the low energy of the Pb L x-ray is that the soft tissue over the bone can attenuate the signal. As the soft tissue thickness increases, the system detects fewer Pb L x-rays and more Compton scattering counts from the soft tissue. Thus, to simulate the soft tissue over bone, we placed Lucite plates of 0 to 5 mm over the 100-ppm bone phantom and measured the phantoms for 15 minutes to calibrate the portable XRF for bone Pb. The calibration line was established as the Pb L_β net counts of the 100-ppm bone phantom change with the Compton scattering peak counts. The *in vivo* bone Pb concentration was calculated by relating an *in vivo* Pb L_β net count to a known count per concentration from the 100-ppm bone phantom, as shown in the following equation. This relation allowed us to use the Compton scattering counts from their measurement to correct for the attenuation of the Pb signal caused by overlying tissue.

$$Pb_{in\ vivo}\ [ppm] = PbNetCounts_{in\ vivo} \times (100ppm\ /PbNetCounts_{100ppm}) \quad \text{(Equation 1)},$$

where, $Pb_{in\ vivo}$ is the bone Pb concentration of an *in vivo* measurement; $PbNetCounts_{in\ vivo}$ is the measured Pb L_β net counts; $PbNetCounts_{100ppm}$ is the Pb L_β net counts of the 100 ppm phantom calculated from the relation between the Pb net counts and Compton scattering counts, where the Compton scattering was from an *in vivo* measurement.

From the portable XRF calibration data, we also determined the relation between Lucite thickness and Compton scattering counts. Using this relation, we estimated the overlying skin

thickness for an individual participant directly from the XRF spectrum of their portable XRF bone Pb measurement.

In previous studies [126, 137], a 0-ppm bone phantom was used to estimate the background under the Pb L_β peak, and the Pb net counts were calculated by subtracting the estimated background counts from the gross counts under the peak of interest. However, for *in vivo* measurements, this background subtraction method overestimated the background and resulted in an underestimated Pb signal and higher uncertainty. Instead, we directly extracted the Pb L_β net count through the peak fitting and compared to the tissue thickness, appropriate 100-ppm bone phantom counts to determine concentration.

Because Pb K x-rays have much higher energy than the L x-rays, the KXRF signals were not attenuated as much by the soft tissue over the bone as the portable XRF signals. Hence, the standard calibration for the KXRF calibration uses nine Pb-doped phantoms with concentrations ranging from 0 to 100 ppm. The phantoms were positioned in front of a ^{109}Cd source, and a 30-minute measurement was performed. The Pb $K_{\alpha,\beta}$ peaks were normalized to the coherent peak for the correction of the measurement geometry, bone mineral normalization, and soft tissue attenuation. The calibrations lines were plotted as the ratios of Pb K_α and K_β peaks over coherent peak versus the bone Pb concentrations.

2.2.5 Detection Limit of the XRF Systems

The DL of the KXRF system was defined as twice the uncertainty of the measurement of the 0-ppm bone phantom. Soft tissue overlying the tibia bone increases the uncertainty and hence the DL of the portable XRF measurement. Thus, we calculated the DL of portable XRF using 3-minute measurements of 0 and 100 ppm Pb-doped bone-equivalent phantoms covered with Lucite of thicknesses ranging from 1 to 8 mm. The DL was calculated as

$$DL_{portable\ XRF} = 2 \times \sigma_{0ppm} = 2 \times \sqrt{\frac{1}{\frac{1}{\sigma^2_{\alpha,0ppm}} + \frac{1}{\sigma^2_{\beta,0ppm}}}} \quad \text{(Equation 2)},$$

where

$$\sigma_{\alpha,\beta,0ppm} = 100\ ppm \times \frac{\sqrt{BKG_{\alpha,\beta,0ppm}/180s}}{Gross_{\alpha,\beta,100ppm} - BKG_{\alpha,\beta,0ppm}},$$

The DL was estimated from both Pb L_α and Pb L_β peaks. $Gross_{\alpha,\beta,100ppm}$ is the gross count rate under the L_α and L_β area measured with a 100 ppm Pb bone phantom in 3 minutes, and $BKG_{\alpha,\beta,0ppm}$ is the total count rate under the L_α and L_β area measured with a 0-ppm bone phantom.

The estimated DL for the phantoms with a given Lucite thickness is the minimum bone Pb concentration that can be reliably detected with that thickness. However, the discrepancy between the Lucite plates and human overlying soft tissue can result in slightly lower estimates of the DL for the phantom with Lucite. Hence, the DL for *in vivo* measurement is expected to be slightly higher than that from the phantom. In this study, we used twice the uncertainty of *in vivo* measurement to approximately estimate the DL for an *in vivo* situation.

2.2.6 Statistical Analyses

Because the bone Pb concentration estimated by the instruments oscillate around the actual value, negative estimates may occur when a participant's actual *in vivo* bone Pb concentration is close to zero. We retained these negative data points to provide unbiased estimates of the comparison between bone Pb measurements [166, 167].

We compared the uncertainty of the different measurement times with the portable XRF. We calculated the average uncertainty of *in vivo* measurement within 3 minutes and 5 minutes, at different soft tissue thickness, and determined the uncertainty reduction factor by only calculating their ratio.

We compared estimates of bone Pb concentration generated by the two measurement systems using linear regression models. From these analyses, we computed Pearson correlation coefficients R and calculated the 95% CI based on Fisher R to Z transformation. Overlying soft tissue tends to increase the uncertainty in the portable XRF estimates, and we took two approaches to evaluate the influence of this uncertainty on the estimated linear regression and Pearson correlation coefficients. First, we repeated the analyses that were progressively restricted to participants with thinner overlying soft tissue. Second, we conducted analyses in which we weighted observations in inverse proportion to their portable XRF measurement uncertainty [168].

We evaluated associations of the portable XRF bone Pb concentrations with two known predictors of cumulative Pb exposure: age and occupational exposure to Pb. Older adults have had more time to accumulate Pb in bone than younger adults, and in the United States, many older adults who are alive today were exposed to a substantial amount of Pb before the ban of leaded

gasoline and paint. Hence, bone Pb concentrations estimated by XRF are expected to be higher with older participant age. We assessed the association between the portable XRF bone Pb concentrations and the age of the participants by regressing bone Pb concentration measured by the portable XRF on age. In addition, we compared the bone Pb concentrations of occupationally and non-occupationally exposed participants by calculating the mean bone Pb concentrations measured via portable XRF. For this comparison, because the occupationally exposed participants were all male and had a more restricted age range (N=10; 63 ± 14 years), we limited the comparison to non-occupationally exposed males of similar age distribution (N=24; 68 ± 8 years). Since the bone Pb concentrations were not normally distributed in these two populations, a two-sample Kolmogorov-Smirnov (K-S) test was used to evaluate the mean difference and compute the p-value. We repeated all of these analyses using KXRF estimates as well.

Finally, to further explore the usefulness of the portable XRF in large-scale studies of older adults, we evaluated the relation of age to soft tissue thickness by regressing soft tissue thickness on age. An inverse association between the two would indicate that soft tissue thickness gets thinner with age, and so would be a less dominant contributor to measurement uncertainty in older adults.

2.3 Results

2.3.1 Study Population

Table 1 shows the selected characteristics of the 71 participants. Ten participants, ages ranged from 45 to 87 years, and all males were occupationally exposed.

Table 1. Age and soft tissue thickness of participants from different sites, occupational and non-occupational participants in the study.

	West Lafayette	East Chicago	Muncie	Occupational	Non-occupational	Total
Participants, N	41	19	11	10	61	71
Male, N (%)[a]	19 (46%)	9 (47%)	9 (82%)	10 (100%)	27 (44%)	37 (52%)
Age (Mean ± SD, years)	64 ± 8	62 ± 17	62 ± 12	63 ± 14	63 ± 11	63 ± 11
Soft tissue thickness (Mean ± SD, mm)	4.7 ± 1.4	5.5 ± 1.5	4.2 ± 1.2	4.4 ± 1.0	4.9 ± 1.5	4.8 ± 1.5
Soft tissue thickness < 5mm, N (%)	25 (61%)	7 (34%)	8 (73%)	7 (70%)	33 (54%)	40 (56%)

[a] All other participants were female.

2.3.2 Calibration of the XRF systems

Compton scattering counts from the portable XRF increased with a thicker Lucite plate (Figure 4). The Pb L_β net counts decreased with progressively higher Compton scattering counts ($R^2 > 0.99$) due to the signal attenuation from increased Lucite thickness (Figure 5). Through this relation, the count per concentration from the 100 ppm bone phantom was calculated with the Compton scatterings counts from an individual *in vivo* XRF spectrum. The *in vivo* bone Pb concentration was then calculated by relating an *in vivo* Pb L_β net count to this known count per concentration ratio using Equation 1.

Figure 6 and Figure 7 show the calibration lines for one of the four detectors of the KXRF system for K_α and K_β peaks, where K_α/coherent and K_β/coherent were plotted against the bone phantom Pb concentrations ($R^2 = 0.99$).

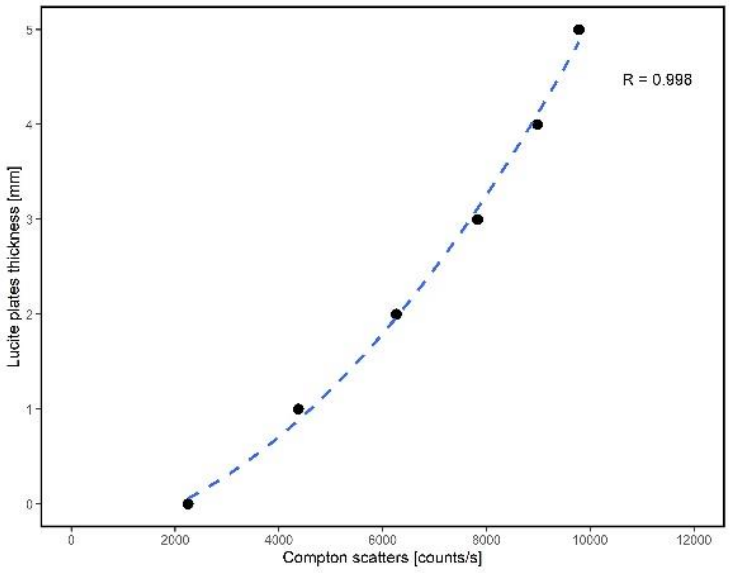

Figure 4. Soft tissue thickness versus Compton scattering signal, measured with portable XRF.

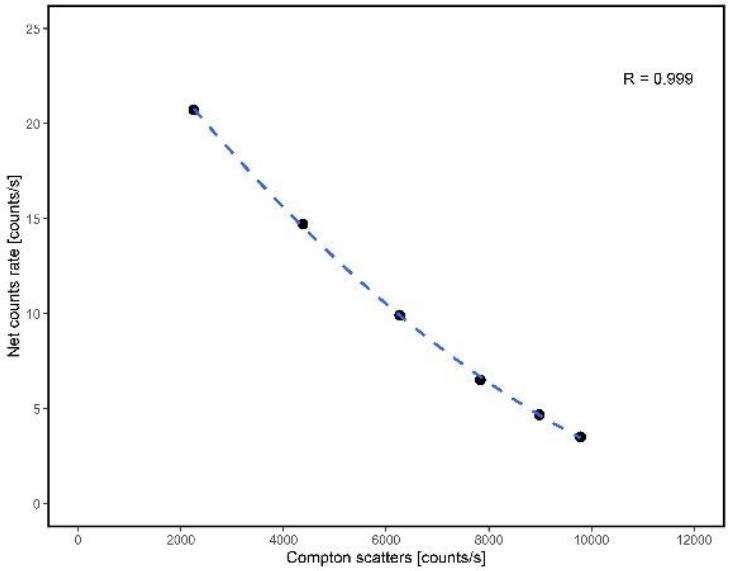

Figure 5. Net counts rate of Pb L_β versus Compton scattering signal with 100ppm Pb bone phantom analyzed by the peak fitting.

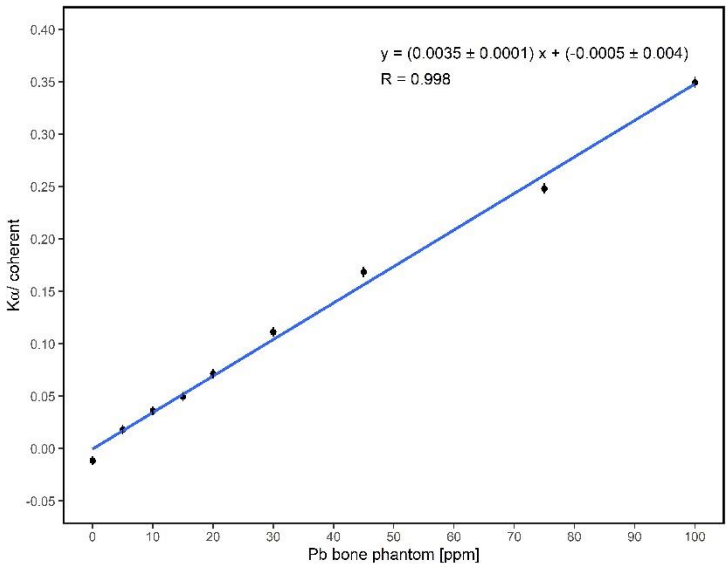

Figure 6. K_{α} /coherent versus the Pb concentration in bone equivalent phantom measured with the KXRF system.

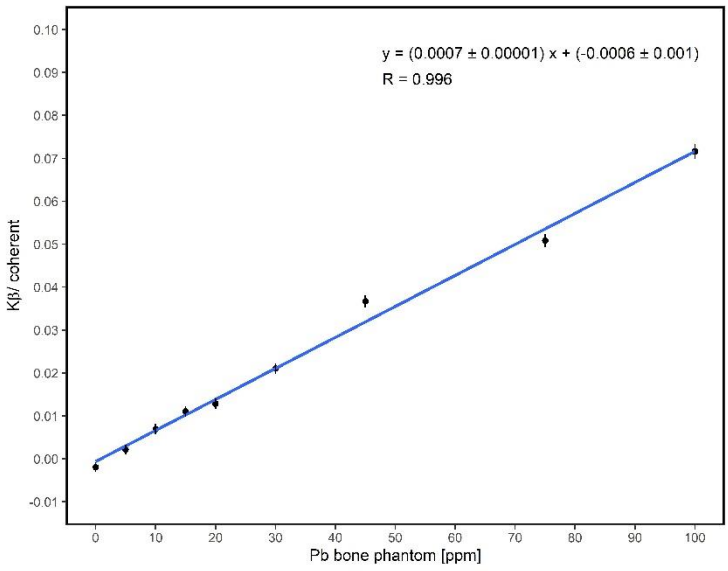

Figure 7. K_{β} /coherent versus the Pb concentration in bone equivalent phantom measured with the KXRF system.

2.3.3 Detection Limit of the XRF systems

The attenuation of the net signal caused by soft tissue overlying the bone resulted in a higher DL of bone Pb by the portable XRF than by the KXRF. These tendencies were borne out in both the measurements of bone-equivalent phantoms covered with Lucite and the *in vivo* measurements. With progressively thicker Lucite covering the bone-equivalent phantom, the DL of the 3-minute portable XRF measurements was substantially higher, with DLs ranging from 7.6 to 38.6 ppm for Lucite thicknesses ranging from 4 to 8 mm (Figure 8). These results extend those from a previous study, in which DLs calculated with the bone-equivalent phantoms ranged from 1.2 to 11 ppm with Lucite thicknesses from 1 to 5 mm [126]. The mean DL of the bone Pb concentration measured by the KXRF using the phantoms was 2.3 ppm and varied little by soft tissue thickness.

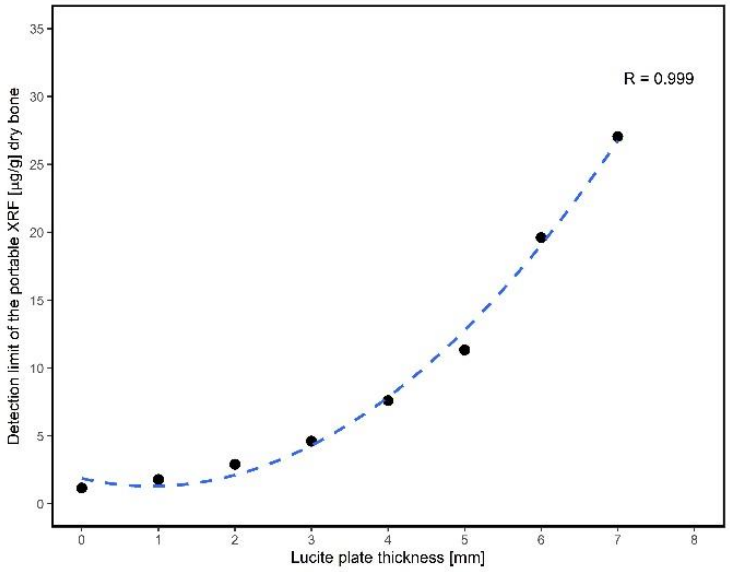

Figure 8. The detection limit of the portable XRF versus the Lucite plate thickness.

Likewise, the uncertainty of *in vivo* bone Pb measurements using the portable XRF was higher with progressively thicker overlying soft tissue, whereas the uncertainty of corresponding KXRF measurements was not affected by soft tissue thickness. Sixty participants underwent measurements with the 3-minute portable XRF and the older ^{109}Cd source (all participants from the West Lafayette and East Chicago sites). Among these participants, with a maximum soft tissue thickness of 7.5 mm, the mean uncertainty of portable XRF bone Pb measurement was 10.6 ± 8.2

μg/g dry bone (Table 2). Among those with soft tissue thicknesses < 5 mm (N=32), the corresponding mean uncertainty was 4.9 ± 1.7 μg/g dry bone. The mean uncertainty of the *in vivo* KXRF measurements was 3.1 ± 1.0 μg/g bone mineral, and it did not vary meaningfully by soft tissue thickness.

Table 2. Mean uncertainty [a], by overlying soft tissue thickness, of 3-minute *in vivo* bone Pb measurements using the portable XRF and KXRF systems (N=60).

Soft tissue thickness	< 5 mm	< 6 mm	< 7 mm	< 8 mm
N (% of study population)	32(53%)	41 (68%)	54 (90%)	60 (100%)
Portable XRF measurements				
Mean uncertainty ± SD (μg/g dry bone)	4.9 ± 1.7	6.1 ± 2.8	8.6 ± 5.4	10.6 ± 8.2
% of observations > 2*uncertainty	28%	24%	22%	23%
KXRF measurements				
Mean uncertainty ± SD (μg/g bone mineral)	3.0 ± 0.7	2.9 ± 0.7	2.9 ± 0.6	3.1 ± 1.0
% of observations > 2*uncertainty	72%	63%	56%	53%

[a] The DL of the XRF systems is approximately twice the mean uncertainty.

Table 3 shows the mean uncertainty of the 5-minute measurements (all Muncie participants, N=11) in different soft tissue thickness. Compared with the mean uncertainty of these 3-minute portable XRF measurements, the mean uncertainty of the 5-minute measurements was lower by a factor of 1.4, with soft tissue thicknesses up to a maximum thickness of 6.3 mm. The uncertainty for KXRF measurements among the Muncie participants was approximately 2 μg/g bone mineral, lower than the 3 μg/g bone mineral for other participants because of the use of a newer ^{109}Cd source in this group.

Table 3. Mean uncertainty [a], by overlying soft tissue thickness, of 5-minute *in vivo* bone Pb measurements using the portable XRF and KXRF systems (N=11).

Soft tissue thickness	< 5 mm	< 6 mm	< 7 mm
N (% of study population)	8 (73%)	10 (91%)	11 (100%)
Portable XRF measurements			
Mean uncertainty ± SD (μg/g dry bone)	3.7 ± 1.5	4.3 ± 1.8	5.2 ±3.6
% of observations > 2* uncertainty	75%	80%	82%
KXRF measurements			
Mean uncertainty ± SD (μg/g bone mineral)	2.0 ± 0.3	1.9 ± 0.3	1.9 ± 0.3
% of observations > 2*uncertainty	64%	60%	63%

[a] The DL of the XRF systems is approximately twice the mean uncertainty.

2.3.4 Comparison of Portable XRF and KXRF Bone Pb concentrations

The mean tibia bone Pb concentration in the study population, as measured by the portable XRF, was 12.3 ± 16.7 μg/g dry bone. As measured by the KXRF system, the mean bone Pb was 7.7 ± 8.8 μg/g bone mineral.

As the uncertainty of *in vivo* bone Pb concentration via portable XRF decreased with thinner overlying soft tissue, the correlation between bone Pb concentrations measured by the portable XRF and KXRF systems, in turn, increased when we restricted analyses to data from persons with thinner overlying tissue (Table 4). The correlation among all participants (N=71) was R =0.48, 95% CI (0.27, 0.64) (Table 4 and Figure 9), but was much higher among participants with soft tissue thicknesses < 5 mm (R =0.78, 95% CI: 0.61, 0.87; N=40, Table 4 and Figure 10). The highest bone Pb concentration of 61 ppm was obtained from a gentleman who had been working in a battery factory for many years. If this data was excluded from the linear regression model, the β coefficient would be 1.05 ± 0.30, and the correlation coefficient R would be 0.39 for all the participants; for participants with soft tissue thickness less than 5 mm, the β coefficient would be 0.56 ± 0.17, R = 0.48. The correlations from inverse-uncertainty-weighted regression models were more consistent across tissue thicknesses, although slightly lower than unweighted correlations at thicknesses < 6 mm. Figure 11 shows the bone Pb concentrations measured by both devices for the participants with soft tissue thickness less than 5 mm, and thicker or equal to 5 mm.

Table 4. Associations between *in vivo* bone Pb measurements via portable XRF and via KXRF (N=71).

Soft tissue thickness	< 5 mm	< 6 mm	< 7 mm	< 8 mm
Correlation between bone Pb concentrations estimated by portable XRF and KXRF				
Unweighted	0.78	0.73	0.46	0.48
Uncertainty-weighted[a]	0.71	0.68	0.63	0.62

[a] Observations weighted in inverse proportion to the uncertainty of portable XRF bone Pb estimate.

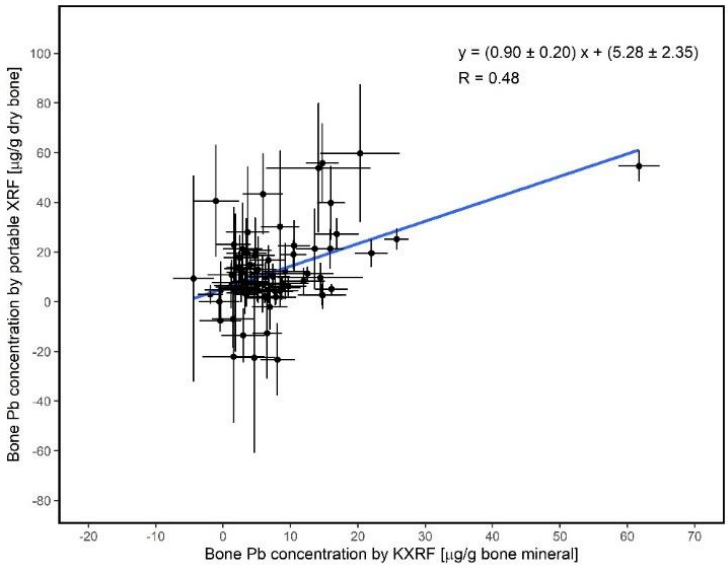

Figure 9. Correlation of bone Pb measured by the portable XRF and KXRF for all participants.

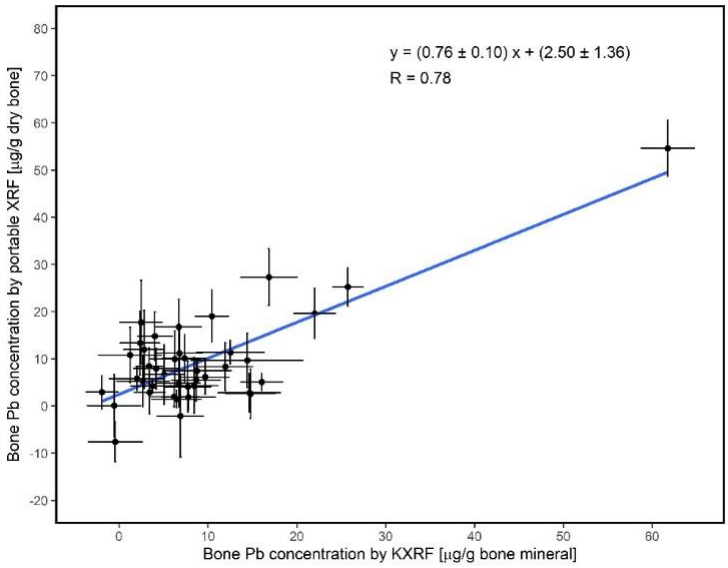

Figure 10. Correlation of bone Pb measured by the portable XRF and KXRF for the participants with soft tissue thinner than 5 mm.

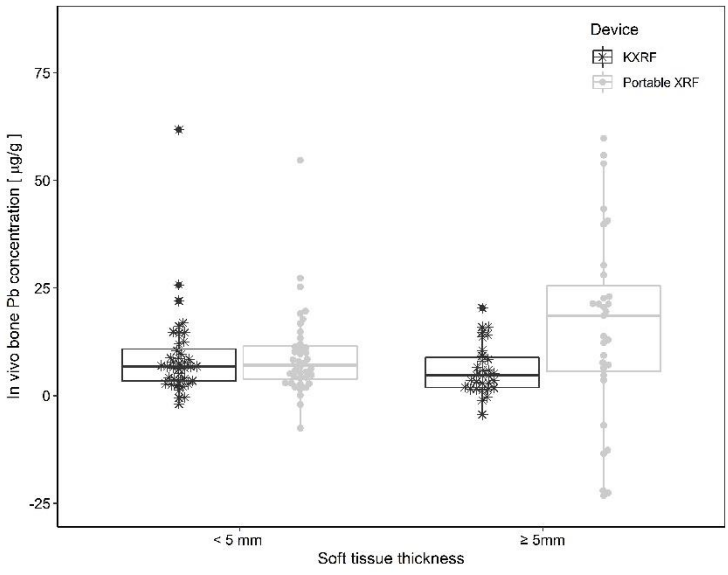

Figure 11. Bone Pb measured by the portable XRF and KXRF for the participants with soft tissue thinner, at, and thicker than 5 mm.

2.3.5 *In Vivo* Bone Pb Concentration with Age and Occupational Exposure to Pb

Older age appeared associated with higher estimated bone Pb concentration, as measured by either system. Bone Pb concentrations measured by KXRF was 1.66 μg/g bone mineral (95% CI: 0.80 to 2.50) higher per five years of age; the corresponding association using the portable XRF was weaker (0.65 μg/g dry bone higher per five years of age; 95% CI: -1.05 to 2.45). The reduced precision in the portable XRF association likely resulted from the increased measurement uncertainty, which, in turn, resulted from overlying soft tissue. Table 5 shows the mean difference in bone Pb concentrations per five years, estimated from the linear regression model, at different soft tissue thicknesses. The precision of the estimate from portable XRF measurements gets worse at higher tissue thickness.

Table 5. Mean difference in bone Pb concentration per 5 years in age, as estimated with bone Pb measured via the portable XRF and KXRF, by soft tissue thickness.

Soft tissue thickness	< 5mm (N=40)	≥ 5mm (N=31)	All (N=71)
Age (years, Mean ± SD)	66 ± 12	60 ± 11	63 ± 11
Portable XRF measurements (μg/g dry bone per 5 years in age)	0.87 (-0.50, 2.50)	1.60 (-2.10, 5.25)	0.65 (-1.05, 2.45)
KXRF measurements (μg/g bone mineral per 5 years in age)	1.87 (0.40, 3.30)	1.30 (0.45, 2.15)	1.66 (0.80, 2.50)

In the analysis of occupational Pb exposure, the mean tibia bone Pb concentration of participants with occupational and non-occupational Pb exposure measured via the portable XRF was 20.5 ± 16.1 and 12.0 ± 16.4 μg/g dry bone, respectively. The mean difference was 8.5 (95% CI: -4.0 to 21.0) μg/g dry bone with a p-value of 0.14. The results obtained from the KXRF were 15.9 ± 17.9 μg/g bone mineral (occupational) and 8.5 ± 4.0 μg/g bone mineral (non-occupational). Their mean difference was 7.4 (95%CI: -0.3 to 15.1) μg/g bone mineral with a p-value of 0.07.

2.3.6 Age and Soft Tissue Thickness

Older age was inversely associated with the thickness of soft tissue overlying the tibia (Figure 12). For each 10-year increase in age, overlying soft tissue was about 0.3 mm thinner, on average (-0.33 mm, 95% CI: -0.03 to -0.63).

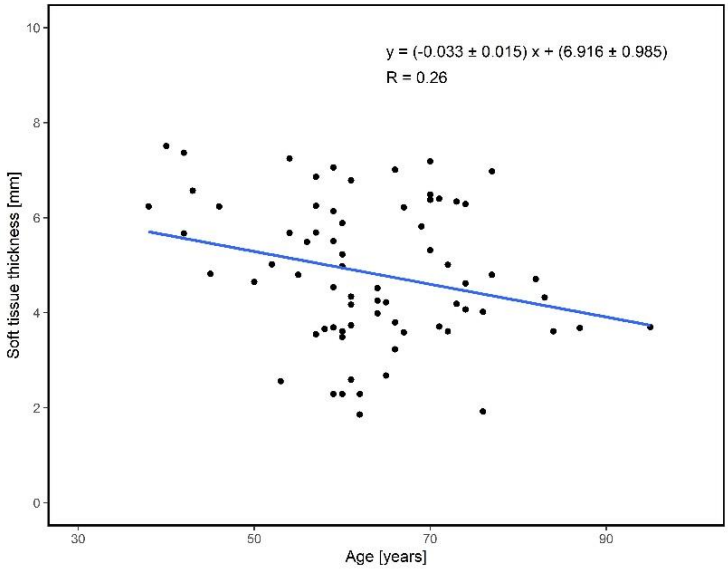

Figure 12. Correlation of soft tissue thickness over bone and age of participants.

2.4 Discussion and Conclusion

Using the portable XRF method, we were able to detect and quantify bone Pb concentrations in a study population of community-recruited adults, some of whom had been occupationally exposed. The *in vivo* bone Pb concentration measured by the portable XRF was strongly correlated with the concentration measured by KXRF, but the absolute bone Pb concentration measured by these devices differed. This is likely in part because these two devices scan different parts of the bone. The lower energy of L-x-rays detected by the portable XRF allows it to scans about 0.5 mm into the surface, whereas the higher energy of the K-x-rays detected by KXRF penetrates the bone more than 1 cm beneath the surface; thus the resulting signal is averaged across that span of bone. If Pb concentrations differ slightly in these regions, we would not expect the two methods to generate identical concentration estimates even under ideal conditions.

Because the higher overlying soft tissue thickness leads to higher signal attenuation for the portable XRF, participants with thicker soft tissue had a higher measurement uncertainty. Thus,

the correlation of bone Pb measured with the two systems for all the participants (N=71) was less precise than it was for the participants with soft tissue thinner than 6 mm (72% of the study population). In epidemiologic studies, investigators routinely use bone Pb measurements less than the DL from the conventional KXRF, as they still provide useful information in the distribution of the overall measures [167]. Hence, the DL, although useful for purposes of determining individual measurement validity, is less useful in population-level diagnostics. The DL of both XRF systems is approximately twice the mean uncertainty of *in vivo* measurements. Nonetheless, while the DL of the portable XRF (~ 7 - 10 ppm) was higher than that we obtained with the cloverleaf KXRF (~ 4 ppm), the portable XRF DL is roughly the same or less than the DL for conventional KXRF systems (~ 8 - 10 ppm) [121] that were used in most of the prior research on health effects of bone Pb, especially if one considers the DL for the portable XRF when tissue thickness is less than 5mm (~ 7 ppm).

Older age was associated with higher estimated bone Pb concentration, as measured by both systems. With thinner overlying tissue, this association was more evident with the portable XRF measurements, even though the β coefficient was slightly smaller than that at higher skin thickness. The associations of age with KXRF estimates were consistent at all soft tissue thicknesses.

The correlation of age and soft tissue thickness suggests that the portable XRF may be especially suitable for studies among older adults. Our results showed that there was a 0.3 mm decrease in soft tissue thickness per 10 years of age. This trend, combined with the minimal logistical barriers of the portable XRF, makes this instrument especially appealing for Pb exposure research among older adults and other populations who may have reduced access to study site visits or less tolerance of the long-measurement times of conventional KXRF.

For the portable XRF to be applied in a large-scale population study, we increased the measurement time from 3 min to 5 min for the Muncie participants, which reduced the measurement uncertainty by a factor of 1.4 overall. This actual reduction factor was even higher than the theoretical reduction factor we had calculated of 1.3. Even though the whole-body effective dose would be increased from 2.4 μSv to 4.0 μSv, it is still negligible compared to the dose for a standard AP chest x-ray of 100 μSv or one day of natural radiation from cosmic sources with a dose of 10 μSv. In addition, as noted above, the DL of the portable XRF is comparable or better than the sensitivity of conventional KXRF, particularly for participants with soft tissue

thickness thinner than 5 mm, which has been extensively used for past bone Pb epidemiology studies. In the current study, the overall bone Pb concentrations in the recruited population were much lower than other studies with similar populations from 20-30 years ago [15, 16, 169], which is likely due to the drastic reduction in environmental sources of Pb.

In conclusion, in this study of community- and occupationally exposed volunteers, bone Pb concentrations obtained from the portable XRF system were strongly correlated with concentrations measured with a KXRF system. The correlation was greater when we excluded the participants with thicker soft tissue or used a weighted least square regression method to weight observations based on soft tissue thickness. However, measuring with the portable XRF for five minutes rather than just three, improved the sensitivity. The portable XRF is a valuable tool for population studies on Pb exposure, avoiding many of the disadvantages of the KXRF measurements, and the method is ready to be used for large-scale population studies where the KXRF is not accessible or not practical.

CHAPTER 3. QUANTIFICATION OF STRONTIUM IN HUMAN BONE IN VIVO AMONG ADULTS USING PORTABLE X-RAY FLUORESCENCE

3.1 Introduction

Strontium (Sr) is a ubiquitous element in food and drinking water, and over 99% of the total body Sr burden is deposited in bone and teeth [20]. Diet is the primary source of Sr exposure, and the average daily Sr intake is approximately 2 to 4 mg [19]. The concentration of Sr varies in different types of food. For example, vegetables, grain, and seafood contain more Sr than meats [20], and cereal and vegetables are the dominant sources of Sr exposure from a person's regular diet [21]. Hence, the amount of Sr intake through diet and its accumulation in human tissue may vary in different geographic areas and races based on their diet.

Sr is a bone-seeking element. Excessive intake of Sr could disturb calcium metabolism [20, 40], causing bone abnormalities [40-42]. On the other hand, low-dose Sr supplements have been used to treat bone diseases over the decades [26, 44, 151]. A few *in vivo* studies and clinical trials have shown that the use of low-dose of strontium ranelate content can lead to bone formation, reducing the fracture incidences caused by osteoporosis [20, 31, 32], especially in the treatment for postmenopausal women [33-35]. Increased risks of myocardial infarction, however, have been investigated [36, 37], and the recent reassessment of the benefit-risk balance for strontium ranelate by the European Medicines Agency (EMA) suggested its use in patients with severe osteoporosis but without cardiovascular contraindications [38, 39].

Osteoporosis-oriented bone fracture rate is different across race and sex [170-173], and Sr may play a role in this difference. However, the relation between bone fracture and bone Sr level in different sex, age, and race is still unknown. In order to understand the effect of Sr in bone health, it is critical to have a practical technology that can measure the bone Sr levels *in vivo*. The long-term retention of Sr in bones [174, 175] allows us to measure and monitor the Sr level in bone over time. In this study, we used the portable x-ray fluorescence technology (XRF) developed in our group [126, 139, 142] to non-invasively quantify the cumulative bone Sr concentration among adults and determine the usefulness of this technology for large-scale population studies. Moreover, we looked at the variation of bone Sr concentrations in different sex and race of our study population.

This chapter demonstrates the methodology of spectral analysis and system calibration for *in vivo* bone Sr measurement. Signal normalization using coherent scatterings was investigated for the first time in this study. This chapter uses data collected from two different populations: one is the American population, who is the same as studied in Chapter 2; the other one is the Chinese population, which was measured by our research group with the same portable XRF device and settings back in Shanghai, China

3.2 Material and Methods

3.2.1 Study Population and *In Vivo* Measurement

The seventy-six participants studied here were the same as studied in the bone Pb project (Chapter 2). Among them, twenty-one participants were African Americans (10 women and 11 men; age 38-95 years), and fifty-two participants were Caucasians (24 women and 28 men; age 43-87 years). Moreover, twenty-nine Chinese adults (15 women and 14 men; age 53-82 years) living in Shanghai, China, were also studied in this project. The data of the Chinese population was collected by our research group a few years ago back in China, and the same portable device had been used for the bone measurements [128]. However, the represented data results only included 102 of the 105 recruited participants. The remaining three participants had a very thick layer of soft tissue overlying their tibia bone (> 9.3 mm), resulting in very high uncertainty or unrealistically negative bone Sr concentrations.

The Institutional Review Board of Purdue University, Boston University, Harvard University, and Xinhua Hospital affiliated to Shanghai Jiaotong University have approved this study. All participants provided their informed consent forms before undergoing the study procedures.

The procedure of *in vivo* measurements with the portable XRF is described in Chapter 2. A 2-minute measurement was performed on the twenty-nine Chinese participants. To investigate the effect of longer measurement time on system DL reduction, we took 3-minute measurements on sixty-two American participants and 5-minute measurements on the rest of eleven Americans participants

3.2.2 Portable XRF system

The portable XRF system and the device settings used here were the same as used for the bone Pb project in Chapter 2. Although the device setting was initially optimized for bone Pb measurement, it also provided the best system sensitivity for bone Sr measurements, due to the similarity of the K-shell electron binding energy of Sr (16.105 keV) to the L-shell electron binding energy of Pb (15.861 keV). Moreover, the Sr level in bone is typically much higher than the Pb level in bone, so its detection will be more accessible than Pb. Therefore, we could take advantage of multi-metal detection with the portable XRF device, and simultaneously measure the Sr levels and Pb levels in one bone measurement without irradiating participants for the second time.

3.2.3 Spectral Analyses

Sr K-shell characteristic x-rays were generated in the measurements with energies of 14.17 keV (K_α) and 15.84 keV (K_β). Only K_α peak was used for the bone Sr concentration calculation because it has a lower background under the Sr peak region. Moreover, K_β peak only represents 14% of the total characteristics x-rays, which will not predominately contribute to the total Sr concentration calculation. We used peak fitting with least-squares algorithms to extract the net counts of Sr K_α, where a Gaussian function was used to fit the Sr K_α peak and an exponential function to describe the background level.

3.2.4 Calibration of the Portable XRF

The bone Sr concentration was measured in μg/g dry bone (ppm) by the portable XRF. As the same as of bone Pb, the Sr K x-rays signal was also attenuated by the soft tissue overlying bone due to its low penetration ability. Hence, we used Compton scattering to estimate the soft tissue thickness and correct for the signal attenuation. This calibration method is described in Chapter 2.2. We calibrated the portable XRF system using a 200 ppm Sr-doped bone-equivalent phantom. This phantom was made in our group for the previous study [139], and it had a Sr contamination level of approximately 74 ppm. Besides, we used Lucite plates of thickness range from 0 to 8 mm, with an increment of 1 mm, to simulate different soft tissue thickness. All the calibration data were collected from 3-minutes measurements with the portable XRF. The determination of the *in vivo*

bone Sr concentrations was the same as described in Equation 1 of Chapter 2; however, the contamination of 74 ppm Sr was added to the 200 ppm Sr phantom for a more accurate calculation.

3.2.4.1. Normalization to Coherent Scattering Peak

As described in the previous chapter, the overlying soft tissue thickness will influence the results of bone measurements with the portable XRF. However, other factors could influence the measurement accuracy as well, such as the bone geometry and the device positioning during the measurement. Therefore, the variability in bone and soft tissue between individuals may create a challenge to the data analysis and bone Sr quantification. For the KXRF system, the above variables are eliminated by using the coherent scattering peak in signal normalization. This correction is useful because the coherent scatterings can reflect the bone interaction by determining the amount of bone mineral being irradiated. To explore a signal correction method for the portable XRF system, we have followed the methodology proposed in Somervaille *et al.* [118] and evaluated the use of coherent scatterings in signal normalization for the portable XRF measurements in this subsection.

The coherent scattering is elastic, and photon loses none of its energy essentially. Hence, the coherently scattered photons had the same energy as that of the x-ray beam produced by the portable XRF device, which was approximately 22 keV. The coherent scattering has importance at such low incident energy due to a large scattering angle. The coherent atomic cross-section is proportional to the squared ratio of the atomic number of the scattering material Z and incident photon energy $h\nu$:

$$\sigma_{coh} \propto Z^2/(h\vartheta)^2 \quad \text{(Equation 3).}$$

The differential cross-section can be expressed as a function of scattering angle θ and relativistic atomic form factor F.

$$d\sigma/d\Omega = \frac{1}{2} r_e^2 (1 + cos^2\theta) F(x, Z)^2 [cm^2 sr^{-1} atom^{-1}] \quad \text{(Equation 4),}$$

where r_e is the classical electron radius; $F(x, Z)$ depends on the $h\nu$, θ and Z [176]; $d\Omega$ is the solid angle. The form factor of a compound was calculated by multiplying the square of the form factor of each element by the elemental concentrations in moles per gram [177].

Using coherent scattering for signal normalization was first thoroughly investigated by Somervaille *et al.* [118] in the study of *in vivo* bone Pb measurement with the KXRF system. In that study, the normalization method was considered valid because the signal ratio of Pb net counts to coherent counts was independent of soft tissue thickness and source to sample distance. The following four criteria were evaluated in that study to satisfy the validity of the normalization and summarized by Keldani *et al.* [178]:

1. the Pb K x-rays and coherent scatter signals must be produced from the same fluence;
2. both signals must be created from the same location in the sample;
3. both signals must have the same angular distribution;
4. both signals must be attenuated similarly on their way back to the detector.

Criteria 1: the energy of source Cd-109 γ-ray (88.035 keV) was very close to the binding energy of Pb K-edge (88.005 keV); hence, the Pb x-rays were mostly generated from the primary incident γ-rays instead of any secondary fluence.

Criteria 2: the coherently scattered photons were about 88 keV with a measurement angle of approximately 153º. At this energy level and measurement angle, the detected coherent scattering was mostly generated from the bone mineral [118], not from other non-bone tissues such as soft tissue: the coherent cross-section in bone was about 28 times higher than in the soft tissue [118], and the relativistic atomic form factor F of soft tissue was only 1.38% of that of bone mineral [177].

Criteria 3: the differential coherent cross-section of main bone compositions was almost constant in the backward direction (angles from 120º to 180º), even though the coherent scattering was not isotropic as the Pb K x-rays.

Criteria 4: the similar energies of coherent scattering and Pb K x-rays made their difference in attenuation almost negligible.

Keldani *et al.* [178] have followed the principle of Somervaille *et al.* to test the validity of coherent normalization in his research topic, which is to measure the Gd (gadolinium) in bone *in vivo* using a similar KXRF system as Somervaille *et al.* did. The major difference between these

two studies was that the energy of Gd K-edge (50.24 keV) was much lower than the energy of coherent scattering (88 keV). Thus, criteria 1 and 4 were unsatisfied, while 2 and 3 remained satisfied. However, both experimental data from the phantom and Monte Carlo simulation have shown that the ratio of Gd net counts to coherent counts remained independent of soft tissue thickness in the range of 0 to 12.2 mm of soft tissue; thus, the coherent normalization was considered valid in that study as well. This result could be explained by that as the soft tissue thickness increased, more Gd K x-rays were produced from the secondary fluence, while fewer coherent scattering was detected due to the signal attenuation. However, the decrease of coherent scattering and the differential attenuation between the Gd K x-rays and the coherent scatterings were counteracted by the increase of Gd K x-rays.

To exam the validity of coherent normalization in the study, we have evaluated the four criteria one by one through the similar methods introduced by Somervaille *et al.* and Keldani *et al*. In the study, the x-ray beam has incident energy of 22.16 keV, and the measurement angle is approximately 145^{o}:

Criteria 1: the Sr K-edge binding energy is 16.105 keV and is 6 keV below the 22 keV incident x-rays. Hence, any photons from secondary fluence with energy between 16.105 keV and 22 keV could undergo photoelectric interaction with Sr in bone and produce Sr K x-rays. The energy of scattered photons from Compton interaction depends on the incident photon energy and scattering angle (Equation 5). If we consider the maximum energy loss in Compton scattering, which is Compton backscattering ($\varphi = 180^{o}$), the scattered photons still have energy 2.4 keV above the Sr K-edge energy. Therefore, it is likely that Sr K x-rays are generated by both secondary fluence from Compton scatter and primary fluence from the incident x-ray beam, while the coherent scatterings are generated by the primary fluence. The contribution of each fluence to the Sr photoelectric scatters, however, is unknown to satisfy this criterion.

$$h\vartheta' = \frac{h\vartheta}{1+(h\vartheta/m_0c^2)(1-cos\varphi)} \quad \text{(Equation 5)},$$

where $h\nu$ is the incident photon energy, $h\nu'$ is the scattered photon energy, φ is the scattering angle, and m_0c^2 is 0.511 MeV (the rest energy of the electron).

Criteria 2: we calculated the form factors of compounds [176] for cortical bone [179], soft tissue, skin, adipose tissue, and whole blood [180] with a photon energy of 22.16 keV and measurement angle of approximately 145^{o} (Table 6). The form factor of the bone mineral elements (hydrogen, oxygen, phosphor, and calcium) was 92% of the total form factor of the cortical bone. Therefore, bone mineral predominates the coherent scattering from cortical bone. On the other hand, the coherent cross-section of cortical bone was only about twice higher than the of non-bone tissues. This ratio is significantly lower compared to that of the bone and was 28 times higher than that of the non-bone tissues with the KXRF system in Somervaille *et al*. We could roughly estimate that a third of the generated total coherent scatterings were from soft tissue and the rest was from bone mineral. Therefore, the criteria of both coherent and Sr K-rays signals must be created from the same location in the sample is not satisfied here.

Criteria 3: similar to the coherent scattering of 88 keV, the different coherent cross-section with 22 keV is also almost constant in the backward direction; hence, both Sr K x-rays and the coherently scattered photons have the same angular distribution.

Criteria 4: the mass attenuation coefficient in soft tissue for Sr K x-rays (14.165 keV) is 2.31 [cm^2/g], while for coherent scattering (22.16 keV) is 0.73 [cm^2/g]. The difference in attenuation is significant for thicker soft tissue since the signal attenuation is exponentially proportional to the soft tissue thickness. 93% of coherent signals and 78% of Sr signals are detected after penetration of 1 mm soft tissue; 54% of coherent signals and only 14% of Sr signals are detected after penetrating 8 mm soft tissue. Such differences in attenuation, therefore, makes the proposed criteria 4 in Somervaille *et al.* not being satisfied here.

In summary, only one of the four proposed criteria was satisfied in the current study, challenging the application of coherent normalization. To experimentally test the validity of coherent normalization, we placed Lucite plates of 0 to 8 mm, with an increment of 1 mm, above a 200 ppm Sr-doped bone phantom, and measured 3 minutes with the portable XRF. We extracted the net counts of Sr K_α peak and the coherent peak to look at the relation between the ratio of Sr to coherent signals and the soft tissue thickness. There are two Compton peaks on each side of and overlapping with the coherent peak. The one at the left edge of the coherent peak is generated from the target Ag K_α with 20.54 keV; the other one at the right edge of the coherent peak is generated from the target Ag K_β with 22.90 keV. For this reason, we used multiple peaks fitting with least-squares algorithms to extract the net counts of the coherent peak. Each peak was fitted by a

Gaussian distribution, and the background level was described by an exponential function (Equation 6). The results are shown in the next section.

$$A_0 e^{-\frac{(x-b_0)^2}{2\sigma_{coherent}^2}} + A_1 e^{-\frac{(x-b_1)^2}{2\sigma_{Compton}^2}} + A_2 e^{-\frac{(x-(b_1+2.37))^2}{2\sigma_{Compton}^2}} + A_3 e^{-xA_4} \quad \text{(Equation 6)},$$

where A_0, A_1, and A_2 are the amplitude of peaks, b_0 and b_1 are positions of peaks, $\sigma_{coherent}$ and $\sigma_{Compton}$ are widths of peaks, and A_3 and A_4 describe the background.

Table 6. Form factors of cortical bone and non-bone tissues and the relative contribution to the bone, calculated with a photon energy of 22.16 keV and scattering angle of 145º.

	Form factor	% of the form factor for cortical bone
Cortical bone (Woodard 1962)	6.71×10^{-2}	100.0
Soft tissue (ICRU 44)	3.55×10^{-2}	52.8
Adipose tissue (ICRU 44)	2.70×10^{-2}	40.2
Whole blood (ICRU 44)	3.94×10^{-2}	58.7
Skin (ICRP 23)	3.58×10^{-2}	53.4

The coherent cross-section is related to different material compositions. Thus, the discrepancy between the in lab materials and human tissues might lead to slight errors in the estimation of *in vivo* bone Sr concentrations when using the coherent peak for signal normalization. The conversion factor of coherent scattering (CCF) between the phantoms and *in vivo* matrices could be calculated as: [177]:

$$CCF_{in\ lab\ to\ in\ vivo} = \frac{(d\sigma/d\Omega)_{in\ vivo}}{(d\sigma/d\Omega)_{in\ lab}} = \frac{F(x,Z)^2_{in\ vivo}}{F(x,Z)^2_{in\ lab}} \quad \text{(Equation 7)}$$

In this study, the Sr-doped bone phantoms were made using Mowiol 4-88 and bone meal derived from the ground cow bone [139, 181]. The interspecies differences in bone composition could be significant. For example, cow cortical bone has slightly higher ash content in dry bone than that of human cortical bone, whereas human trabecular bone has higher ash content than that

of cow trabecular bone [182]. Since the bovine bone meal used in the bone phantoms could contain different parts of the bone, it is difficult to determine the accurate chemical composition and calculate the form factors. The chemical composition of bone mineral is similar to the synthetic stoichiometric hydroxyapatite (HA) mineral [183, 184]. Therefore, to estimate the coherent scatterings from the bone phantom, we used the compositions of natural hydroxyapatite extracted from bovine cortical bone ash [185] to calculate the form factor. Moreover, we used the chemical composition of the HA to simulate the human bone mineral composition. The composition of the acrylic Lucite (polymethyl methacrylate) was adopted from the NIST database (National Institute of Standard and Technology) for the estimation of coherent form factor. Table 7 summarizes the form factors and CCF for each material. The CCF converting from bone phantom to the human mineral was 0.73, and from Lucite plates to soft tissue was 1.25.

Table 7. Form factors and coherent conversion factors (CCF) for the phantoms and human tissue, calculated with a photon energy of 22.16 keV and scattering angle of 145º.

	Form factor	CCF (from in lab to *in vivo*)
Bone phantom (HA from bovine cortical bone)	1.29×10^{-1}	0.73
Human bone mineral (HA)	9.37×10^{-2}	
Lucite plates (polymethyl methacralate)	2.84×10^{-2}	1.25
Human soft tissue	3.55×10^{-2}	

3.2.5 Detection Limit of the Portable XRF

The detection limit (DL) of the portable XRF for *in vivo* bone Sr measurements was determined by Specht *et al.* [139]. Instead of using one 200 ppm bone phantom, a set of bone phantoms with different Sr concentrations of 0 to 200 ppm were used to determine the DL. Since the soft tissue thickness could influence the signal detection, Lucite plates of 0 to 9 mm were placed between the bone phantoms and detector to determine the DL for each Lucite thickness. The previous study demonstrated that the DL increased with thicker Lucite, varying from 1.3 ppm with a 0 mm Lucite to around 15 ppm with a 9 mm Lucite. However, the discrepancy between the human soft tissue and Lucite plates could result in inaccurate DL estimates for the phantom with Lucite; thus, the uncertainty of *in vivo* bone Sr measurement for each participant was used to represent the system sensitivity for the *in vivo* setting in this study.

3.2.6 Statistical Analyses

The bone Sr concentrations were not normally distributed; thus, the nonparametric Kruskal-Wallis One-way (K-W) test was used to compare the Sr concentrations across the three races, while the Kolmogorov-Smirnov (K-S) test was used to evaluate the discrepancy between two different datasets. Moreover, the geometric mean was calculated to describe the overall bone Sr concentration values in different races and sex. In addition, we used a linear regression model with adjustment of possible confounders, including race, sex, and age, to exam the bone Sr concentration in different populations. Since Sr intake is highly related to diet and continuously accumulated in the bones, older adults may have more cumulated Sr in their bone. Hence, we regressed bone Sr concentration onto age to study the relation between bone Sr and age among adults in stratified sex and country (USA and China) and computed the Pearson correlation coefficients and the β coefficients of the linear regression model.

3.3 Results

3.3.1 Study Population

Table 8 shows the demographic data of the 102 participants in different races and sex.

Table 8. Age, sex, and soft tissue thickness of participants with different races in the study.

Race	African American	Caucasian	Chinese
N of participants	21	52	29
Age (Mean ± SD, years)	61 ± 15	64 ± 9	71 ± 9
Male Participants:			
N (% study population)	11 (52%)	28 (54%)	14 (48%)
Age (Mean ± SD, years)	68 ± 16	66 ± 10	73 ± 8
Female Participants:			
N (% study population)	10 (48%)	24 (46%)	15 (52%)
Age (Mean ± SD, years)	54 ± 13	62 ± 7	69 ± 9
Soft tissue thickness (Mean, 95% CI, mm)	5.6 (4.7, 6.4)	4.7 (4.3, 5.2)	5.1 (4.3, 5.9)

3.3.2 Calibration of the Portable XRF

Figure 13 shows the net counts of coherent peak changing with Lucite thickness with a 200 ppm Sr-doped bone phantoms. As the soft tissue thickness increases, more coherent scatterings were detected. This fact could be explained by that the attenuated coherent scatterings produced from the bone through soft tissues were counteracted by the increase of coherent scatterings produced from soft tissue.

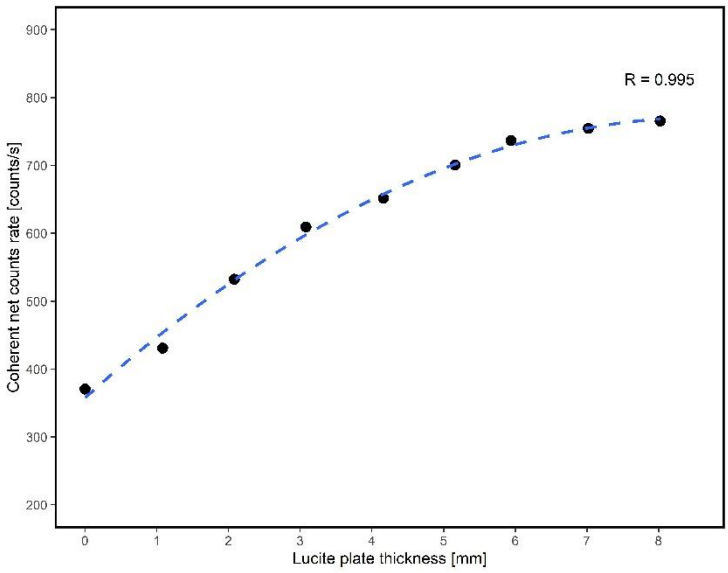

Figure 13. Coherent net counts versus soft tissue thickness.

For the coherent normalization to be valid, the ratio of Sr Kα signals to coherent signals needs to be almost constant over soft tissue thickness. Nevertheless, Figure 14 shows this ratio decreased with thicker soft tissue thickness; thus, a careful interpretation is needed when using the coherent scatterings for signal normalization for this study. The result also revealed that even though more Sr Kα signals could be produced from the secondary fluence as the soft tissues increased, this increased amount only contributed to a tiny portion of the total detected Sr signals and was not enough to counteract the signal attenuation.

Since more interpretations are required to use the coherent normalization as a valid method, at this stage, we have established the traditional calibration line without the normalization method and used it to calculate the *in vivo* Sr level calculation. Figure 15 shows the Compton scattering

counts increasing with thicker Lucite plate (R^2 = 0.999), while Figure 16 shows that the Sr K_α net counts decreasing with higher Compton scattering counts, measured from a 200 ppm bone Sr phantom, due to the signal attenuation (R^2 = 0.998). The calibration method explained here was the same as described in Chapter 2.

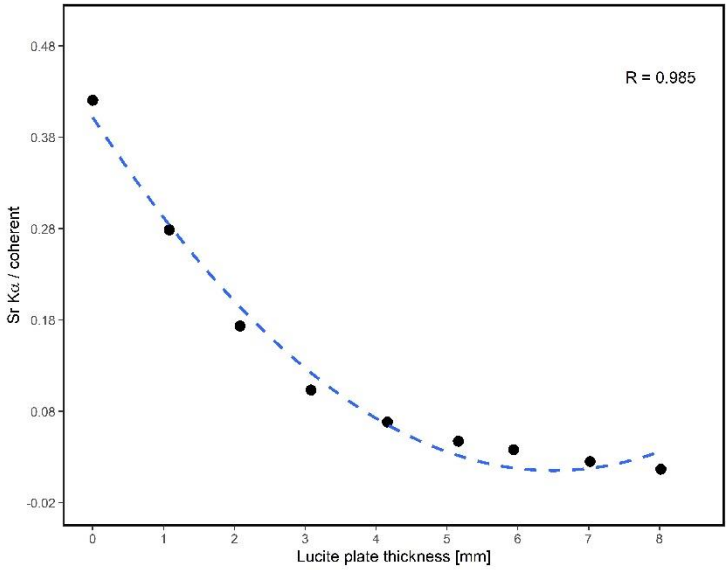

Figure 14. The ratio of Sr K_α net signals to coherent net signals versus soft tissue thickness.

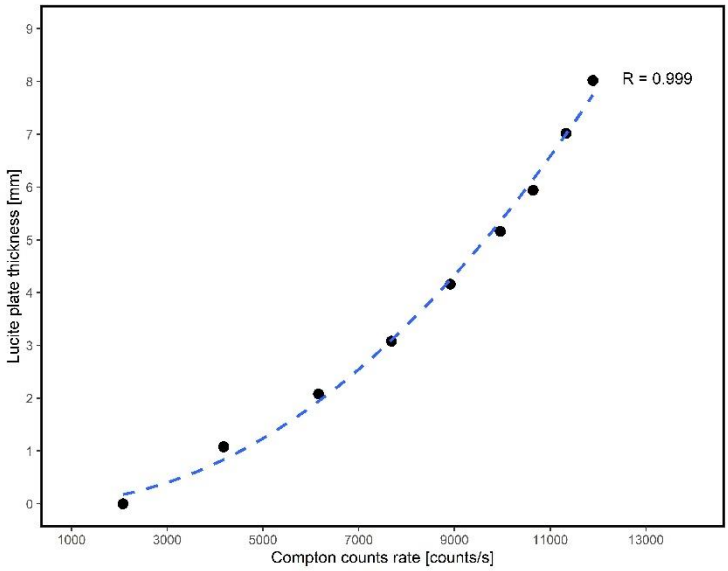

Figure 15. Soft tissue thickness versus Compton scattering signal.

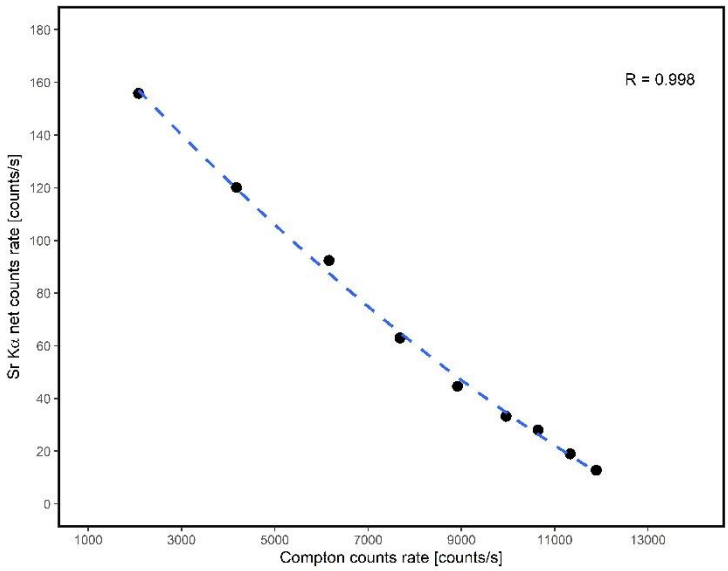

Figure 16. Net counts rate of Sr K_α versus Compton scattering signal with a 200 ppm Sr bone phantom analyzed by the peak fitting.

3.3.3 Comparison between the calibration methods

To compare the *in vivo* bone Sr concentrations estimated from both normalized and non-normalized calibration methods, we used a linear regression model to evaluate the association between the measurements from both methods (Figure 17). The slope of 0.73 represented a conversion factor between the two methods. When the *in vivo* Sr signals were normalized to the coherent scatterings, it should be considered the coherent conversion factor (CCF) of 0.73 from the bone phantom to the human bone mineral, CCF of 1.25 from the Lucite plates to the human soft tissue. Since the coherent scattering from soft tissue was about 38% of the bone mineral, the weighted CCF was calculated considering both Lucite and bone phantoms and obtained as 0.87. This CCF, however, was slightly different from the actual value since the chemical composition of the bone phantoms was adopted from the literature. Nevertheless, this factor converting from in lab *to in vivo* did not counteract the observed slope of the linear regression model in Figure 17. In contrast, it would decrease the *in vivo* Sr concentration calculated by the coherent normalization method and further decrease the slope of the linear regression line to 0.54. The discrepancy between the two calibration methods still needs further investigation.

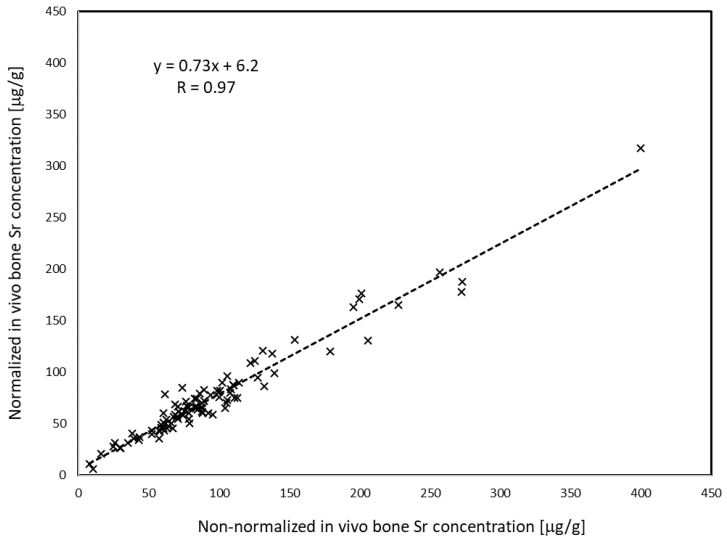

Figure 17. Correlation between the *in vivo* bone Sr concentrations calculated with and without coherent normalization.

3.3.4 Detection Limit of the Portable XRF

A consequence of signal attenuation by soft tissue over the bone was that the system DL calculated from the phantoms and Lucite plates decreased with a thicker plate. Likewise, the uncertainty of *in vivo* bone Sr measurements using portable XRF was higher with progressively thicker overlying soft tissue (Table 9). Extending the measurement time from 2 minutes to 3 minutes reduced the uncertainty by a factor of 1.2. Similarly, extending the measurement time from 3 minutes to 5 minutes further reduced the uncertainty by a factor of 1.3. The measured *in vivo* bone Sr concentration was greater than twice the uncertainty for all the participants (N=102) regardless of overlying soft tissue.

Table 9. Uncertainty, by overlying soft tissue thickness, of *in vivo* bone Sr within different measurement time using the portable XRF (N = 102).

Soft tissue thickness	< 5 mm	< 6 mm	< 7 mm	< 8 mm	< 9 mm
2 minutes of measurements (N=29)					
N (% of study population)	14(48%)	21(72%)	23(79%)	25(86%)	29(100%)
Mean uncertainty, ppm	2.6	3.3	3.6	4.3	8.0
3 minutes of measurements (N=62)					
N (% of study population)	33(53%)	41(66%)	52(84%)	61(98%)	62(100%)
Mean uncertainty, ppm	2.3	2.6	3.2	4.2	4.4
5 minutes of measurements (N=11)					
N (% of study population)	7(64%)	10(91%)	11(100%)	--	--
Mean uncertainty, ppm	1.8	2.2	2.4	--	--

3.3.5 *In Vivo* Bone Sr Concentration in Different Race and Gender

Figure 18 shows the measured bone Sr concentrations of participants with different race and sex, and the statistics are summarized in Table 10. The overall Sr concentrations differed across the three races of the study population (p-value of K-W test was 0.12). Among them, the overall Caucasian participants had the highest bone Sr concentrations, whereas the African Americans had the lowest values, and the difference between these two groups was significant (p-value = 0.01). Moreover, the bone Sr concentrations of the overall Chinese was marginally higher than that of the African Americans (p-value = 0.07), while a non-significant difference was found between the Chinese and Caucasian participants (p-value = 0.63).

Comparing the bone Sr concentrations in different sex within the same race, African American and Caucasian male participants had higher median bone Sr concentrations than the female participants, whereas Chinese men had lower median bone Sr than women. However, these differences were not significant, and the p-value for African Americans, Caucasians, and Chinese was 0.66, 0.60, and 0.76, respectively. Comparing the bone Sr in different races within the same sex, the bone Sr concentrations of male participants differed across the three races (p-value = 0.19), while such a trend was not observed in the female participants (p-value = 0.47). Among the male participants, the bone Sr concentration in the African Americans was lower than that of Caucasians (p-value = 0.055) and slightly lower than that of Chinese (p-value = 0.30). No significant difference was observed between Caucasians and Chinese (p-value = 0.73). Among the female

participants, the overall African Americans had the lowest bone Sr concentrations, while the Caucasians had a similar median with the Chinese. The difference between African American women and Caucasian women (p-value = 0.10) was more pronounced than that of the comparisons between other races, i.e., p-value = 0.22 between African Americans and Chinese and p-value = 0.50 between Caucasians and Chinese. Interestingly, Chinese women had higher geometric mean than Caucasian women. Similar results persisted when a linear regression model with adjusted age and sex used to analyze the Sr concentration across different races.

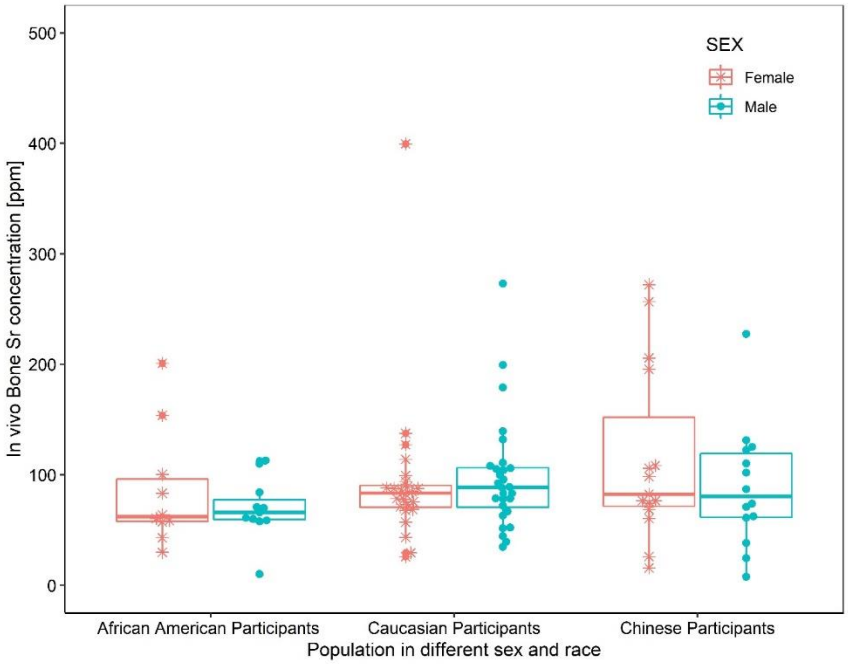

Figure 18. Bone Sr concentrations measured by the portable XRF for the participants with different races and gender.

Table 10. *In vivo* bone Sr concentration of the participants in different race and sex (N=102).

	Race	Median	1st Quartile	3rd Quartile	GM[a] ± GSD
All Participants	African American (N=21)	63.8	52.8	92.2	66.5 ± 1.8
	Caucasian (N=52)	85.5	69.3	105.1	84.6 ± 1.6
	Chinese (N=29)	82.5	61.8	123.7	79.4 ± 2.2
Male Participants	African American (N=11)	65.9	58.9	84.1	60.1 ± 1.8
	Caucasian (N=28)	88.6	68.1	107.5	88.2 ± 1.6
	Chinese (N=14)	80.5	55.5	123.0	69.8 ± 2.3
Female Participants	African American (N=10)	62.2	53.8	113.7	73.1 ± 1.7
	Caucasian (N=24)	83.6	69.3	92.7	80.7 ± 1.7
	Chinese (N=15)	82.5	68.6	195.6	89.7 ± 2.1

[a]: GM = geometric mean; GSD = geometric standard deviation

Since the participants were from the USA and China, we also looked at the bone Sr concentrations in different countries (Table 11 and Figure 19). No significant difference in the bone Sr concentrations was observed between the overall Chinese and US participants (p-value = 0.52). Among them, the Chinese male participants had slightly lower Sr concentrations than the US men (p-value = 0.86), whereas the US female participants had marginally higher concentrations than the Chinese women (p-value = 0.58). The same results persisted in the analysis of a linear regression model that adjusted for both age and sex.

Table 11. *In vivo* bone Sr concentration of the participants in different countries and sex (N=102).

	Country	Median	1st Quartile	3rd Quartile	GM ± GSD
All Participants	USA (N=73)	82.4	60.7	102.3	78.9 ± 1.7
	China (N=29)	82.5	61.8	123.7	79.4 ± 2.2
Male Participants	USA (N=39)	83.2	61.0	105.9	79.5 ± 1.7
	China (N=14)	80.5	55.5	123.0	69.8 ± 2.3
Female Participants	USA (N=34)	80.5	60.0	95.3	78.3 ± 1.7
	China (N=15)	82.5	68.6	195.6	89.7 ± 2.1

Note: GM = geometric mean; GSD = geometric standard deviation

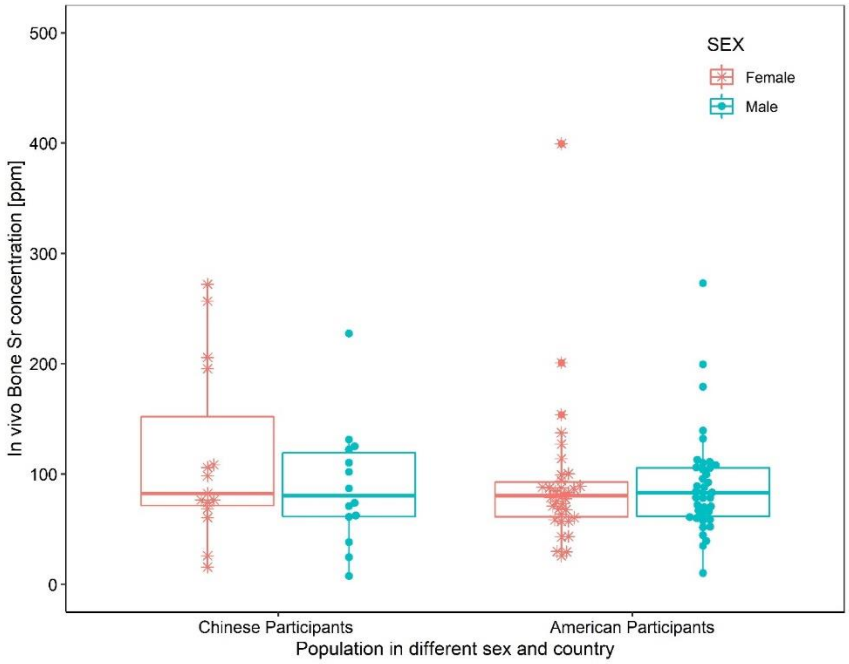

Figure 19. Bone Sr concentrations measured by the portable XRF for the participants with different gender and country.

3.3.6 *In Vivo* Bone Sr Concentration with Age

Table 12 shows the β coefficients and p-values from the linear regression of bone Sr concentration onto age for participants from different countries and sex, and the associations are shown in Figure 20 and Figure 21. In the analyses, the highest bone Sr concentration of 400 ppm was excluded from the American female participants since possible Sr supplements taking, or external Sr contamination was suspected. A significant positive correlation was found between bone Sr concentrations and age among the American female participants (Spearman coefficient = 0.42, N = 33). This correlation persisted but not significant if all the dataset was included in the analysis (N=34), where the β coefficient would be 1.99 (95%CI: -0.38 to 4.35) with a p-value of 0.10. The same positive correlations were observed in the American male (Spearman coefficient = 0.19, N = 39) and Chinese male (Spearman coefficient = 0.46, N = 14) participants. Interestingly, the bone Sr concentrations of the Chinese female participants were inversely associated with ages (Spearman coefficient = -0.17, N = 15).

Table 12. Mean difference (β coefficient) in bone Sr concentration (95% CI) per year age for participants with different sex and country.

Sex	USA (N=72)	China (N=28)
Male (ppm per year)	1.10 (-0.17, 2.36) p = 0.09	1.91 (-1.74, 5.58) p = 0.3
Female (ppm per year)	1.92 (0.74, 3.10) p < 0.01	-2.39 (-6.75 2.07) p = 0.3

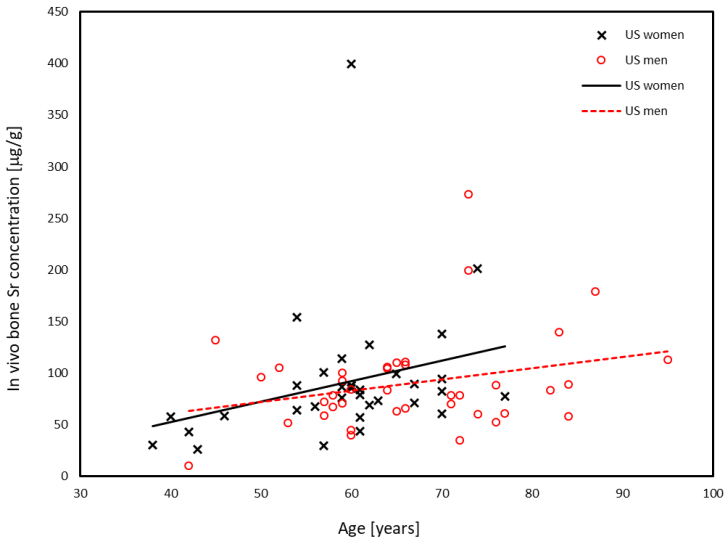

Figure 20. Correlation between the *in vivo* bone Sr concentrations and ages among US male and female participants.

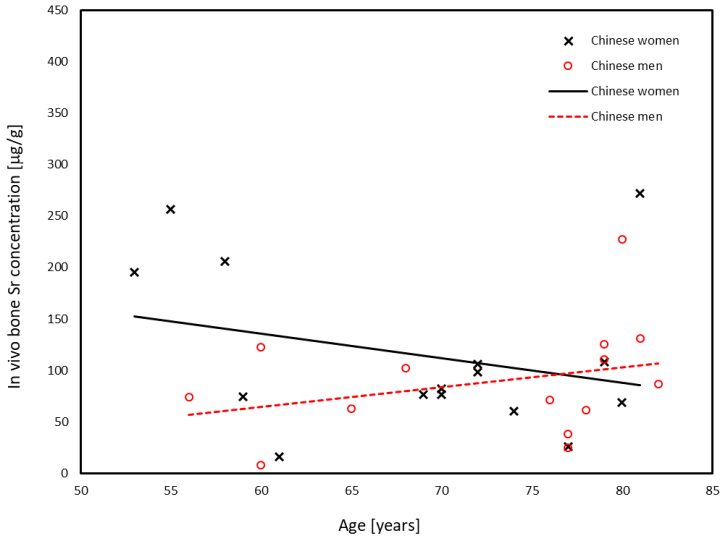

Figure 21. Correlation between the *in vivo* bone Sr concentrations and ages among Chinese male and female participants.

3.4 Discussion and Conclusion

Since signal attenuation increases with soft tissue thickness over the bone, participants with thicker soft tissue had higher uncertainties of the bone Sr measurements. Among the 2-minute measurements with the portable XRF, the uncertainties of individual *in vivo* measurement ranged from 1.1 ppm to 8.0 ppm, with overlying soft tissue thickness ranging from approximately 1.6 mm to 8.8 mm. The extending measurement time from 2 minutes to 3 minutes and from 2 minutes to 5 minutes reduced the uncertainty of *in vivo* measurements by a factor of 1.2 and 1.5, respectively. Even though the total-body effective dose would be increased from about 1.6 μSv (2-minute measurement) to 4.0 μSv (5-minute measurements), it is still negligible compared to the dose for a standard AP chest x-ray of 100 μSv or one day of natural radiation from cosmic sources with a dose of 10 μSv. In this study, all the participants had bone Sr concentrations higher than twice the measured uncertainty.

Since the coherent scatterings are generated from both the bone and overlying soft tissues, the coherent normalization method should reduce the uncertainty induced by, not only the bone geometry of the measurements but also the variances in the non-bone tissues between individual subjects. Nevertheless, the changing of normalized signals with the soft tissue thickness makes the normalization method questionable to calculate the *in vivo* Sr concentration, since more

variabilities are induced during the process, and the measurement uncertainty will be higher than the non-normalized method. Furthermore, the coherent normalization method has resulted in a discrepancy of the *in vivo* bone Sr levels from the traditional non-normalization method, and this conversion factor still needs to be better understood with further investigations.

The results showed that the bone Sr concentrations differed across the races. The overall Caucasian participants had the highest Sr concentrations, while African Americans had the lowest concentrations. Since calcium is the major component of bone mineral and Sr can displace it in bones [21], we could also compare the measured bone Sr concentrations in the study to the bone mineral density (BMD) and bone fracture rate from the literature review, among the different population. Nam, Shin [186] showed that among the US Caucasian, African American, and Hong Kong Chinese men aged 65 years above, African American men had significantly higher BMD than Caucasian men at the total hip, femoral neck, and lumbar spine. And similar hip BMD was found in Caucasian and Chinese men. As Sr has a much higher atomic number, higher BMD indicates higher Sr (or vice versa). That is not what we observed in this study. In this study population, the bone Sr levels in Caucasian men were higher than African American men (p-value = 0.055), and slightly higher than Chinese men (p-value = 0.73). The same result persisted with adjustment for age.

Comparing different races of the same sex in the US population, Hochberg [187] showed that among American adults aged 50 years and above, African Americans had significantly higher total body BMD than Caucasians for both sexes. In this study, the bone Sr concentrations in Caucasian participants were significantly higher than that of African Americans (p-value = 0.01). Among them, the difference in men was more pronounced than that in women. Comparing different sexes of the same race in the US population, Hochberg [187] and Looker, Melton [188] found that men had higher total body BMD than women for both Caucasian and African American. In this study, both Caucasian and African American men had marginally higher bone Sr levels than women, although the differences were not significant. These findings are not abnormal as there are many other factors that can affect the BMD in a population. However, as Sr is a bone-seeking metal and over 99% of the total Sr burden deposits in bone, it is expected that bone Sr levels are related to bone health. Future study with well-adjusted study design is warranted to further explore the association between Sr intake and bone health.

Furthermore, a significant positive correlation between the bone Sr concentrations and age was observed in American women. Similar positive but not significant correlations were found in both American men and Chinese men. This could be expected since cumulative Sr in bone might increase over time. However, regardless of race and sex, BMD decreases with age [188, 189]. Hence, the increasing of Sr in bone with the increasing of age could be offset by the decreasing of BMD with age, which results in the complex relations shown in the previous paragraph. Interestingly, a negative association between the bone Sr levels and age was found in Chinese women.

In conclusion, portable XRF is a valuable technology to quantify Sr concentration in bone and study the Sr-related bone health outcomes among adults. The detection limit of the portable XRF can be reduced by extending measurement time. The 5-minute measurements can provide fine sensitivity while the induced radiation dose is still negligible comparing to one day of natural radiation from cosmic sources. Furthermore, different bone Sr concentrations were observed in populations with different race and sex. Further study carefully designed study population is warranted to investigate the relation between bone Sr concentration, BMD, and bone health among different populations.

CHAPTER 4. QUANTIFICATION OF MANGANESE AND MERCURY IN TOENAIL IN VIVO USING PORTABLE X-RAY FLUORESCENCE

4.1 Introduction

Manganese (Mn) is an essential nutrient that can be found in food, water, and soil. No oral Minimal Risk Level (MRL) was set for Mn, but an Adequate Intake (AI) was established for adult men and women at 2.3 and 1.8 mg/day, respectively. Moreover, a Tolerable Upper Intake Level (UL) for adults of 11 mg/day was established by the Food and Nutrition Board of the Institute of Medicine [70]. Overexposure of Mn has been related to many chronic health effects [74, 190, 191]. Occupational populations such as ferromanganese welders [192] and steel smelting workers [193] are under the risk of Mn overexposure. The brain is the most vulnerable target of Mn accumulation and Mn induced damage to the central nervous system can lead to chronic neurobehavioral disorders resembling Parkinson's disease, which were confirmed in many studies [192, 194, 195].

Mercury (Hg) is a toxic heavy metal. Adverse health outcomes from Hg exposure to the general population have been a significant public health issue for many decades. The Environmental Protection Agency (EPA) recently announced to reduce the reference dose (RfD) for methylmercury (MeHg) intake from 0.3 μg/kg/day to 0.1 μg/kg/day [196]. As a common element of seafood, MeHg is a chemical form of Hg that cumulates in the human body and becomes a neurotoxicant targeting brain. Therefore, Hg exposure has been related to chronic neurological disorders and human developmental, such as disability of fine motor skills and verbal memory [197, 198].

In contrast to the short half-life of Mn and Hg in traditional biomarkers, including blood and urine, the toenail can reflect exposures in a relatively long period, for example, over 7-12 months for Mn [112]. Since total-Hg concentrations in toenails are significantly correlated to the concentrations of MeHg in blood and occipital lobe cortex [113], the toenail can be a good indicator for MeHg exposure. Furthermore, the toenail is generally less contaminated compared to hair and fingernail. Standard approaches to quantify toenail Mn and Hg concentrations include ICP-MS and AAS. These approaches require the collection of nail clippings, which could be difficult for some populations with slow nail growth. In addition, sample preparation and data analysis are time-consuming, especially for the Hg analysis, since its volatility requires a more sophisticated operation. The *in vivo* measurement with the portable XRF device does not require

the collection of toenail clippings, and data analysis can be processed in a more time- and cost-effective way.

This chapter demonstrates the methodology of spectral analysis and system calibration for *in vivo* toenail Mn and Hg measurement and determines the DLs of the portable XRF. It also shows the measured radiation dose induced by the portable XRF.

4.2 Material and Methods

4.2.1 Portable XRF System

The portable XRF system used here was the same as used for the bone Pb and Sr projects in Chapters 2 and 3; however, the device setting was optimized for toenail Mn and Hg measurements: voltage of 40 kVp, current of 50 μA, and a silver (Ag) and iron (Fe) combination filter. These settings provide the best DL for the simultaneous Mn and Hg quantification in human nails. Figure 22 illustrates a schematic configuration of metal assessment in a nail with the portable XRF device. In response to irradiation, photons undergo photoelectric interaction with Mn atoms in the nail, generating Mn K-shell-characteristic x-rays with an energy of 5.90 keV (K_α), while Hg atoms in nail generate Hg L-shell characteristic x-rays with an energy of 9.99 keV (L_α). Those detected x-rays are further processed and digitized by employed electronics in the device.

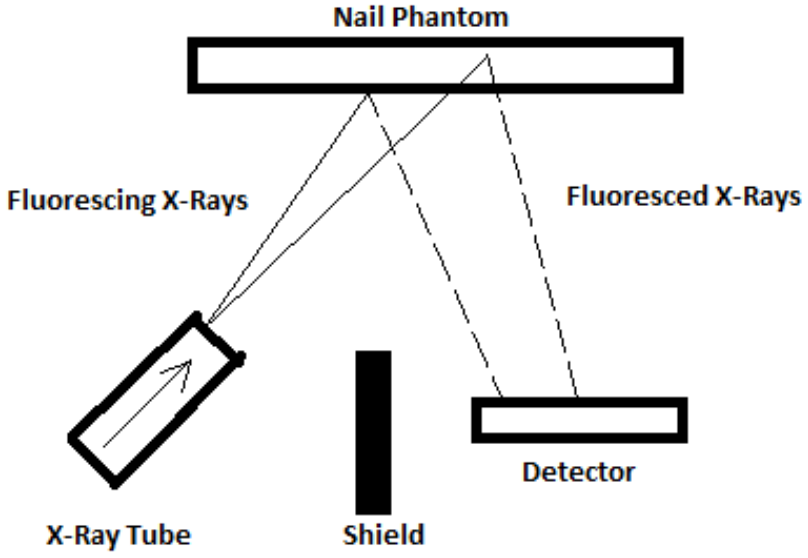

Figure 22. Schematic configuration of portable XRF device in nail phantom measurement.

4.2.2 Nail Phantoms

A mixture of polyester resin and salt was chosen to simulate human nails. Table 13 summarizes the elemental composition and density of each material [147]. To make a valid nail phantom, the attenuation properties of the phantom must match to human nail. Hence, we looked at the mass attenuation coefficients for each material at energies of Mn K_α (5.90 keV) and Hg L_β (9.99 keV), showing in Table 13 and found out that mixing a mass of 95% commercial polyester resin (Bondo Corp. Atlanta, GA) and 5% commercial salt (Morton Salt Inc, Chicago, IL) could successfully stimulate human nails. The selection of the composition was confirmed with the identical photoelectric absorption attenuation at the energy of incident x-ray beams (22.16 keV) for both nail phantoms and human nails (Table 13).

Table 13. Elemental composition, density, total mass attenuation coefficient, and photoelectric absorption coefficient for resin, salt, nail phantom, and human nail.

Substance	Elemental composition [by % mass]	Density [g/cm^3]	Total mass attenuation coefficient [cm^2/g]		Photoelectric absorption coefficient [cm^2/g]
Energy			5.90 keV	9.99 keV	22.16 keV
Resin	5 H, 60 C, 35 O	1.2	17.13	3.63	0.25
Salt	39 Na, 61 Cl	2.16	181.10	42.20	3.85
Nail Phantom	4.75 H, 57 C, 33.25 O, 1.97 Na, 3.05 Cl	1.25	25.34	5.56	0.43
Human Nail	7 H, 45 C, 15 N, 29 O, 4 S	1.3	25.38	5.57	0.43

To make the nail phantoms, we first dissolved salt into a small amount of water and then mixed with the resin. Magnetic stirrer with a stirring bar was used to guarantee a homogenous resin-salt mixture. In the next step, different concentrations of Mn and Hg, ranging from 0 to 50

ppm (0, 5, 10, 15, 20, 30, 45, 50 ppm), were doped into the nail-equivalent phantoms with the pipettes. For Mn nail phantoms, we used a manganese (II) nitrate solution (Flinn Scientific Inc, Batavia, IL) with a concentration of 0.24 g/mL. For Hg phantoms, the Hg solution was atomic absorption spectrometry standard (Fisher scientific company LLC, Bridgewater, NJ) with a concentration of 1 mg/mL. To ensure the homogeneity of phantoms, we diluted the solutions and mixed it well with the phantoms using a magnetic stirrer. Finally, we poured the well-mixed phantom into individual plastic rectangular shape molds with a dimension of 2.2 cm x 2.4 cm. The human big toenail thickness found by Johnson and Shuster [199] ranged from 0.83 to 1.69 mm. Moreover, the average thickness for men was 1.65mm, while for women, it was 1.38mm. Therefore, we made two sets of nail phantoms for each metal with a thickness of 1.0 mm and 3.0 mm to cover the thickness range and to study how the thickness will affect the calibration process and the results.

4.2.3 Spectral Analyses

Mn and Hg spectra were analyzed independently, and multiple-peak fitting with least-squares algorithms was conducted. The Mn K_α peak region (5.90 keV) was fitted over a range from 5.7 keV to 6.2 keV. Another Fe K_α peak with an energy of 6.4 keV was significantly interfering with the Mn K_α peak. This peak was generated from the surrounding shielding of the portable XRF device. Hence, we simultaneously fitted both peaks with a Gaussian distribution for each to represent the net x-ray count (Equation 8).

$$A_0 e^{-\frac{(x-b_0)^2}{2\sigma_{Mn}^2}} + A_1 e^{-\frac{(x-b_1)^2}{2\sigma_{Fe}^2}} + A_2 x + A_3 \qquad \text{(Equation 8)},$$

where A_0 and A_1 represent the amplitude of peaks, b_0 and b_1 are the positions of peaks, σ_{Mn} and σ_{Fe} are the width of peaks, and A_2 and A_3 describe the background level. Besides the Fe peak, a small number of scatterings were collected that formed a peak with the energy around 6.3 keV. Thus, we used an additional Gaussian function to fit this peak together with other peaks, to obtain a more accurate Mn net signals.

The Hg $L_{\alpha 1}$ peak region (9.99 keV) was fitted over a range from 8.90 keV to 10.32 keV. Such a wide fitting range was needed because of the interference from multiple peaks. The first interfering peak was tungsten (W) $L_{\beta 1}$ peak and located at the left edge of and significantly overlapping with the Hg $L_{\alpha 1}$ peak. The W $L_{\beta 1}$ peak has an energy of 9.67 keV and a relative density of 67%. The second interfering peak was W $L_{\beta 2}$ peak with an energy of 9.96 keV and a relative density of 21%. And the last peak was W Compton peak with energy about 9.35 keV, significantly interfering with the W $L_{\beta 1}$ peak. The W peaks come from the portable XRF device that W is the main composition of the collimator and tube base in the device.

In the fitting algorithm, the W $L_{\beta 2}$ peak was not fitted as an independent Gaussian function; instead, we used one Gaussian function to fit both the Hg $L_{\alpha 1}$ peak and W $L_{\beta 2}$ peak. Since the W $L_{\beta 2}$ peak was only two channels away from the Hg $L_{\alpha 1}$ peak (this peak dislocation was even smaller than the peak resolution, which was about 5 to 6 channels), this peak was indistinguishable from the Hg $L_{\alpha 1}$ peak. Hence, an additional Gaussian function for the W $L_{\beta 2}$ peak will result in inaccurate fitting results and very high uncertainty of the Hg net counts, especially for an *in vivo* measurement with a very low-level of Hg. The W peaks were generated from the portable device itself; thus, the measured W peaks should be consistent with the same device setting among the phantoms; consequently, the interference of W $L_{\beta 2}$ peak could be extracted from the intercept of the calibration line [142]. The following equation represents the fitting algorithm for the Hg spectrum.

$$A_0 e^{-\frac{(x-b_0)^2}{2\sigma_{Hg}^2}} + A_1 e^{-\frac{(x-b_1)^2}{2\sigma_{W1}^2}} + A_2 e^{-\frac{(x-b_2)^2}{2\sigma_{Wcompton}^2}} + A_3 e^{-xA_4}$$

(Equation 9),

where A_0, A_1 and A_2 represent the amplitude of peaks, b_0 b_1 and b_2 are the positions of peaks, σ_{Hg}, σ_{W1} and $\sigma_{Wcompton}$ are the width of peaks, and A_3 and A_4 describe the background.

4.2.4 Calibration and Detection Limit of the Portable XRF

To investigate the effects of nail thickness on system calibration, we established calibration lines for Mn and Hg nail phantoms with thicknesses of 1 mm and 3 mm. After that, we investigated

the effects of soft tissue underneath the nail on system calibration by using Lucite plates with different thicknesses. We first placed a 0 phantom above the Lucite plates of thickness ranging from 0 to 14.56 mm with an increment of 1 mm and regressed the background counts under the Mn K_α peak onto Lucite thickness to determine the correlation. The same measurement procedure was repeated for a 50 ppm phantom, we regressed the net counts of Mn K_α onto Lucite thickness and determined the correlation. The β coefficient and the p-value were computed from these linear regression models. Following the above investigations, we selected the 1 mm nail phantoms and a 10 mm soft tissue backing to establish a standard calibrations line for Mn and Hg. All the measurements for system calibration were performed in 3 minutes with the portable XRF device.

The DL was calculated using the following equation:

$$MDL = 2 \times \sqrt{BKG}/Slope \quad \text{(Equation 10)},$$

where BKG is the background under the Mn K_α or Hg L_β peak measured from 0 ppm nail phantoms, and *Slope* is obtained from the calibration curve of all the eight phantoms at a particular Lucite thickness.

4.2.5 Radiation Dose Assessed with TLDs

Four thermoluminescent dosimeters chips (TLDs) with a diameter of 0.5 cm were used to estimate the dose at the skin surface induced by a 3-minute portable XRF measurement. The four TLD chips were placed at the window surface of the device, covering about 1 cm^2 area, and a 3 mm bare nail phantom was placed on top of the TLDs. The device setting was the same as used for toenail measurements: 40 kV, 50 μA, and an Ag and Fe combination filter. Following a 3-minute measurement, the TLDs were read out by a TLD reader equipment Harshaw TLD 4000 (Harshaw Partnership, Solon, OH, USA). For the TLD calibration, each of them was exposed three times to doses of 0, 25, 50, 75, 100, 125, 250, 500, and 1000 mR, via a gamma irradiator at Purdue University, and has been calibrated independently by our research group. The gamma irradiator is a Gammacell 220 (Nordion International Inc., Ottawa, Canada) containing a cobalt-60 radioisotope source with known exposure rates. All the obtained calibration regression lines had $R^2 > 0.995$, ensuring the quantification and accuracy of results obtained using these TLDs.

4.3 Results

4.3.1 Spectrum Fitting for Mn and Hg

Figure 23 shows the Mn spectrum with the fitting curve, measured from a 50 ppm Mn nail phantom with 1mm thickness. As described in the methods section, Fe K_α peak generated from surrounding shieldings of the device was interfering with the Mn K_α peak, causing difficulty in determining the net counts under the Mn K_α peak, especially for lower Mn concentrations. The χ^2 of fitting results for all the phantoms measurements ranged from 0.89 to 1.40.

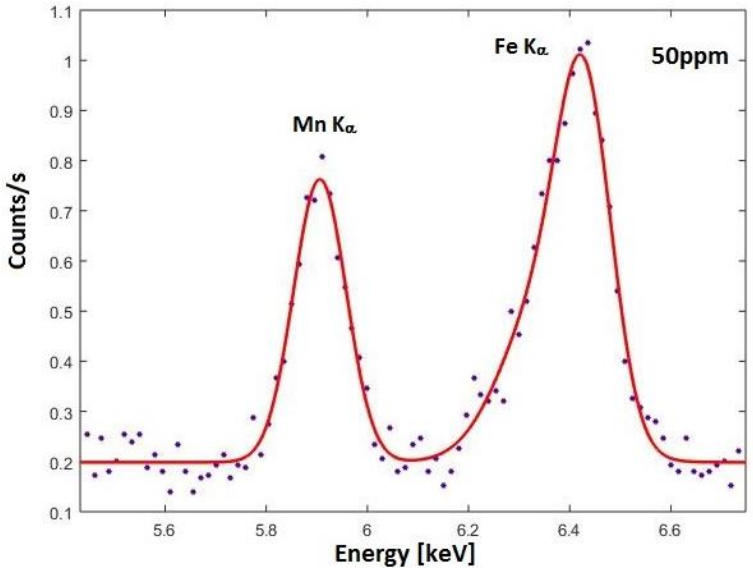

Figure 23. Observed and fitted Mn K_α peak and Fe K_α peak measured from a 50 ppm Mn toenail phantom.

The multiple-peak fitting algorithm was also applied in the Hg spectrum analysis. Figure 24 and Figure 25 show the Hg spectrum and fitting curve, measured from the 1 mm Hg nail phantoms of 50 ppm and 0 ppm, respectively. The W $L_{\beta 2}$ peak of 9.96 keV was indistinguishable from the Hg $L_{\alpha 1}$ peak but remarkable in the spectrum of a 0 ppm Hg phantom (Figure 25). The χ^2 of fitting results for all the phantom measurements ranged from 1.31 to 1.85.

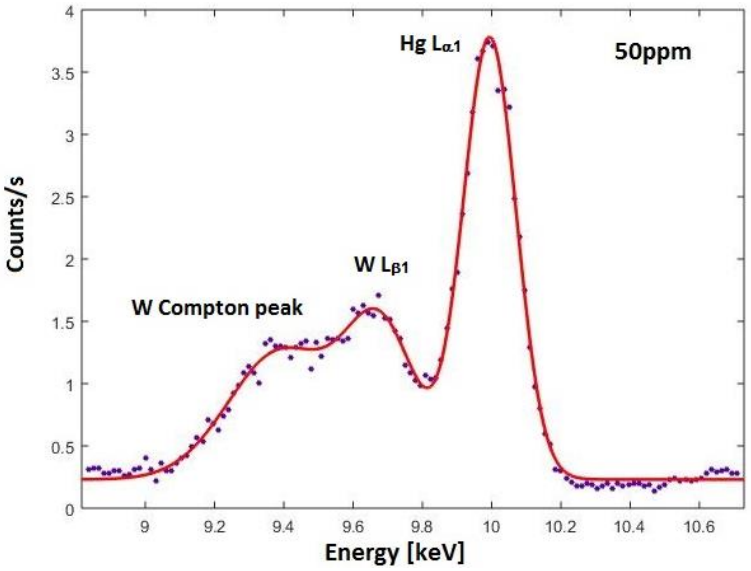

Figure 24. Observed and fitted Hg $L_{\alpha 1}$ peak, W $L_{\beta 1,2}$ peaks, and its Compton peak measured from a 50 ppm Hg toenail phantom.

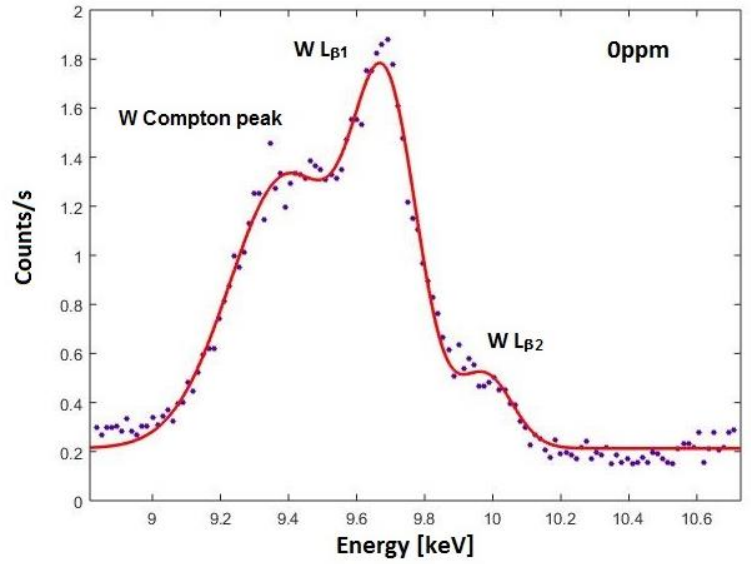

Figure 25. Observed and fitted Hg $L_{\alpha 1}$ peak, W $L_{\beta 1,2}$ peaks, and its Compton peak measured from a 0 ppm Hg toenail phantom.

4.3.2 Effect of Soft Tissue and Nail Thickness

Figure 26 shows the calibration lines measured with the Mn-doped nail phantoms of 1 mm and 3 mm thicknesses, while Figure 27 shows the calibration lines for toenail Hg. Based on the theoretical calculations, 97% of Mn K_α x-rays with the energy of 5.90 keV would be attenuated by a 3 mm nail phantom on their way back to the detector, in comparison to 95% of them were attenuated by a 1 mm phantom. Similar to Mn, the signal attenuation of Hg L_α x-rays (9.99 keV) in phantoms of 1 mm to 3 mm ranged from 50% to 87%. Due to the high signal self-absorption in the phantoms, the attenuation of signals in the first 1 mm thickness of a 3 mm phantom partially counteracted the extra amount of characteristic x-rays produced beyond the first 1mm in the phantom. Therefore, the net signals of Mn K_α x-rays were almost identical in the 1 mm and 3mm toenail phantoms, as shown in Figure 26, and the same result was observed for the toenail Hg as well.

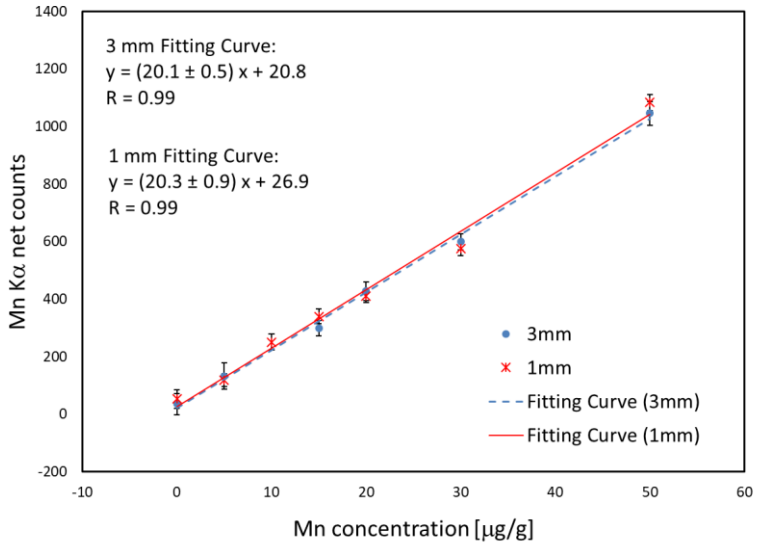

Figure 26. Calibration line of 1 mm and 3mm Mn-doped phantoms measured with portable XRF.

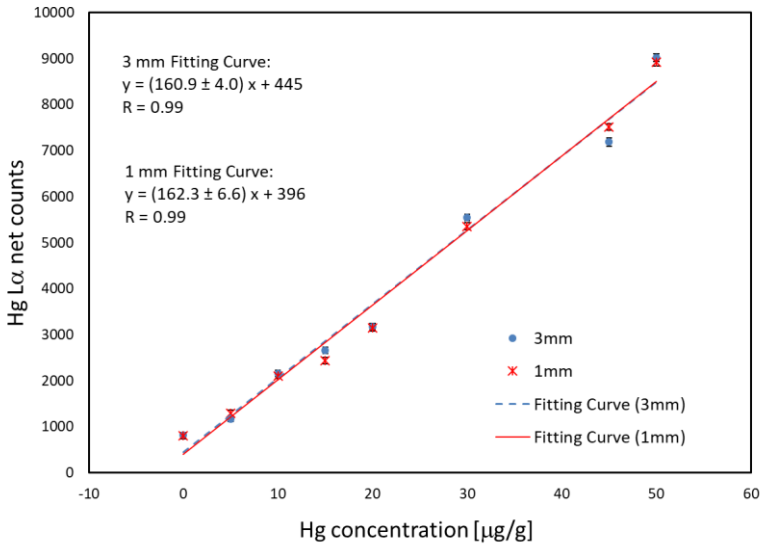

Figure 27. Calibration line of 1 mm and 3mm Hg-doped phantoms measured with portable XRF.

Figure 28 shows the total background counts under the Mn K_α peak of a 0 ppm phantom, changing with the thickness of soft tissue underneath the nail. The background counts increased with thicker soft tissue and then flattened at around 10 mm. This was expected because more secondary scatterings were generated from thicker soft tissues, increasing the background count until it saturated at a certain thickness due to the signal attenuation. Figure 29 shows the net counts of Mn K_α peak measured from a 50 ppm phantom, changing with the thickness of soft tissue underneath the nail. We used a linear regression model to exam the association between the net signals and soft tissue thickness and obtained the β coefficient of 0.01, with the p-value = 0.73. The statistical results indicated that the slope of the linear regression was not significantly different from zero at a 5% level; thus, the Mn K_α net count was not associated with the soft tissue thickness, especially within the estimated range of *in vivo* soft tissue thickness (above 10 mm).

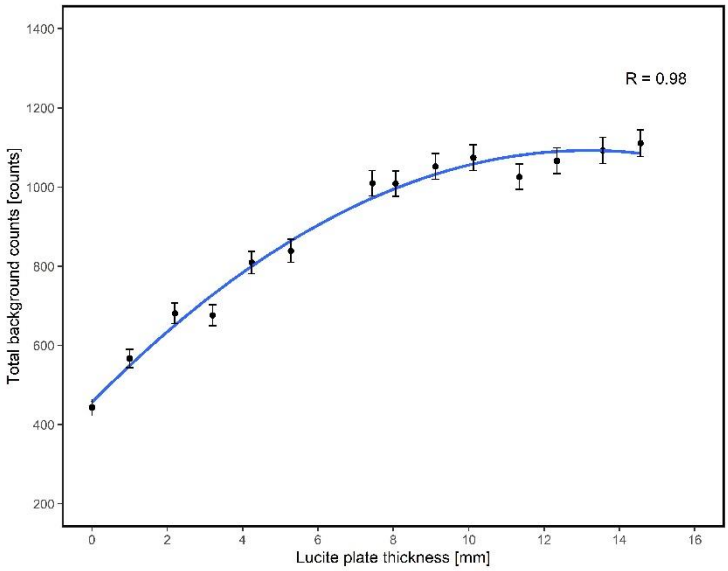

Figure 28. Total background counts under Mn K_α peak versus soft tissue thickness, measured from a 0 ppm Mn-doped phantom.

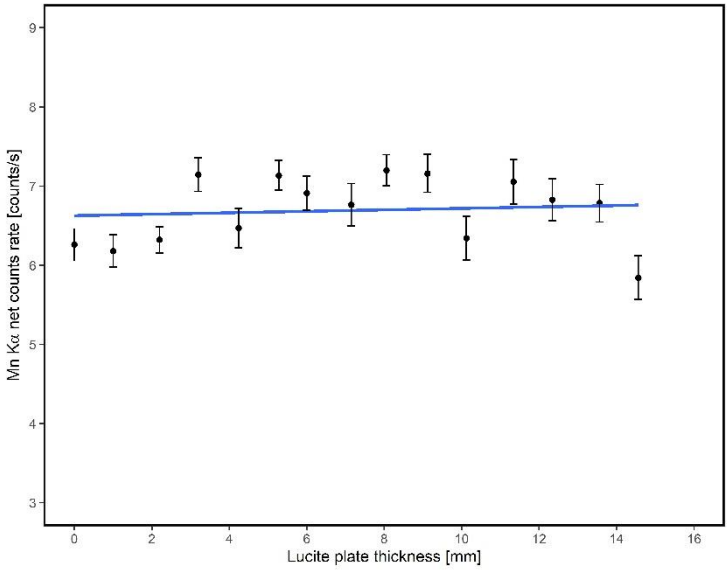

Figure 29. Net counts rate under Mn K_α peak versus soft tissue thickness, measured from a 50 ppm Mn-doped phantom.

4.3.3 Calibration of the Portable XRF System

Since the net signals and background signals have saturated with soft tissue thinner than 10 mm, and the human's big toenail ranges approximately from 0.8 mm to 1.7 mm [199], we have selected 1 mm Mn- and Hg- doped nail phantoms with a 10 mm backing for methodology exploration and system calibration. Figure 30 and Figure 31 show the calibration lines for Mn and Hg with obtained R, respectively. The toenail Mn and Hg concentrations from an *in vivo* measurement can be calculated from the calibration lines.

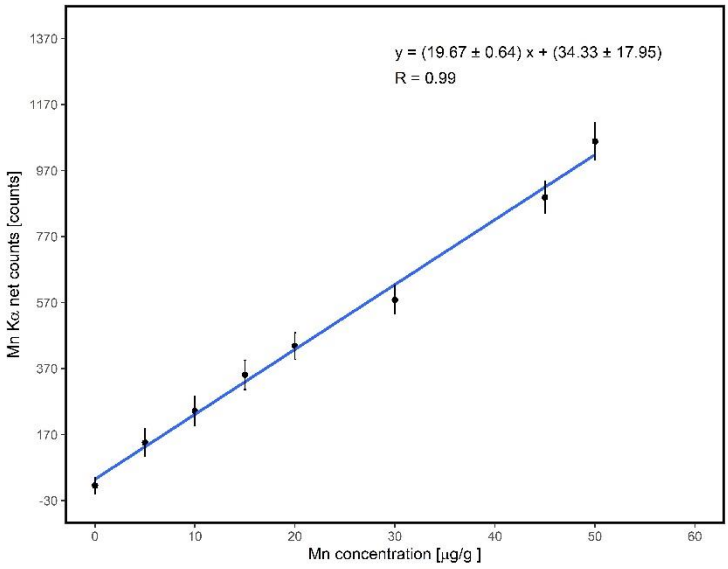

Figure 30. Calibration line for *in vivo* toenail Mn exposure assessment, measured from 1 mm Mn-doped phantoms and a 10 mm Lucite backing with portable XRF.

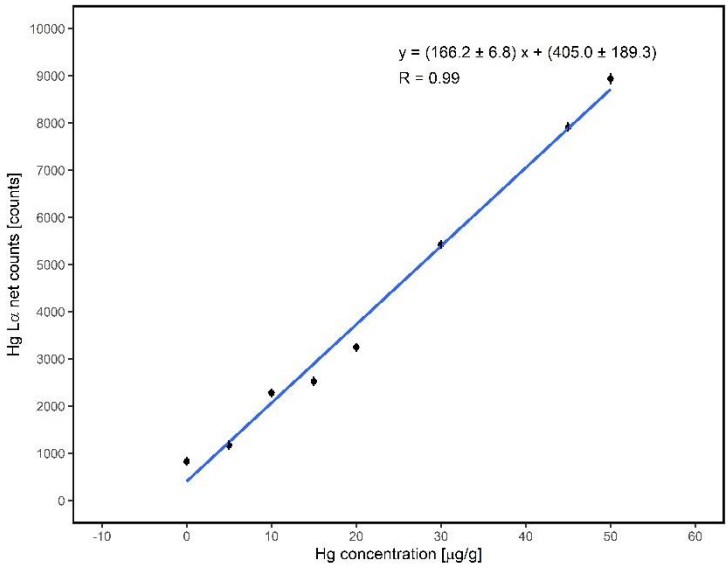

Figure 31. Calibration line for *in vivo* toenail Hg exposure assessment, measured from 1 mm Hg-doped phantoms and a 10 mm Lucite backing with portable XRF.

4.3.4 Detection Limit of the Portable XRF System

Table 14 shows the DL of portable XRF for the *in vivo* toenail Mn and Hg exposure assessment, measured from the 1 mm nail phantoms with and without a 10 mm Lucite backing. The significant increase of background under Mn and Hg peaks produced by the backing did not counteract the subtle rise of photoelectric x-rays produced by secondary fluence from the backing. As a consequence, adding soft tissue backing led to a worse system DL as shown in the following table.

Table 14. Detection limit for Mn and Hg in vivo exposure assessment with portable XRF, measured from 1 mm nail phantoms with and without a 10 mm soft tissue.

	Mn K_{α} [μg/g]	Hg $L_{\alpha 1}$ [μg/g]
1 mm bare phantom	2.03	0.50
1 mm phantom with 10 mm Lucite	3.59	0.58

4.3.5 Dose Induced by the Portable XRF System

We used four TLDs (TLD 700-1 to 700-4) to measure the radiation dose induced by a 3-minute measurement with the portable XRF, and obtained an average entrance radiation dose of approximately 43 mSv to 1 cm^2 nail area. Slightly less radiation dose to the soft tissue underneath the nail was expected. For a conservative estimate, we assumed the skin entrance dose was the same as the entrance radiation dose, which was 43 mSv. Since the estimated skin surface area for a reference man is approximately 1.9 m^2 [200], the estimate of whole-body effective dose induced by a 3-minute portable XRF measurement was 2.3 μSv.

4.4 Discussion and Conclusion

Even though thicker toenails can produce more characteristic x-rays, the high attenuation of those x-ray signals in the first 1 mm of toenail led to the detected number of x-ray signals that were almost identical for the 1 mm and 3 mm phantoms. Therefore, the toenail thickness will not significantly affect signal detection, allowing the use of a standard calibration line, measured with phantoms of one thickness, in calculating the *in vivo* Mn or Hg concentrations.

Unlike bones, toenails are unencumbered by overlying tissues. Thus, net signals are attenuated by the soft tissues underneath the nail and affecting the metal quantification in toenails using the portable XRF. As the soft tissue thickness increases, more characteristic x-rays can be generated by the secondary fluence coming from the soft tissue. At the same time, a higher background can be resulted from secondary scatterings. Since the increase of background is much more significant than the increase of characteristic x-rays, a higher system DL is observed with the soft tissue backing than the one without backing. Moreover, the increase of net signals was very subtle in the first couple mm thicknesses and quickly saturated with soft tissue thickness about 4 mm. No correlation was observed between the net signals and soft tissue thickness. Similar to the net signals, the background was slightly increased with the soft tissue thickness and saturated at about 10 mm. Therefore, a standard calibration line measured with soft tissue backing of one thickness can be used to calculate the *in vivo* Mn or Hg concentrations.

The DL of portable XRF for *in vivo* toenail Mn quantification was 3.59 μg/g, and this was comparable to the weighted mean nail Mn concentration of 4.22 μg/g in the general population found by Slotnick *et al.* [201]. Even though the sensitivity of Mn was not as good as of Hg for

low-level exposure assessment, the portable XRF is still a competitive technique for a population with high Mn exposure. Note that in the Mn spectrum analysis, a scattering peak was found in the region around 6.3 keV. Based on the theoretical calculation, Compton scatterings from the Fe K_α peak had an energy of about 6.25 keV. Thus, at least a small amount of that scattering peak might have come from the Compton scatterings of Fe. However, the amplitude of this peak was not consistent over all the Mn nail phantoms, while the Fe peak was consistent within uncertainty. Thus, the identification of that peak remained unclear. We used an additional Gaussian function to fit this peak together with other peaks, constraining the position and width of the peak with a narrow range. Therefore, although this peak would induce a higher uncertainty of Mn concentration, especially for the low-level of Mn, it would not affect the determination of the Mn absolute value due to the small counts of this peak.

The system DL for *in vivo* toenail Hg exposure assessment was achieved as 0.58 μg/g. The system sensitivity was comparable to the toenail Hg concentration found in the general population by Ohno *et al.* [202] and Alfthan [115], making it a competitive approach to non-invasively quantify *in vivo* toenail Hg concentration for environmentally exposed populations. In addition, the portable XRF technique overcomes some disadvantages of the traditional techniques, such as ICP-MS and CVAS (cold vapor atomic fluorescence spectroscopy), and is able to perform measurement and data analysis in a more time- and cost-effective way.

The total body effective dose induced by a 3-minute toenail measurement, with the portable XRF setting of 40 kV and 50 μA, was about 2.2 μSv. The induced risk is negligible compared to the annual background radiation dose of 3.6 mSv for the general population in the USA. The shallow-dose is defined as the dose averaged over a 10 cm^2 area of skin; thus, the 43 mSv entrance skin dose to 1 cm^2 skin is only about 1% of the allowable yearly occupational extremity dose limit of 500 mSv.

In conclusion, the current study explored the use of portable XRF technology for the assessment of Mn and Hg in toenail *in vivo*. The obtained system DLs for toenail Mn and Hg were 3.59 μg/g and 0.58 μg/g, respectively. The whole-body effective dose induced by a 3-minute measurement was 2.2 μSv. The future study involves the validation of the portable XRF for the toenail Mn and Hg exposure assessment with a population study, and it is described in the next chapter.

CHAPTER 5. EVALUATION OF THE PORTABLE XRF SYSTEM FOR IN VIVO TOENAIL MN AND HG QUANTIFICATION AMONG A US POPULATION

5.1 Introduction

Adverse health effects of manganese (Mn) and mercury (Hg) exposure have been recognized over the decades. Overexposure of Mn can typically occur among the occupational population who inhale Mn dust and fumes during the work and adversely affect health, resulting in neurological dysfunction [203, 204]. In the US, millions of construction workers, welders, and smelters are at risk of occupationally overexposing to Mn. However, health risks induced by low-level environmental Mn exposure, such as contaminated food and drinking water, have been recently investigated [68, 205, 206].

Different chemical forms of Hg exposure are associated with different routes of exposure, metabolism, and toxicity [82]. Inorganic Hg compounds are significantly accumulated in kidneys and induce kidney diseases [207]. Elemental Hg and organic Hg compounds are most toxic in the central nervous system inducing neurological disorders [82]. Among the organic Hg compounds, methylmercury (MeHg) that commonly presents in seafood, is the primary source of environmental Hg exposure. The Hg exposure induced neurological disorders not only manifest in adults but more pronounced in fetuses and infants who can suffer from developmental brain dysfunction and early sensorimotor dysfunction [152, 153].

Traditional biomarkers for Mn and Hg exposure assessment involve blood and urine, which can reflect metal exposures typically one to two months retroactively. On the other hand, nail integrates Mn and Hg over a relatively more extended period on the order of months to a year [112, 208, 209], making it a more appropriate biomarker for cumulative exposure assessment. The toenail is a useful biomarker to assess not only the high-level occupational Mn exposure [112, 210] but also the low-level environmental exposure. Studies have shown that the Mn levels in toenail were significantly correlated with the Mn concentration in drinking water for children and women during pregnancy and postpartum [99, 211]. Significant correlations between toenail Mn levels and performance in several neuropsychological tests were found in the residents living near a ferromanganese refinery [212]. Besides, increased Mn levels in toenail was observed in patients with epilepsy compared to the healthy controls [213]. In addition to Mn, the toenail is also a useful

biomarker for Hg exposure assessment, especially to evaluate the exposure from fish consumption [114]. Many studies have used toenail as a successful biomarker to evaluate the Hg-related health outcomes, including children with autism [214], women with prenatal MeHg exposure [91], and cognitive function [215] and amyotrophic lateral sclerosis risks [216] in adults.

The standard approach to quantify metal concentrations in human nail clippings is inductively coupled plasma mass spectrometry (ICP-MS). This approach can measure level in as low as parts per trillion range, but the preparation and process for data analysis can be very time and cost consuming. An alternative method to measure nail clippings is the portable XRF; however, calibration methods can be challenging since the geometry of nail samples to the device is very sensitive to cause higher uncertainty of the measurements [138, 217]. Therefore, we have explored the portable XRF technique to measure Mn and Hg exposure on toenail *in vivo*. The methodology of system calibration and the system detection limit are described in Chapter 4 [142]. In this chapter, we have evaluated the use of portable XRF for *in vivo* toenail Mn and Hg quantification within a population study and compared the results against the measurements of their nail clippings via ICP-MS.

This chapter combines *in vivo* toenail data measured by the portable XRF from two studies with different populations. The first one is the environmentally exposed population that is the same as in the bone Pb and Sr projects described in Chapters 2 and 3. Measurements for this population were performed at Purdue University. The second one is the occupationally exposed population, which was performed by our collaborators at Harvard T.H. Chan School of Public Health. Portable XRF devices with the same model and system design were used in both research sites.

5.2 Material and Methods

5.2.1 Study Population

At Purdue University, we have performed *in vivo* toenail measurements on seventy participants living in Indiana, USA. Among them, sixteen participants (9 women and 7 men; ages 38-95 years) were recruited from East Chicago. Forty-one participants (22 women and 19 men; ages 43-83 years) were recruited from the vicinity around West Lafayette. And thirteen participants (3 women and 10 men; ages 45-87 years) were recruited from the region around Muncie. Besides the *in vivo* measurements with the portable XRF, fifty participants' toenail

clippings were analyzed by ICP-MS. However, data from two participants were excluded from the analysis for toenail Mn, because they had nail polish with Mn contamination on the big toenail during the measurement, resulting in unacceptable high uncertainty and unrealistically positive toenail Mn concentrations. Moreover, data from another participant was excluded from the ICP-MS analysis for toenail Hg due to insufficient amounts of samples. Therefore, the data analysis of the comparison between the portable XRF and ICP-MS measurements represented forty-eight data for toenail Mn, and forty-nine data for toenail Hg.

To better validate the portable XRF system with a broader range of toenail Mn and Hg concentrations, we also analyzed the data collected from the occupational populations by our collaborators in Boston. Among them, sixteen male welding participants (ages 22-61 years) were recruited from a local Boilermaker union in Quincy, MA. Ten female nail salon workers (ages 21-50 years) were recruited from several nail salons around the Boston area.

5.2.2 *In Vivo* Toenail Measurement with Portable XRF

The portable XRF system used here was the same as used for the projects in previous chapters. The device setting was optimized for Mn and Hg measurements: 40 kV, 50 μA, and a silver and iron combination filter. For the portable XRF measurements, the participant sat on a chair with feet resting on a piece of clean paper placed on the ground. Participants were asked not to trim or paint their toenails for a few days before the visit. Before the measurement, we cleaned the participant's big toenail with alcohol swabs to eliminate any extraneous contamination. We used a contamination-free marker to mark the center of the participant's big toenail and then placed the portable XRF in the center of the big toenail via the camera inside the device itself (Figure 32). We performed a 3-minute measurement with the portable XRF on participants from West Lafayette and East Chicago. To determine the extent to which a longer scan time would reduce the DL of the device, we extended the measurement to 5 minutes for Muncie participants. The portable XRF measurement was followed by a collection of nail clippings samples from all ten toes. All the toenails were cleaned once again with alcohol swabs, and we used a clean stainless-steel toenail clippers to cut the nails. The nail clippings were placed in a small clean plastic zip bag labeled outside and sent to the laboratory at Harvard T.H. Chan School of Public Health for the analysis of ICP-MS.

Nail clippings were not collected from four participants from West Lafayette and three participants from East Chicago during their visit, because they have had their nails trimmed just before being contacted by us, and it was too short of cutting. They have mailed back their nail samples following our instruction of cleaning. However, their nail clippings samples and the ones of participants from Muncie (thirteen) were collected after we have mailed out the nail samples to Boston for ICP-MS analysis. Hence, the nail clippings of only fifty participants were analyzed by ICP-MS. The rest of the nail clippings samples are stored in our laboratory at Purdue University and will undergo ICP-MS analysis soon.

For the occupational population in Boston, a similar measurement procedure was followed by our collaborators to measure the big toenail within 3 minutes. However, a different portable XRF device setting was used in the measurements: 50 kV and 40 μA instead of the 40 kV and 50 μA. A higher background under the peaks of interest was observed with the device settings used in Boston.

Figure 32. *In vivo* toenail measurement with the portable XRF system.

5.2.3 System Calibration

The calibration method used here was the same as described in Chapter 4. Two calibration lines were used to calculate the *in vivo* toenail Mn and Hg concentrations of the general population measured at Purdue University: one was measured with the 1 mm bare nail phantoms, the other one was measured with 1 mm phantoms and a 10 mm Lucite backing. The comparison of the results would help to evaluate the validity of using one standard calibration line in the *in vivo* metal quantification. The occupational population in Boston was measured with different device settings from the general population; thus, our collaborators have re-measured the same set of phantoms with the corresponding device setting and established new calibration lines to calculate the *in vivo* Mn and Hg concentrations. The same fitting algorithm was used in the spectral analysis for both populations.

The estimated system DL from the 1 mm phantoms with a 10 mm Lucite backing is the minimum toenail Mn and Hg concentrations that can be reliably detected. However, the discrepancy between the phantoms and human toenails may result in different estimates of the DL for the phantoms. Therefore, we could use twice the uncertainty of *in vivo* measurement to approximately estimate the DL for an *in vivo* situation. We calculated the average uncertainty of *in vivo* measurement within 3 minutes and 5 minutes and determined the uncertainty reduction factor by simply calculating their ratio.

5.2.4 Statistical Analyses

Similar to the bone Pb and Sr measurements, the toenail Mn and Hg concentrations estimated by the instruments also oscillate around the actual value; hence, negative estimates may occur when a participant's actual *in vivo* toenail Mn and Hg concentration is close to zero. We retained these negative data points to provide unbiased estimates of the comparison between toenail measurements.

We used the Shapiro-Wilk test to first examine the normality of the *in vivo* toenail Mn estimates obtained from the two calibration lines (one with bare nail phantoms and the other one with a Lucite backing). We calculated the mean toenail Mn concentration and used a two-sample t-test with pooled variance or two-sample Kolmogorov-Smirnov test when appropriate to evaluate the mean difference and compute the p-value. Also, we used a linear regression model to compare

the estimates and computed β coefficient (95% CI) with its p-value. These analyses were repeated using toenail Hg estimates as well.

In addition, we used a linear regression model to compare the *in vivo* toenail Mn concentrations measured by the portable XRF to the toenail clippings Mn concentrations measured by ICP-MS. Pearson correlation coefficient R and p-value were computed. The *in vivo* Mn concentrations were calculated based on the calibration line with a 10 mm Lucite backing. The same analysis was repeated for toenail Hg data. We also analyzed the data collected from the occupational population by our collaborators in Boston. This population had moderate- to high-levels of Mn and Hg in toenails, broadening the examining range of metal levels and allowing a better evaluation of the correlations between measurements via both techniques.

5.3 Results

5.3.1 Study Population

Table 15 summarizes the demographic data of the seventy participants recruited from the general population in Indiana. Among them, 33 were female participants, and 35 were male participants. This table also shows the data of 50 participants whose nail clippings samples were analyzed by the ICP-MS.

Table 15. Age and sex of participants measured with portable XRF alone and with both portable XRF and ICP-MS.

	Portable XRF measurements	Portable XRF and ICP-MS measurements
N of participants	70	50
Age (Mean ± SD , years)	63 ± 11	64 ± 11
Male Participants:		
N (% study population)	36 (51%)	22 (44%)
Age (Mean ± SD, years)	68 ± 8	67 ± 13
Female Participants:		
N (% study population)	34 (49%)	28 (56%)
Age (Mean ± SD, years)	63 ± 6	61 ± 8

5.3.2 Calibration method testing with *in vivo* measurement

Table 17 shows the *in vivo* Mn concentrations of the general population (N=68, two were excluded due to external contamination), calculated based on the two calibration lines, and the Shapiro-Wilk p-values of the normality test. Table 17 shows the results of Hg (N = 70). The normality of toenail Mn and Hg concentrations, measured from both calibration methods, was strongly supported by the p-values for the Shapiro-Wilk test. Therefore, we used a two-sample t-test to evaluate the mean difference for both metals: the mean difference for toenail Mn was 0.22 ppm, with a p-value of 0.61, and the mean difference for toenail Hg was 0.06 ppm, with a p-value of 0.64. The statistical results indicated that no significant difference was observed between the *in vivo* metals concentrations calculated from the two calibration methods. Moreover, the correlation coefficient of the linear regression model for both metals was 1.0, and the β coefficient was 0.975 for Mn and 0.977 for Hg. Since adding the Lucite backing to nail phantoms could simulate better the *in vivo* situation, we used the calibration line of backing to determine the *in vivo* metal concentrations in the following sections.

Table 16. *In vivo* toenail Mn concentration calculated based on the calibration line of bare nail phantoms with and without Lucite backing (N = 68) in the general population measured at Purdue University.

Toenail Mn	From calibration line with 1mm bare nail phantom [ppm]	From calibration line with 1 mm nail phantom and 10 mm Lucite backing
Median	0.83	0.62
1st Quartile	-0.47	-0.72
3rd Quartile	1.80	1.62
Mean ± SD	0.70 ± 2.34	0.49 ± 2.42
Shapiro-Wilk p-value	0.19	0.19

Table 17. *In vivo* toenail Hg concentration calculated based on the calibration line of bare nail phantoms with and without Lucite backing (N = 70) in the general population measured at Purdue University.

Toenail Hg	From calibration line with 1mm bare nail phantom [ppm]	From calibration line with 1 mm nail phantom and 10 mm Lucite backing
Median	2.07	2.01
1st Quartile	1.44	1.49
3rd Quartile	2.53	2.60
Mean ± SD	2.07 ± 0.73	2.01 ± 0.71
Shapiro-Wilk p-value	0.98	0.98

5.3.3 *In vivo* toenail Mn and Hg concentration

Table 18 shows the toenail Mn and Hg concentrations of the general population, measured via both the portable XRF and ICP-MS techniques. The DL of ICP-MS for toenail clippings Mn and Hg were 0.046 ng/ml and 0.003 ng/ml, respectively. Among the toenail clipping samples, only four samples had Mn concentration higher than 1 ppm, ranging from 1.01 ppm to 1.29 ppm; and two samples had Hg concentration higher than 0.50 ppm, which were 1.71 ppm and 0.60 ppm. Table 19 summarizes the toenail Mn concentrations of the welders and the toenail Hg concentrations of the salon workers, measured by both techniques. The average Mn concentration in the toenail clippings of the welders was about three times higher than that of the general population, while the average Hg concentration of the salon workers was almost ten times higher than that of the general population.

Table 18. Toenail Mn and Hg concentrations of the general population, measured by the portable XRF and ICP-MS at Purdue University.

	Mn concentration (N = 48)		Hg concentration (N=49)	
	Portable XRF [ppm]	ICP-MS [ppm]	Portable XRF [ppm]	ICP-MS [ppm]
Median	0.56	0.22	2.01	0.03
1st Quartile	-0.86	0.11	1.44	0.02
3rd Quartile	1.55	0.35	2.54	0.07
Mean ± SD	0.38 ± 2.39	0.31 ± 0.31	2.03 ± 0.75	0.10 ± 0.26

Table 19. Toenail Mn concentrations of the welders and toenail Hg concentration of the salon workers, measured by the portable XRF and ICP-MS at Harvard University.

	Mn concentration (N = 16)		Hg concentration (N = 10)	
	Portable XRF [ppm]	ICP-MS [ppm]	Portable XRF [ppm]	ICP-MS [ppm]
Median	1.8	1.1	1.35	0.97
1st Quartile	-8.4	0.1	0.63	0.77
3rd Quartile	17.0	3.9	2.21	1.04

For toenail Hg measurements with the portable XRF, the average uncertainty (SD) of *in vivo* measurement within 3 minutes (N = 57) was approximately 0.24 (0.07) ppm, and the average uncertainty of 5-minute (N = 13) measurements was 0.21 (0.07) ppm. For toenail Mn measurement, the average uncertainty (SD) of 3-minute (N = 55) and 5-minute (N = 13) measurements was 1.78 (1.71) ppm and 0.95 (0.54) ppm, respectively. The uncertainty reduction factor for toenail Hg was about 1.14, while for toenail Mn was about 1.8.

5.3.4 Comparison of Portable XRF and ICP-MS Toenail Mn and Hg concentrations

Figure 33 shows the correlation between the *in vivo* toenail and toenail clippings Mn concentrations of the general population (N = 48), measured by the portable XRF and ICP-MS. The correlation coefficient was R = 0.33, and the β coefficient was 2.65 (95%CI: 0.15 to 4.89),

with a p-value of 0.02. If we restricted data to those with Mn concentration higher than twice their uncertainty (N = 8), measured via the portable XRF, the Spearman correlation coefficient between portable XRF and ICP-MS measurements would be 0.50, and the β coefficient obtained would be 1.97 (95%CI: -1.90 to 5.84) with a p-value of 0.35.

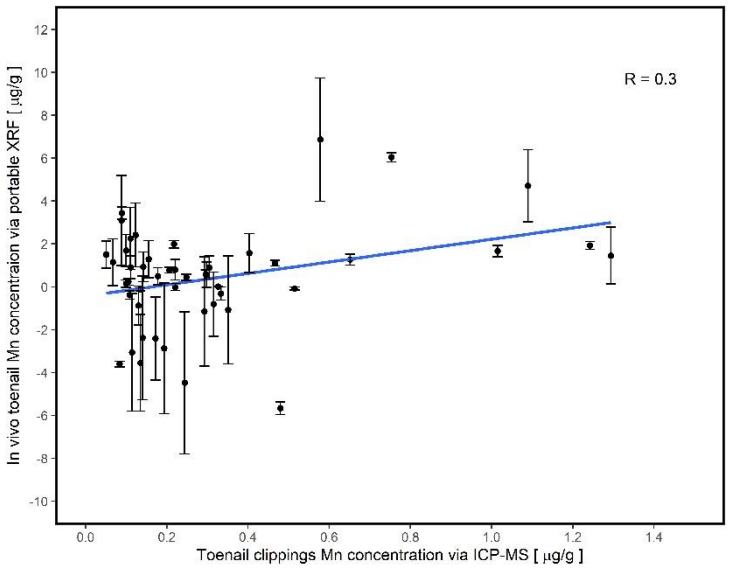

Figure 33. Correlation between the *in vivo* toenail Mn measured via portable XRF and the toenail clippings Mn measured via ICP-MS in the general population (N = 48).

No correlation was found between the toenail Hg concentrations measured by both techniques in the general population (R < 0.01, N = 49). Since the ICP-MS had excellent sensitivity for the Hg quantification in nail clippings (DL = 0.003 ng/ml), we could use the estimates from ICP-MS as a reference to reevaluate this correlation. If we excluded the maximum Hg concentration measured by ICP-MS (1.71 ppm), it would zoom in the linear regression model to a maximum Hg concentration of 0.6 ppm (N = 48). Then the correlation coefficient would increase to R = 0.3, and the β coefficient would be 2.2 (95% CI: 0.1 to 4.3) with a p-value of 0.04 (Figure 34).

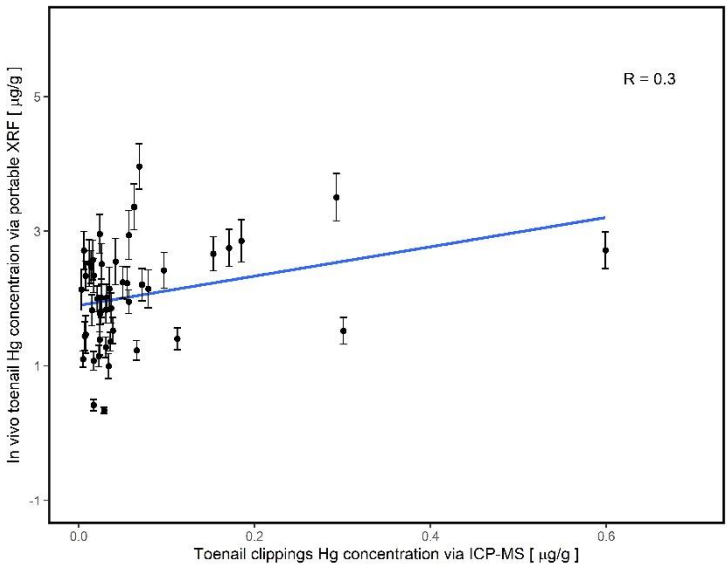

Figure 34. Correlation between *in vivo* toenail Hg measured via portable XRF and toenail clippings Hg measured via ICP-MS in the general population, excluding the highest Hg concentration measured by ICP-MS (N = 49).

Nevertheless, there was a significant correlation between the toenail portable XRF and ICP-MS measurements in the occupational population for both Mn and Hg. For the toenail Mn measurements in the welders (N = 16), the correlation coefficient was 0.59, and the β coefficient was 3.97, with a p-value of 0.02. Combining the data from both the general and occupational populations, the overall correlation coefficient for the toenail Mn measurements obtained was 0.22 (N = 64). For the toenail Hg measurements in the nail salon workers (N = 10), the correlation coefficient was 0.74, and the β coefficient was 1.46, with a p-value of 0.02. Furthermore, the overall correlation coefficient of the combined data was 0.19 (N=59).

5.4 Discussion and Conclusion

As described earlier in Chapter 4, the net signals of Mn and Hg were independent on the soft tissue thickness underneath the nails, and the background signals increased with thicker soft tissue but abruptly flattened out around 10 mm soft tissue. The difference of metal concentration calculated based on the two calibration lines (one of the bare phantoms and the other one of 10 mm backing) would approximately reflect the maximum disagreement of the metal estimates for an individual *in vivo* measurement. For both the Mn and Hg measurements, statistical results

showed a non-significant difference in the overall metal concentrations calculated based on the two calibration lines. The individual Hg concentration was almost identical for both calibration methods. The small difference obtained from the two calibration lines was observed in the individual Mn concentration that might influence the estimate of absolute values. However, the uncertainty of individual Mn measurement was much higher than this difference; thus, the *in vivo* Mn concentration calculated from one standard calibration line should still be reliable.

Significant correlations were observed between the toenail portable XRF and ICP-MS measurements for both Mn (R = 0.59) and Hg (R = 0.75) in the occupational populations. These promising results demonstrated the suitability of portable XRF for *in vivo* Mn and Hg toenail exposure assessment, especially for participants who have moderate- to high-level of toenail Mn and Hg concentrations. Since toenail is a biomarker for cumulative exposure assessment, the toenail growth rate, and the half-life of metals in it could result in slightly different exposure windows on different parts of the toenail. Therefore, such difference might decrease the correlation coefficient between the estimates of toenail clippings via ICP-MS and *in vivo* toenail via portable XRF, resulting in an underestimated correlation from the actual correlation of both measurements.

In the environmentally exposed population, a positive correlation (R = 0.33) was found in the toenail Mn concentrations measured by both techniques, while the non-significant correlation was found in the toenail Hg concentrations. These weaker correlations, compared to that of the occupational population, could be explained by that their toenail Mn and Hg concentrations were remarkably lower than the system DLs, especially for Hg. The DL of portable XRF for toenail Hg measurement was about 0.6 ppm shown in Chapter 4. However, the mean toenail clippings Hg concentration was only about 0.1 ppm measured by ICP-MS, and the mean *in vivo* toenail Hg concentration of the general population was about 2 ppm via the portable XRF. The system DL for toenail Mn was higher than that of toenail Hg, which was about 3.6 ppm shown in Chapter 4. However, the mean *in vivo* toenail Mn concentration of the general population was only about 0.38 ppm, measured via portable XRF, and the mean toenail clippings Mn concentration was 0.3 ppm, via ICP-MS.

The uncertainty of *in vivo* Mn measurements was significant and widely varied among individual measurements, as shown in Figure 33. One of the reasons was that most of the Mn peaks were not notably different from the background under the peaks, resulting in high uncertainty of measurements from the peak fitting. Also, the interference of the unidentified peak of 6.3 keV

(discussed Chapter 4), overlapping with the Mn peak, was inconsistent among *in vivo* measurements; thus, the fitting algorithm developed for the system calibration lines shown in Chapter 4 might not be optimized for the spectral analysis of some *in vivo* measurements. As described in the previous chapter, a W $L_{\beta 2}$ peak was indistinguishable from the Hg peak. The intercept of the calibration line was used to extract the W $L_{\beta 2}$ peak since the W peaks were consistent among the phantoms. However, the variability in the curve of individual human toenail and geometry of *in vivo* measurement could result in slightly different W counts for individual measurements. Hence, the toenail Hg concentration calculated from the calibration line could be overestimated, especially for the low-level of Hg, as shown in Table 18.

Compared to the theoretical reduction factor of 1.3, the average measurement uncertainty for toenail Hg has reduced by a factor of 1.2, with the extending measurement time from 3 minutes to 5 minutes. And the average uncertainty for toenail Mn has reduced by a factor of 1.8. Among participants who were measured with 3 minutes, a few of them had unacceptably high uncertainty for Mn due to the non-optimal positioning of the device during measurements and very low level of Mn. These high uncertainties increased the average uncertainty for 3 minutes measurements, resulting in a reduction factor of 1.8 that was much higher than the theoretical value. Even though the whole-body effective dose would be increased from 2.3 μSv to 4.0 μSv with the extending measurement time, it is still negligible compared to one day of natural radiation from cosmic sources with a dose of 10 μSv.

In conclusion, portable XRF is a valuable tool that can effectively assess the cumulative Mn and Hg exposure in toenail *in vivo*, especially for moderate- to high-level of Mn and Hg concentrations. Measurement sensitivity can be improved by extending the measurement time from 3 minutes to 5 minutes while retaining the low induced radiation dose, which is negligible compared to the dose of natural radiation from cosmic sources. Further actions such as spectral fitting optimization will improve the detection limit and provide better estimates of toenail Mn and Hg exposure assessment.

CHAPTER 6. SUMMARY AND FUTURE DIRECTIONS

This work evaluated the use of the portable XRF technology on *in vivo* bone Pb and Sr, and toenail Mn and Hg quantification. My primary contribution of this work included: 1. I have improved the methodology of data analysis for bone Pb and Sr determination with the portable XRF; 2, developed the methodology for toenail Mn and Hg quantification with the portable XRF. 3, performed the experiences within a population study for the validation of portable XRF.

A significant correlation between bone Pb concentrations measured via the portable XRF and KXRF systems was found in adults of the general population in USA. Participants with thicker soft tissue overlying bone had higher measurement uncertainties; hence, a stronger correlation between the estimates from both measurements was observed in participants with thinner soft tissue. Elevated bone Pb concentrations were found in older participants, and the soft tissue thickness was inversely associated with age.

The detection limit of portable XRF for *in vivo* bone Sr measurement also increased with thicker soft tissue, varying from 2.7 ppm to 9.0 ppm with soft tissue thickness ranging from approximately 2 mm to 8 mm within 3-minute measurements. For both bone Sr and Pb measurements, system sensitivity was improved by a factor of about 1.4 with the extending measurement time from 3 to 5 minutes. A strong positive correlation between bone Sr concentrations and age was observed among the US populations, suggesting possible cumulative Sr in bone over time. Furthermore, a trend of different bone Sr concentrations was found in the study population with different races and sexes, which opens the possibility of studying associations between the accumulation of Sr in bone and bone health among people with different demographic characteristics.

Methodology development and validation were conducted for the quantification of Mn and Hg in toenail using the portable XRF device. Mn- and Hg-doped nail phantoms were made with different thicknesses to establish system calibration lines. The thickness of the toenail and soft tissue underneath it would not make considerable differences in the determination of the metal concentrations. Thus, we established the calibration lines by using the 1 mm nail phantoms and a 10 mm Lucite backing. The detection limit of the portable XRF for *in vivo* toenail Mn and Hg measurements was 3.6 ppm and 0.6 ppm for Hg, respectively.

Significant correlations between the toenail portable XRF and ICP-MS measurements were observed for Mn (R = 0.59) and Hg (R = 0.75) in the occupational population. A positive correlation (R = 0.3) was found for toenail Mn measurements in the environmentally exposed population, while a non-significant correlation was found for toenail Hg measurements due to the extremely low-level of Hg (Mean = 0.1 ppm) in the study population. Since the exposure window could be different in different parts of the toenail, it might underestimate the correlation between the two measurements (portable XRF and ICP-MS) from the actual correlation.

In conclusion, portable XRF will be a valuable tool for population studies on bone Pb exposure, especially for the elderly, avoiding many of the disadvantages of the KXRF measurements. The portable XRF is a competitive device to quantify *in vivo* Sr levels in bone in a large-scale population with a promising detection limit. Thus, it can be used to study further the associations between bone Sr levels and bone health. Lastly, the current portable XRF device could be a promising tool to measure *in vivo* toenail Mn and Hg, especially for moderate to high-level Mn and Hg.

In future works, coherent normalization method for the *in vivo* bone Sr quantification can be further investigated by: first, using Monte Carlo simulation to understand how much coherent scatterings and Sr signals are generated from each primary and secondary fluences, with different soft tissue thickness; second, identify the conversion factor between the *in vivo* Sr levels measured with and without the coherent normalization; lastly, use human cadaver bone with known Sr concentration to validate the portable XRF device and the normalization method.

In addition to the data analysis, it will be interesting to explore more studies using the portable XRF: first, investigate the long-term Sr deposition in different types of bone (cortical and trabecular) with cadaver bones and population study; second, study the accumulation of Sr in different populations and how does it relate to bone health. Since many factors can influence Sr metabolisms, such as age, sex, and diet, a well-adjusted study is needed. Moreover, DXA or quantitative ultrasound scans can be used to determine BMD and study the relation between BMD and bone Sr levels for different populations.

For toenail Mn, different device settings with the current system design can be further investigated to achieve a better detection limit. The current study used an optimized device setting that allows the simultaneous detection of Mn and Hg. However, this might not be ideal for measuring Mn and Hg individually. For example, the current incident x-ray beam has an energy

of about 22 keV produced from a silver target, which is much higher than the 6.5 keV K-edge binding energy of Mn. Thus, filters with lower Z targets can be an option to increase the photoelectric cross-section of Mn and increase the signal to noise ratio.

The current device setting has achieved a promising detection limit for the toenail Hg measurements. Nevertheless, a tungsten peak located only two channels away from the Hg peak challenged the peak fitting for spectral analysis. This tungsten peak was extracted by using the intercept of the calibration line; however, the variability of *in vivo* measurement, such as the curvature of nails, positioning of the device during measurements, could result in slightly different tungsten peak amplitudes and influence the determination of absolute Hg concentration. In the future system design, materials other than tungsten can be considered in constructing the device tube base and collimator in order to eliminate the interference of the tungsten peak.

Besides the system settings, nail phantoms with more consistent thickness and homogeneity can be made; a more sophisticated calibration set up can be explored to simulate the *in vivo* situation, such as using bone underneath the nail and using nail phantoms with different curvature.

REFERENCES

1. Occupational Safety and Health Administration. *Lead*. 2018; Available from: https://www.osha.gov/SLTC/lead/index.html.
2. Agency for Toxic Substances and Disease Registry, *Toxicological profile for Lead*, P.H.S. U.S. Department of Health and Human Services, Editor. 2019: Atlanta, GA.
3. Futures, H.B.B. *What's in my Baby's Food?* 2019; Available from: https://www.healthybabyfood.org/sites/healthybabyfoods.org/files/2019-10/BabyFoodReport_FULLREPORT_ENGLISH_R5b.pdf.
4. Ziegler, E.E., et al., *Absorption and retention of lead by infants.* Pediatr Res, 1978. **12**(1): p. 29-34.
5. Heard, M.J. and A.C. Chamberlain, *Effect of minerals and food on uptake of lead from the gastrointestinal tract in humans.* Hum Toxicol, 1982. **1**(4): p. 411-5.
6. Watson, W.S., et al., *Food iron and lead absorption in humans.* Am J Clin Nutr, 1986. **44**(2): p. 248-56.
7. Barry, P.S., *A comparison of concentrations of lead in human tissues.* Br J Ind Med, 1975. **32**(2): p. 119-39.
8. Navas-Acien, A., et al., *Lead exposure and cardiovascular disease--a systematic review.* Environ Health Perspect, 2007. **115**(3): p. 472-82.
9. Obeng-Gyasi, E., *Lead Exposure and Cardiovascular Disease among Young and Middle-Aged Adults.* Med Sci (Basel), 2019. **7**(11).
10. Poreba, R., et al., *Environmental and occupational exposure to lead as a potential risk factor for cardiovascular disease.* Environ Toxicol Pharmacol, 2011. **31**(2): p. 267-77.
11. He, L., et al., *Low-level lead exposure and cardiovascular disease: the roles of telomere shortening and lipid disturbance.* J Toxicol Sci, 2018. **43**(11): p. 623-630.
12. Lanphear, B.P., et al., *Low-level lead exposure and mortality in US adults: a population-based cohort study.* Lancet Public Health, 2018. **3**(4): p. e177-e184.
13. Canfield, R.L., T.A. Jusko, and K. Kordas, *Environmental lead exposure and children's cognitive function.* Riv Ital Pediatr, 2005. **31**(6): p. 293-300.
14. Lanphear, B.P., et al., *Erratum: "Low-Level Environmental Lead Exposure and Children's Intellectual Function: An International Pooled Analysis".* Environ Health Perspect, 2019. **127**(9): p. 99001.
15. Weuve, J., et al., *Cumulative exposure to lead and cognition in persons with Parkinson's disease.* Mov Disord, 2013. **28**(2): p. 176-82.
16. Weisskopf, M.G., et al., *Cumulative lead exposure and prospective change in cognition among elderly men: the VA Normative Aging Study.* Am J Epidemiol, 2004. **160**(12): p. 1184-93.
17. Bandeen-Roche, K., et al., *Cumulative lead dose and cognitive function in older adults.* Epidemiology, 2009. **20**(6): p. 831-9.
18. Skoryna, S.C., *Effects of oral supplementation with stable strontium.* Can Med Assoc J, 1981. **125**(7): p. 703-12.
19. Agency for Toxic Substances and Disease Registry, *Toxicological profile for Strontium*, P.H.S. U.S. Department of Health and Human Services, Editor. 2004: Atlanta, GA.
20. Cabrera, W.E., et al., *Strontium and bone.* J Bone Miner Res, 1999. **14**(5): p. 661-8.
21. Pors Nielsen, S., *The biological role of strontium.* Bone, 2004. **35**(3): p. 583-8.

22. International Programme on Chemical Safety & Inter-Organization Programme for the Sound Management of Chemicals. *Strontium and strontium compounds*. 2010; Available from: https://apps.who.int/iris/handle/10665/44280.
23. Comar, C.L., et al., *Strontium metabolism and strontium-calcium discrimination in man.* Proc Soc Exp Biol Med, 1957. **95**(2): p. 386-91.
24. Dahl, S.G., et al., *Incorporation and distribution of strontium in bone.* Bone, 2001. **28**(4): p. 446-53.
25. Hendrix, Z.J., N.W. Alcock, and R.M. Archibald, *Competition between Calcium, Strontium, and Magnesium for Absorption in the Isolated Rat Intestine.* Clin Chem, 1963. **12**: p. 734-44.
26. Canalis, E., et al., *The divalent strontium salt S12911 enhances bone cell replication and bone formation in vitro.* Bone, 1996. **18**(6): p. 517-23.
27. Johnson, A.R., *The influence of strontium on characteristic factors of bone.* Calcif Tissue Res, 1973. **11**(3): p. 215-21.
28. Daniella Marxa, A.R.Y., MarcelloPapini, MarkTowler, *A review of the latest insights into the mechanism of action of strontium in bone*. 2020: Bone Reports.
29. Boivin, G., et al., *Strontium distribution and interactions with bone mineral in monkey iliac bone after strontium salt (S 12911) administration.* J Bone Miner Res, 1996. **11**(9): p. 1302-11.
30. Leeuwenkamp, O.R., et al., *Human pharmacokinetics of orally administered strontium.* Calcif Tissue Int, 1990. **47**(3): p. 136-41.
31. Farlay, D., et al., *Long-term strontium ranelate administration in monkeys preserves characteristics of bone mineral crystals and degree of mineralization of bone.* J Bone Miner Res, 2005. **20**(9): p. 1569-78.
32. Marie, P.J., D. Felsenberg, and M.L. Brandi, *How strontium ranelate, via opposite effects on bone resorption and formation, prevents osteoporosis.* Osteoporos Int, 2011. **22**(6): p. 1659-67.
33. Meunier, P.J., et al., *The effects of strontium ranelate on the risk of vertebral fracture in women with postmenopausal osteoporosis.* N Engl J Med, 2004. **350**(5): p. 459-68.
34. Meunier, P.J., et al., *Strontium ranelate: dose-dependent effects in established postmenopausal vertebral osteoporosis--a 2-year randomized placebo controlled trial.* J Clin Endocrinol Metab, 2002. **87**(5): p. 2060-6.
35. Reginster, J.Y., *Strontium ranelate in osteoporosis.* Curr Pharm Des, 2002. **8**(21): p. 1907-16.
36. Reginster, J.Y., *Cardiac concerns associated with strontium ranelate.* Expert Opin Drug Saf, 2014. **13**(9): p. 1209-13.
37. Yu, J., et al., *History of cardiovascular events and cardiovascular risk factors among patients initiating strontium ranelate for treatment of osteoporosis.* Int J Womens Health, 2015. **7**: p. 913-8.
38. Reginster, J.Y., et al., *The position of strontium ranelate in today's management of osteoporosis.* Osteoporos Int, 2015. **26**(6): p. 1667-71.
39. European Medicines Agency. *Assessment report—periodic safety update report (EPAR - Protelos-H-C-560-PSU31).* 2013; Available from: http://www.ema.europa.eu/docs/en_GB/document_library/EPAR_-_Assessment_Report_-_Variation/human/000560/WC500147168.pdf.

40. Morohashi, T., T. Sano, and S. Yamada, *Effects of strontium on calcium metabolism in rats. I. A distinction between the pharmacological and toxic doses.* Jpn J Pharmacol, 1994. **64**(3): p. 155-62.
41. Neufeld, E.B. and A.L. Boskey, *Strontium alters the complexed acidic phospholipid content of mineralizing tissues.* Bone, 1994. **15**(4): p. 425-30.
42. Ozgur, S., H. Sumer, and G. Kocoglu, *Rickets and soil strontium.* Arch Dis Child, 1996. **75**(6): p. 524-6.
43. Gonzalez-Reimers, E., et al., *Relative and combined effects of ethanol and protein deficiency on strontium and barium bone content and fecal and urinary excretion.* Biol Trace Elem Res, 1999. **68**(1): p. 41-9.
44. Omdahl, J.L. and H.F. DeLuca, *Rachitogenic activity of dietary strontium. I. Inhibition of intestinal calcium absorption and 1,25-dihydroxycholecalciferol synthesis.* J Biol Chem, 1972. **247**(17): p. 5520-6.
45. Leggett, R.W., *An age-specific kinetic model of lead metabolism in humans.* Environ Health Perspect, 1993. **101**(7): p. 598-616.
46. Nilsson, U., et al., *Kinetics of lead in bone and blood after end of occupational exposure.* Pharmacol Toxicol, 1991. **68**(6): p. 477-84.
47. Specht, A.J., M. Weisskopf, and L.H. Nie, *Childhood lead biokinetics and associations with age among a group of lead-poisoned children in China.* J Expo Sci Environ Epidemiol, 2019. **29**(3): p. 416-423.
48. Sommar, J.N., et al., *Investigation of lead concentrations in whole blood, plasma and urine as biomarkers for biological monitoring of lead exposure.* J Expo Sci Environ Epidemiol, 2014. **24**(1): p. 51-7.
49. Smith, D., et al., *The relationship between lead in plasma and whole blood in women.* Environ Health Perspect, 2002. **110**(3): p. 263-8.
50. Li, J., et al., *Maternal serum lead level during pregnancy is positively correlated with risk of preterm birth in a Chinese population.* Environ Pollut, 2017. **227**: p. 484-489.
51. Niculescu, T., et al., *Relationship between the lead concentration in hair and occupational exposure.* Br J Ind Med, 1983. **40**(1): p. 67-70.
52. Mehra, R. and M. Juneja, *Biological monitoring of lead and cadmium in human hair and nail and their correlations with biopsy materials, age and exposure.* Indian J Biochem Biophys, 2004. **41**(1): p. 53-6.
53. Wibowo, A.A., et al., *The feasibility of using lead in hair concentration in monitoring environmental exposure in children.* Int Arch Occup Environ Health, 1980. **46**(3): p. 275-80.
54. D'Haese, P.C., et al., *Measurement of strontium in serum, urine, bone, and soft tissues by Zeeman atomic absorption spectrometry.* Clin Chem, 1997. **43**(1): p. 121-8.
55. Usuda, K., et al., *Determination of reference concentrations of strontium in urine by inductively coupled plasma atomic emission spectrometry.* Environ Health Prev Med, 2006. **11**(1): p. 11-6.
56. Ulanova, T.S., et al., *[Determination of strontium content in whole blood and urine by icp-ms]*. Biomed Khim, 2015. **61**(5): p. 613-6.
57. Rentschler, G., et al., *Platinum, palladium, rhodium, molybdenum and strontium in blood of urban women in nine countries.* Int J Hyg Environ Health, 2018. **221**(2): p. 223-230.
58. Tipple, B.J., L.O. Valenzuela, and J.R. Ehleringer, *Strontium isotope ratios of human hair record intra-city variations in tap water source.* Sci Rep, 2018. **8**(1): p. 3334.

59. Vautour, G., A. Poirier, and D. Widory, *Tracking mobility using human hair: What can we learn from lead and strontium isotopes?* Sci Justice, 2015. **55**(1): p. 63-71.
60. Prejac, J., et al., *Hair for a long-term biological indicator tissue for assessing the strontium nutritional status of men and women.* J Trace Elem Med Biol, 2017. **42**: p. 11-17.
61. Doublier, A., et al., *Effects of strontium on the quality of bone apatite crystals: a paired biopsy study in postmenopausal osteoporotic women.* Osteoporos Int, 2013. **24**(3): p. 1079-87.
62. Arlot, M.E., et al., *Histomorphometric and microCT analysis of bone biopsies from postmenopausal osteoporotic women treated with strontium ranelate.* J Bone Miner Res, 2008. **23**(2): p. 215-22.
63. Blake, G.M. and I. Fogelman, *Effect of bone strontium on BMD measurements.* J Clin Densitom, 2007. **10**(1): p. 34-8.
64. Nielsen, S.P., et al., *Noninvasive measurement of bone strontium.* J Clin Densitom, 2004. **7**(3): p. 262-8.
65. Wittmers, L.E., Jr., et al., *Lead in bone. IV. Distribution of lead in the human skeleton.* Arch Environ Health, 1988. **43**(6): p. 381-91.
66. Todd, A.C., et al., *Individual variability in human tibia lead concentration.* Environ Health Perspect, 2001. **109**(11): p. 1139-43.
67. Bellis, D.J., et al., *Measurement of the microdistribution of strontium and lead in bone via benchtop monochromatic microbeam X-ray fluorescence with a low power source.* J Anal At Spectrom, 2009. **24**(5): p. 622-626.
68. O'Neal, S.L. and W. Zheng, *Manganese Toxicity Upon Overexposure: a Decade in Review.* Curr Environ Health Rep, 2015. **2**(3): p. 315-28.
69. Aschner, J.L. and M. Aschner, *Nutritional aspects of manganese homeostasis.* Mol Aspects Med, 2005. **26**(4-5): p. 353-62.
70. Institute of Medicine (US) Panel on Micronutrients, *Dietary Reference Intakes for Vitamin A, Vitamin K, Arsenic, Boron, Chromium, Copper, Iodine, Iron, Manganese, Molybdenum, Nickel, Silicon, Vanadium, and Zinc*. 2001, National Academies Press (US): Washington (DC).
71. Jiang, Y. and W. Zheng, *Cardiovascular toxicities upon manganese exposure.* Cardiovasc Toxicol, 2005. **5**(4): p. 345-54.
72. Chetri, K. and G. Choudhuri, *Role of trace elements in hepatic encephalopathy: zinc and manganese.* Indian J Gastroenterol, 2003. **22 Suppl 2**: p. S28-30.
73. Guilarte, T.R., *Manganese and Parkinson's disease: a critical review and new findings.* Cien Saude Colet, 2011. **16**(11): p. 4549-66.
74. Crossgrove, J. and W. Zheng, *Manganese toxicity upon overexposure.* NMR Biomed, 2004. **17**(8): p. 544-53.
75. Agency for Toxic Substances and Disease Registry, *Toxicological profile for Manganese,* P.H.S. U.S. Department of Health and Human Services, Editor. 2012: Atlanta, GA.
76. Dydak, U., et al., *In vivo measurement of brain GABA concentrations by magnetic resonance spectroscopy in smelters occupationally exposed to manganese.* Environ Health Perspect, 2011. **119**(2): p. 219-24.
77. Racette, B.A., et al., *Welding-related parkinsonism: clinical features, treatment, and pathophysiology.* Neurology, 2001. **56**(1): p. 8-13.
78. Racette, B.A., et al., *Prevalence of parkinsonism and relationship to exposure in a large sample of Alabama welders.* Neurology, 2005. **64**(2): p. 230-5.

79. Rutchik, J.S., et al., *How does an occupational neurologist assess welders and steelworkers for a manganese-induced movement disorder? An international team's experiences in Guanxi, China Part II.* J Occup Environ Med, 2012. **54**(12): p. 1562-4.
80. Rutchik, J.S., et al., *How does an occupational neurologist assess welders and steelworkers for a manganese-induced movement disorder? An international team's experiences in Guanxi, China, part I.* J Occup Environ Med, 2012. **54**(11): p. 1432-4.
81. Agency for Toxic Substances and Disease Registry, *Toxicological profile for Mercury*, P.H.S. U.S. Department of Health and Human Services, Editor. 1999: Atlanta, GA.
82. Park, J.D. and W. Zheng, *Human exposure and health effects of inorganic and elemental mercury.* J Prev Med Public Health, 2012. **45**(6): p. 344-52.
83. Chan, T.Y., *Inorganic mercury poisoning associated with skin-lightening cosmetic products.* Clin Toxicol (Phila), 2011. **49**(10): p. 886-91.
84. Clarkson, T.W., L. Magos, and G.J. Myers, *The toxicology of mercury--current exposures and clinical manifestations.* N Engl J Med, 2003. **349**(18): p. 1731-7.
85. Castoldi, A.F., et al., *Neurotoxicity and molecular effects of methylmercury.* Brain Res Bull, 2001. **55**(2): p. 197-203.
86. Kajiwara, Y., et al., *Methylmercury transport across the placenta via neutral amino acid carrier.* Arch Toxicol, 1996. **70**(5): p. 310-4.
87. Ramon, R., et al., *Prenatal exposure to mercury in a prospective mother-infant cohort study in a Mediterranean area, Valencia, Spain.* Sci Total Environ, 2008. **392**(1): p. 69-78.
88. Stern, A.H. and A.E. Smith, *An assessment of the cord blood:maternal blood methylmercury ratio: implications for risk assessment.* Environ Health Perspect, 2003. **111**(12): p. 1465-70.
89. Sakamoto, M., et al., *Maternal and fetal mercury and n-3 polyunsaturated fatty acids as a risk and benefit of fish consumption to fetus.* Environ Sci Technol, 2004. **38**(14): p. 3860-3.
90. Grandjean, P., et al., *Umbilical cord mercury concentration as biomarker of prenatal exposure to methylmercury.* Environ Health Perspect, 2005. **113**(7): p. 905-8.
91. Sakamoto, M., et al., *Significance of fingernail and toenail mercury concentrations as biomarkers for prenatal methylmercury exposure in relation to segmental hair mercury concentrations.* Environ Res, 2015. **136**: p. 289-94.
92. Bjornberg, K.A., et al., *Transport of methylmercury and inorganic mercury to the fetus and breast-fed infant.* Environ Health Perspect, 2005. **113**(10): p. 1381-5.
93. Vahter, M., et al., *Longitudinal study of methylmercury and inorganic mercury in blood and urine of pregnant and lactating women, as well as in umbilical cord blood.* Environ Res, 2000. **84**(2): p. 186-94.
94. Drexler, H. and K.H. Schaller, *The mercury concentration in breast milk resulting from amalgam fillings and dietary habits.* Environ Res, 1998. **77**(2): p. 124-9.
95. Bose-O'Reilly, S., et al., *Infants and mothers levels of mercury in breast milk, urine and hair, data from an artisanal and small-scale gold mining area in Kadoma / Zimbabwe.* Environ Res, 2020. **184**: p. 109266.
96. Apostoli, P., R. Lucchini, and L. Alessio, *Are current biomarkers suitable for the assessment of manganese exposure in individual workers?* Am J Ind Med, 2000. **37**(3): p. 283-90.
97. Smith, D., et al., *Biomarkers of Mn exposure in humans.* Am J Ind Med, 2007. **50**(11): p. 801-11.

98. Zheng, W., H. Kim, and Q. Zhao, *Comparative toxicokinetics of manganese chloride and methylcyclopentadienyl manganese tricarbonyl (MMT) in Sprague-Dawley rats.* Toxicol Sci, 2000. **54**(2): p. 295-301.
99. Ntihabose, R., et al., *Assessment of saliva, hair and toenails as biomarkers of low level exposure to manganese from drinking water in children.* Neurotoxicology, 2018. **64**: p. 126-133.
100. Wang, D., X. Du, and W. Zheng, *Alteration of saliva and serum concentrations of manganese, copper, zinc, cadmium and lead among career welders.* Toxicol Lett, 2008. **176**(1): p. 40-7.
101. O'Neal, S.L., et al., *Manganese accumulation in bone following chronic exposure in rats: steady-state concentration and half-life in bone.* Toxicol Lett, 2014. **229**(1): p. 93-100.
102. Liu, Y., et al., *In vivo neutron activation analysis of bone manganese in workers.* Physiol Meas, 2018. **39**(3): p. 035003.
103. (US), N.R.C., *Toxicological Effects of Methylmercury*. 2000, National Academies Press (US): Washington (DC).
104. Berglund, M., et al., *Inter-individual variations of human mercury exposure biomarkers: a cross-sectional assessment.* Environ Health, 2005. **4**: p. 20.
105. Grandjean, P., et al., *Cognitive performance of children prenatally exposed to "safe" levels of methylmercury.* Environ Res, 1998. **77**(2): p. 165-72.
106. Cardenas, A., et al., *Prenatal Exposure to Mercury: Associations with Global DNA Methylation and Hydroxymethylation in Cord Blood and in Childhood.* Environ Health Perspect, 2017. **125**(8): p. 087022.
107. Chen, G., et al., *Surveying mercury levels in hair, blood and urine of under 7-year old children from a coastal city in China.* Int J Environ Res Public Health, 2014. **11**(11): p. 12029-41.
108. Counter, S.A., L.H. Buchanan, and F. Ortega, *Mercury levels in urine and hair of children in an Andean gold-mining settlement.* Int J Occup Environ Health, 2005. **11**(2): p. 132-7.
109. Yusa, V., et al., *Biomonitoring of mercury in hair of breastfeeding mothers living in the Valencian Region (Spain). Levels and predictors of exposure.* Chemosphere, 2017. **187**: p. 106-113.
110. Legrand, M., et al., *Biomonitoring of mercury exposure with single human hair strand.* Environ Sci Technol, 2005. **39**(12): p. 4594-8.
111. Li, Y.F., et al., *Scalp hair as a biomarker in environmental and occupational mercury exposed populations: suitable or not?* Environ Res, 2008. **107**(1): p. 39-44.
112. Laohaudomchok, W., et al., *Toenail, blood, and urine as biomarkers of manganese exposure.* J Occup Environ Med, 2011. **53**(5): p. 506-10.
113. Bjorkman, L., et al., *Mercury in human brain, blood, muscle and toenails in relation to exposure: an autopsy study.* Environ Health, 2007. **6**: p. 30.
114. Rees, J.R., et al., *Toenail mercury and dietary fish consumption.* J Expo Sci Environ Epidemiol, 2007. **17**(1): p. 25-30.
115. Alfthan, G.V., *Toenail mercury concentration as a biomarker of methylmercury exposure.* Biomarkers, 1997. **2**(4): p. 233-8.
116. Yaemsiri, S., et al., *Growth rate of human fingernails and toenails in healthy American young adults.* J Eur Acad Dermatol Venereol, 2010. **24**(4): p. 420-3.
117. Ahlgren, L., et al., *X-ray fluorescence analysis of lead in human skeleton in vivo.* Scand J Work Environ Health, 1976. **2**(2): p. 82-6.

118. Somervaille, L.J., D.R. Chettle, and M.C. Scott, *In vivo measurement of lead in bone using x-ray fluorescence.* Phys Med Biol, 1985. **30**(9): p. 929-43.
119. Gordon, C.L., D.R. Chettle, and C.E. Webber, *An improved instrument for the in vivo detection of lead in bone.* Br J Ind Med, 1993. **50**(7): p. 637-41.
120. Chettle, D.R., M.C. Scott, and L.J. Somervaille, *Improvements in the precision of in vivo bone lead measurements.* Phys Med Biol, 1989. **34**(9): p. 1295-300.
121. Nie, H., et al., *In vivo investigation of a new 109Cd gamma-ray induced K-XRF bone lead measurement system.* Phys Med Biol, 2006. **51**(2): p. 351-60.
122. Somervaille, L.J., et al., *In vivo measurements of bone lead--a comparison of two x-ray fluorescence techniques used at three different bone sites.* Phys Med Biol, 1989. **34**(12): p. 1833-45.
123. Nie, H., et al., *The study of age influence on human bone lead metabolism by using a simplified model and X-ray fluorescence data.* J Environ Monit, 2005. **7**(11): p. 1069-73.
124. Todd, A.C., et al., *L-shell x-ray fluorescence measurements of lead in bone: accuracy and precision.* Phys Med Biol, 2002. **47**(8): p. 1399-419.
125. H. Nie, D.C., L. Luo, and J. O'Meara, *Dosimetry study for a new in vivo X-ray fluorescence (XRF) bone lead measurement system.* Nuclear Instruments and Methods in Physics Research. Section B: Beam Interactions with Materials and Atoms, 2007. **263**: p. 225-230.
126. Specht, A.J., M. Weisskopf, and L.H. Nie, *Portable XRF Technology to Quantify Pb in Bone In Vivo.* J Biomark, 2014. **2014**: p. 398032.
127. Specht, A.J., et al., *XRF-measured bone lead (Pb) as a biomarker for Pb exposure and toxicity among children diagnosed with Pb poisoning.* Biomarkers, 2016. **21**(4): p. 347-52.
128. Specht, A.J., et al., *Bone lead levels in an environmentally exposed elderly population in shanghai, China.* Sci Total Environ, 2018. **626**: p. 96-98.
129. Shih, R.A., et al., *Cumulative lead dose and cognitive function in adults: a review of studies that measured both blood lead and bone lead.* Environ Health Perspect, 2007. **115**(3): p. 483-92.
130. Weisskopf, M.G., et al., *Association of cumulative lead exposure with Parkinson's disease.* Environ Health Perspect, 2010. **118**(11): p. 1609-13.
131. Navas-Acien, A., et al., *Bone lead levels and blood pressure endpoints: a meta-analysis.* Epidemiology, 2008. **19**(3): p. 496-504.
132. Wielopolski, L., et al., *Feasibility of noninvasive analysis of lead in the human tibia by soft x-ray fluorescence.* Med Phys, 1983. **10**(2): p. 248-51.
133. Wielopolski, L., et al., *In vivo measurement of cortical bone lead using polarized x rays.* Med Phys, 1989. **16**(4): p. 521-8.
134. Wielopolski, L., et al., *In vivo bone lead measurements: a rapid monitoring method for cumulative lead exposure.* Am J Ind Med, 1986. **9**(3): p. 221-6.
135. Todd, A.C., *L-shell x-ray fluorescence measurements of lead in bone: system development.* Phys Med Biol, 2002. **47**(3): p. 507-22.
136. Todd, A.C., *L-shell x-ray fluorescence measurements of lead in bone: theoretical considerations.* Phys Med Biol, 2002. **47**(3): p. 491-505.
137. Nie, L.H., et al., *In vivo quantification of lead in bone with a portable x-ray fluorescence system--methodology and feasibility.* Phys Med Biol, 2011. **56**(3): p. N39-51.
138. Specht, A.J., et al., *Validation of x-ray fluorescence measurements of metals in toenail clippings against inductively coupled plasma mass spectrometry in a Nigerian population<sup/>*. Physiol Meas, 2018. **39**(8): p. 085007.

139. Specht, A.J., et al., *Measurements of Strontium Levels in Human Bone In Vivo Using Portable X-ray Fluorescence (XRF).* Appl Spectrosc, 2017. **71**(8): p. 1962-1968.
140. Specht, A.J., et al., *Feasibility of a portable X-ray fluorescence device for bone lead measurements of condor bones.* Sci Total Environ, 2018. **615**: p. 398-403.
141. Specht, A.J., et al., *A Dosimetry Study of Portable X-ray Fluorescence in Vivo Metal Measurements.* Health Phys, 2019. **116**(5): p. 590-598.
142. Zhang, X., et al., *Quantification of manganese and mercury in toenail in vivo using portable X-ray fluorescence (XRF).* Biomarkers, 2018. **23**(2): p. 154-160.
143. Specht, A.J., A.S. Dickerson, and M.G. Weisskopf, *Comparison of bone lead measured via portable x-ray fluorescence across and within bones.* Environ Res, 2019. **172**: p. 273-278.
144. Fleming, D.E.B., S.L. Crook, and C.T. Evans, *Assessing zinc from a nail clipping using mono-energetic portable X-ray fluorescence.* Appl Radiat Isot, 2019. **145**: p. 170-175.
145. Fleming, D.E. and C.S. Ware, *Portable x-ray fluorescence for the analysis of chromium in nail and nail clippings.* Appl Radiat Isot, 2017. **121**: p. 91-95.
146. Fleming, D.E., et al., *Assessing arsenic and selenium in a single nail clipping using portable X-ray fluorescence.* Appl Radiat Isot, 2017. **120**: p. 1-6.
147. Roy, C.W., M.R. Gherase, and D.E. Fleming, *Simultaneous assessment of arsenic and selenium in human nail phantoms using a portable x-ray tube and a detector.* Phys Med Biol, 2010. **55**(6): p. N151-9.
148. ThermoFisherScientific. *X-ray Fluorescence (XRF) in Mining*. Available from: https://www.thermofisher.com/blog/mining/technology-focus-x-ray-fluorescence-xrf-in-mining/.
149. Banks, E.C., L.E. Ferretti, and D.W. Shucard, *Effects of low level lead exposure on cognitive function in children: a review of behavioral, neuropsychological and biological evidence.* Neurotoxicology, 1997. **18**(1): p. 237-81.
150. Pilmane, M., et al., *Strontium and strontium ranelate: Historical review of some of their functions.* Mater Sci Eng C Mater Biol Appl, 2017. **78**: p. 1222-1230.
151. Querido, W., A.L. Rossi, and M. Farina, *The effects of strontium on bone mineral: A review on current knowledge and microanalytical approaches.* Micron, 2016. **80**: p. 122-34.
152. Schoeman, K., et al., *Hair mercury levels of women of reproductive age in Ontario, Canada: implications to fetal safety and fish consumption.* J Pediatr, 2010. **157**(1): p. 127-31.
153. Goldman, L.R., M.W. Shannon, and H. American Academy of Pediatrics: Committee on Environmental, *Technical report: mercury in the environment: implications for pediatricians.* Pediatrics, 2001. **108**(1): p. 197-205.
154. Rabinowitz, M.B., *Toxicokinetics of bone lead.* Environ Health Perspect, 1991. **91**: p. 33-7.
155. Hwang, Y.H., C.K. Hsiao, and P.W. Lin, *Globally temporal transitions of blood lead levels of preschool children across countries of different categories of Human Development Index.* Sci Total Environ, 2019. **659**: p. 1395-1402.
156. Grosse, S.D., et al., *Economic gains resulting from the reduction in children's exposure to lead in the United States.* Environ Health Perspect, 2002. **110**(6): p. 563-9.
157. Pirkle, J.L., et al., *The decline in blood lead levels in the United States. The National Health and Nutrition Examination Surveys (NHANES).* JAMA, 1994. **272**(4): p. 284-91.

158. Bellinger, D.C. and H.L. Needleman, *Intellectual impairment and blood lead levels.* N Engl J Med, 2003. **349**(5): p. 500-2; author reply 500-2.
159. Lanphear, B.P., et al., *Low-level environmental lead exposure and children's intellectual function: an international pooled analysis.* Environ Health Perspect, 2005. **113**(7): p. 894-9.
160. ATSDR. *Agency for Toxic Substances and Disease Registry, Priority list of hazardous substances. 2019*. 2019 January 17, 2020; Available from: https://www.atsdr.cdc.gov/spl/index.html#2019spl.
161. Centers for Disease, C. and Prevention, *Very high blood lead levels among adults - United States, 2002-2011.* MMWR Morb Mortal Wkly Rep, 2013. **62**(47): p. 967-71.
162. Rabinowitz, M.B., G.W. Wetherill, and J.D. Kopple, *Kinetic analysis of lead metabolism in healthy humans.* J Clin Invest, 1976. **58**(2): p. 260-70.
163. Specht, A.J., M. Weisskopf, and L.H. Nie, *Childhood lead biokinetics and associations with age among a group of lead-poisoned children in China.* J Expo Sci Environ Epidemiol, 2018.
164. Weisskopf, M.G., et al., *Biased Exposure-Health Effect Estimates from Selection in Cohort Studies: Are Environmental Studies at Particular Risk?* Environ Health Perspect, 2015. **123**(11): p. 1113-22.
165. Nie, H., et al., *An investigation of the 109Cd gamma-ray induced K-x-ray fluorescence (XRF) bone-lead measurement calibration procedure.* Phys Med Biol, 2004. **49**(19): p. N325-34.
166. Whitcomb, B.W. and E.F. Schisterman, *Assays with lower detection limits: implications for epidemiological investigations.* Paediatr Perinat Epidemiol, 2008. **22**(6): p. 597-602.
167. Kim, R., et al., *K x-ray fluorescence measurements of bone lead concentration: the analysis of low-level data.* Phys Med Biol, 1995. **40**(9): p. 1475-85.
168. Behinaein, S., et al., *Age and sex influence on bone and blood lead concentrations in a cohort of the general population living in Toronto.* Physiol Meas, 2017. **38**(3): p. 431-451.
169. Weuve, J., et al., *Cumulative exposure to lead in relation to cognitive function in older women.* Environ Health Perspect, 2009. **117**(4): p. 574-80.
170. Moldawer, M., S.J. Zimmerman, and L.C. Collins, *Incidence of osteoporosis in elderly whites and elderly Negroes.* JAMA, 1965. **194**(8): p. 859-62.
171. Silverman, S.L. and R.E. Madison, *Decreased incidence of hip fracture in Hispanics, Asians, and blacks: California Hospital Discharge Data.* Am J Public Health, 1988. **78**(11): p. 1482-3.
172. Yang, P.L., et al., *Associations between ethnicity, body composition, and bone mineral density in a Southeast Asian population.* J Clin Endocrinol Metab, 2013. **98**(11): p. 4516-23.
173. Curtis, E.M., et al., *Epidemiology of fractures in the United Kingdom 1988-2012: Variation with age, sex, geography, ethnicity and socioeconomic status.* Bone, 2016. **87**: p. 19-26.
174. Moise, H., D.R. Chettle, and A. Pejovic-Milic, *Monitoring bone strontium intake in osteoporotic females self-supplementing with strontium citrate with a novel in-vivo X-ray fluorescence based diagnostic tool.* Bone, 2014. **61**: p. 48-54.
175. Blake, G.M. and I. Fogelman, *Long-term effect of strontium ranelate treatment on BMD.* J Bone Miner Res, 2005. **20**(11): p. 1901-4.

176. Hubbell, J.H. and I. O/verbo/, *Relativistic atomic form factors and photon coherent scattering cross sections.* Journal of Physical and Chemical Reference Data, 1979. **8**(1): p. 69-106.
177. Todd, A.C., *Coherent scattering and matrix correction in bone-lead measurements.* Phys Med Biol, 2000. **45**(7): p. 1953-63.
178. McIver, D.J., et al., *Evaluation of a novel portable x-ray fluorescence screening tool for detection of arsenic exposure.* Physiol Meas, 2015. **36**(12): p. 2443-59.
179. Woodard, H.Q., *The elementary composition of human cortical bone.* Health Phys, 1962. **8**: p. 513-7.
180. ICRU, *Tissue substitutes in radiation dosimetry and measurement.* Journal of the International Commission on Radiation Units and Measurements, 1989. **Report 44**.
181. Mostafaei, F., et al., *Design of a phantom equivalent to measure bone-fluorine in a human's hand via delayed neutron activation analysis.* Physiol Meas, 2013. **34**(5): p. 503-12.
182. Aerssens, J., et al., *Interspecies differences in bone composition, density, and quality: potential implications for in vivo bone research.* Endocrinology, 1998. **139**(2): p. 663-70.
183. Von Euw, S., et al., *Bone mineral: new insights into its chemical composition.* Sci Rep, 2019. **9**(1): p. 8456.
184. Legros, R., N. Balmain, and G. Bonel, *Age-related changes in mineral of rat and bovine cortical bone.* Calcif Tissue Int, 1987. **41**(3): p. 137-44.
185. Bahrololoom. Mohammad, J.M., Javadpour. Sirus, Ma. J., *Characterisation of natural hydroxyapatite extracted from bovine cortical bone ash.* Journal of Ceramic Processing Research, 2009. **10**(2): p. 129-138.
186. Nam, H.S., et al., *Race/ethnic differences in bone mineral densities in older men.* Osteoporos Int, 2010. **21**(12): p. 2115-23.
187. Hochberg, M.C., *Racial differences in bone strength.* Trans Am Clin Climatol Assoc, 2007. **118**: p. 305-15.
188. Looker, A.C., et al., *Age, gender, and race/ethnic differences in total body and subregional bone density.* Osteoporos Int, 2009. **20**(7): p. 1141-9.
189. Duan, Y., et al., *Structural and biomechanical basis of racial and sex differences in vertebral fragility in Chinese and Caucasians.* Bone, 2005. **36**(6): p. 987-98.
190. Rodier, J., *Manganese poisoning in Moroccan miners.* Br J Ind Med, 1955. **12**(1): p. 21-35.
191. Bowman, A.B., et al., *Role of manganese in neurodegenerative diseases.* J Trace Elem Med Biol, 2011. **25**(4): p. 191-203.
192. Wang, J.D., et al., *Manganese induced parkinsonism: an outbreak due to an unrepaired ventilation control system in a ferromanganese smelter.* Br J Ind Med, 1989. **46**(12): p. 856-9.
193. Wennberg, A., et al., *Manganese exposure in steel smelters a health hazard to the nervous system.* Scand J Work Environ Health, 1991. **17**(4): p. 255-62.
194. Levy, B.S. and W.J. Nassetta, *Neurologic effects of manganese in humans: a review.* Int J Occup Environ Health, 2003. **9**(2): p. 153-63.
195. Jiang, Y.M., et al., *Effective treatment of manganese-induced occupational Parkinsonism with p-aminosalicylic acid: a case of 17-year follow-up study.* J Occup Environ Med, 2006. **48**(6): p. 644-9.
196. Agency, U.S.E.P., *Methylmercury (MeHg) (CASRN 22967-92-6).* 2011, lntegrated Risk Information System, U.S. Environmental Protection Agency.: Washington, DC.

197. Staff, N.R.C., *Toxicological Effects of Methylmercury*, ed. C.o.t.T.E.o. Methylmercury, B.o.E.S.a.T. Staff, and P. National Research Council Committee on the Toxicological Effects of Methylmercury. Content. 2000, Washington: Washington : National Academies Press.
198. United States. Agency for Toxic Substances and Disease, R., *Toxicological profile for mercury*. 1999: Atlanta, Ga. : U.S. Dept. of Health and Human Services, Public Health Service, Agency for Toxic Substances and Disease Registry.
199. Johnson, M. and S. Shuster, *Determinants of nail thickness and length.* Br J Dermatol, 1994. **130**(2): p. 195-8.
200. Verbraecken, J., et al., *Body surface area in normal-weight, overweight, and obese adults. A comparison study.* Metabolism, 2006. **55**(4): p. 515-24.
201. Slotnick, M.J., et al., *Profiles of trace elements in toenails of Arab-Americans in the Detroit area, Michigan.* Biol Trace Elem Res, 2005. **107**(2): p. 113-26.
202. Ohno, T., et al., *Total mercury levels in hair, toenail, and urine among women free from occupational exposure and their relations to renal tubular function.* Environ Res, 2007. **103**(2): p. 191-7.
203. Olanow, C.W., *Manganese-induced parkinsonism and Parkinson's disease.* Ann N Y Acad Sci, 2004. **1012**: p. 209-23.
204. Guilarte, T.R., *Manganese neurotoxicity: new perspectives from behavioral, neuroimaging, and neuropathological studies in humans and non-human primates.* Front Aging Neurosci, 2013. **5**: p. 23.
205. Bouchard, M.F., et al., *Low level exposure to manganese from drinking water and cognition in school-age children.* Neurotoxicology, 2018. **64**: p. 110-117.
206. Standridge, J.S., et al., *Effect of chronic low level manganese exposure on postural balance: a pilot study of residents in southern Ohio.* J Occup Environ Med, 2008. **50**(12): p. 1421-9.
207. Counter, S.A. and L.H. Buchanan, *Mercury exposure in children: a review.* Toxicol Appl Pharmacol, 2004. **198**(2): p. 209-30.
208. Bergomi, M., et al., *Environmental exposure to trace elements and risk of amyotrophic lateral sclerosis: a population-based case-control study.* Environ Res, 2002. **89**(2): p. 116-23.
209. Garland, M., et al., *Toenail trace element levels as biomarkers: reproducibility over a 6-year period.* Cancer Epidemiol Biomarkers Prev, 1993. **2**(5): p. 493-7.
210. Grashow, R., et al., *Toenail metal concentration as a biomarker of occupational welding fume exposure.* J Occup Environ Hyg, 2014. **11**(6): p. 397-405.
211. Signes-Pastor, A.J., et al., *Toenail manganese as biomarker of drinking water exposure: a reliability study from a US pregnancy cohort.* J Expo Sci Environ Epidemiol, 2019. **29**(5): p. 648-654.
212. Viana, G.F., et al., *Noninvasive biomarkers of manganese exposure and neuropsychological effects in environmentally exposed adults in Brazil.* Toxicol Lett, 2014. **231**(2): p. 169-78.
213. Ilhan, A., et al., *The comparison of nail and serum trace elements in patients with epilepsy and healthy subjects.* Prog Neuropsychopharmacol Biol Psychiatry, 2004. **28**(1): p. 99-104.
214. Lakshmi Priya, M.D. and A. Geetha, *Level of trace elements (copper, zinc, magnesium and selenium) and toxic elements (lead and mercury) in the hair and nail of children with autism.* Biol Trace Elem Res, 2011. **142**(2): p. 148-58.

215. Mao, X., et al., *Effects of seafood consumption and toenail mercury and selenium levels on cognitive function among American adults: 25 y of follow up.* Nutrition, 2019. **61**: p. 77-83.
216. Andrew, A.S., et al., *Toenail mercury Levels are associated with amyotrophic lateral sclerosis risk.* Muscle Nerve, 2018.
217. Fleming, D., Gherase, M., & Anthonisen, M. , *Calibrations for measurement of manganese and zinc in nail clippings using portable XRF.* X-Ray Spectrometry, 2013. **42**(4): p. 299-302.

VITA

Xinxin Zhang

EDUCATION

Ph.D.	Medical Physics, Purdue University, West Lafayette, IN, USA	2015 – 2020
M.Sc.	Nuclear Physics, University of Sao Paulo, Sao Paulo, Brazil	2013 – 2015
B.Sc.	Physics, University of Sao Paulo, Sao Paulo, Brazil	2008 – 2012

ACADEMIC AWARDS

Purdue University, West Lafayette, IN

Travel Award, AAPM Ohio River Valley Chapter meeting	2019
Bilsland Dissertation Fellowship, Purdue University	2019 – 2020
Purdue Research Foundation Fellowship	2018 – 2019
NIOSH-funded ERC Pilot Research Grant at University of Michigan	2017 – 2018
Research Assistantship, Purdue University	2017 – 2018
Teaching Assistantship, Purdue University	2016 – 2017
Student Fellowship Award, Health Physics Society	2016 – 2017

University of Sao Paulo, SP, Brazil

Best Poster Presentation in the 37th Brazilian Workshop on Nuclear Physics	2014
National Nuclear Energy Commission Fellowship	2013 – 2015
Institutional Program of Scientific Initiation Scholarship	2011 – 2012
National Council for Scientific & Technological Development Scholarship	2009 – 2011

GRADUATE RESEARCH EXPERIENCE

Purdue University, West Lafayette, IN August 2015 – August 2020

- Investigate and validate the portable X-ray fluorescence (XRF) technology for the in vivo quantification of lead and strontium in bone against K-shell XRF (XKRF) bone lead system.
- Design and develop a project that aimed to quantify manganese and mercury concentration in toenail *in vivo* using a portable XRF system.
- Optimize system design to obtain a lower detection limit and develop methods for data analysis.
- Develop and validate an MCNP model to simulate a portable XRF device to measure different materials in bone and toenail.
- Participate in a project designed to map metal distribution in teeth by the synchrotron-μXRF beamline at Argonne National Laboratory, IL.
- Supervise graduate and undergraduate students on projects related to X-ray fluorescence.
- Cumulative GPA 3.93/4.0

University of Sao Paulo, SP, Brazil January 2013 – June 2015

- Studied the coulomb-nuclear interference in the inelastic scattering of ^{6}Li on ^{76}Ge using the Pelletron accelerator.
- Participated in software development of a data acquisition system (digital pulse processing) using LabView.
- Cumulative GPA 3.76/4.0

GRADUATE TEACHING EXPERIENCE

Purdue University, West Lafayette, IN August 2016 – December 2017

HSCI 572 – Radiation Oncology Physics

HSCI 514 – Radiation Instrumentation Laboratory

HSCI 420 – Applied Anatomy for Medicine

HSCI 580 – Occupational Safety and Ergonomics

University of Sao Paulo, SP, Brazil January 2015 – June 2015

Physics in Laboratory

GRADUATE MENTORING EXPERIENCE

Student: Emily Paul June 2019 – September 2019

Sophomore. Department of Physics, University of Chicago

Project: Feasibility study of using in vivo K-X-ray fluorescence to quantify gadolinium in bone.

Poster presented in Fall Undergraduate Research Symposium, University of Chicago.

Student: Emma Wallens August 2016 – April 2019

B.Sc. School of Health Sciences, Undergraduate Research Honors Program, Purdue University

Project: Accuracy of Portable L-X-ray Fluorescence Device to Quantify Lead in Condor Bone In Vivo.

Paper published in Journal of Purdue Undergraduate Research, Vol 8 (2018).

Student: Kevinraj Sukumar May 2017 – June 2018

M.Sc. School of Health Sciences, Purdue University

Project: Detection of Arsenic in Skin in vivo Using Portable X-ray Fluorescence Device.

Theses Completed.

GRANTS

Purdue Research Foundation Fellowship August 2018 – August 2019

Role: Graduate Research Assistant PI: Linda. H. Nie

Title: Portable X-ray Fluorescence (XRF) to Study Strontium and Bone Health.

Funded – Award amount: $20,000

NIOSH-funded ERC Pilot Research Grant at University of Michigan July 2017 – July 2018

Role: Co-PI PI: Linda. H. Nie

Title: Portable XRF Technology for Noninvasive In Vivo Quantification of Uranium (U) in Bone and Arsenic (As) in Skin among a Population with High U- and As- Exposures.

Funded – Award amount: $20,000

PUBLICATIONS

1. **Zhang X**, Specht A, Wells E, Weisskopf M, Weuve J, Nie L (2020) In vivo quantification of lead in bone using portable x-ray fluorescence (XRF) among a US population; Submitted.
2. **Zhang X**, Specht A, Wells E, Weisskopf M, Weuve J, Nie L (2020) In vivo quantification of strontium in human bone among adults using portable x-ray fluorescence; Internal review.
3. Specht AJ, **Zhang X**, Young A, Nguyen V, Christiani DC, Ceballo DM, Allen, JG, Weuve J, Nie LH, Weisskopf MG (2020) Validation of in vivo toenail measurements of manganese and mercury using a portable x-ray fluorescence device. Submitted.
4. Specht AJ, **Zhang X**, Goodman BD, Maher E, Weisskopf MG, Nie LH (2019) A Dosimetry Study of Portable X-ray Fluorescence In vivo Metal Measurements. *Health Physics*, Vol.116(5):590-598.
5. **Zhang X**, Specht A, Weisskopf M, Weuve J, Nie L (2018) Quantification of manganese and mercury in toenail in vivo using portable X-ray fluorescence (XRF). *Biomarkers*, Vol.23(2):154-160.

6. Coyne MD, Neumann C, **Zhang X**, Byrne P, Liu Y, Weaver CM, Nie LH (2018) Compact DD generator-based in vivo neutron activation analysis (IVNAA) system to determine sodium concentrations in human bone. *Physiological measurement*, 23 Vol.39(5)
7. A S Freitas, L Marques, **X X Zhang**, M A Luzio, P Guillaumon, R Pampa Condori and R Lichtenthaler (2016) Woods-Saxon Equivalent to a Double Folding Potential *Braz J Phys* 46: 120-128
8. **X X Zhang**, M R D Rodrigues, T Borello-Lewin, C L Rodrigues, G M Ukita, L R B Benevides, J L M Duarte and L B Horodynski-Matsushigue (2015) Coulomb-nuclear interference in the inelastic scattering of ^{6}Li on ^{76}Ge *J. Phys.*: Conf. Ser. 630 012025

ABSTRACTS AND CONFERENCE POSTER PRESENTATIONS

1. **Zhang X**, Specht AJ, Weisskopf MG, Weuve J, Nie LH (2019). Quantification of Bone Lead with Portable X-ray Fluorescence Technology. Project presented at the AAPM ORVC Fall Symposium, Indianapolis, IN
2. **Zhang X**, Specht AJ, Weisskopf MG, Weuve J, Nie LH (2018). Quantification of Bone Lead and Toenail Manganese and Mercury In Vivo with X-ray Fluorescence Technology. Project presented at the biannually Metals Workshop, Jun.14-15, 2018; Boston, MA
3. Coyne M, Lobene A, **Zhang X**, Neumann C, Lachcik P, Weaver C, Nie LH (2018). Determination of Bone Sodium (Na) and Na Exchange in Pig Leg Using In Vivo Neutron Activation Analysis (IVNAA). Project presented at the biannually Metals Workshop, Boston, MA
4. **Zhang X**, Specht AJ, Weisskopf MG, Weuve J, Nie LH (2018). Quantification of bone lead, toenail manganese and mercury in toenail in vivo with x-ray fluorescence technology. Project presented at the UM-ERC Regional Research Symposium, Chicago, IL
5. **Zhang X**, Specht AJ, Weisskopf MG, Weuve J, Nie LH (2017). Quantification of manganese and mercury in toenail in vivo using portable x-ray fluorescence (XRF). Project presented at the AAPM ORVC Fall Symposium, Indianapolis, IN

6. Specht AJ, **Zhang X**, Weuve J, Nie LH, and Weisskopf MG (2017). In vivo x-ray fluorescence measured toenail manganese as a biomarker of exposure among welders, abstract accepted at the 2017 Annual International Society of Exposure Science meeting, Durham, North Carolina.
7. **Zhang X**, Specht AJ, Weisskopf M, Weuve J, Nie LH (2017). Feasibility of Quantifying the Manganese and Mercury in Toenail In Vivo with Portable X-ray Fluorescence Technology. Abstract published and project presented at the 62nd HPS annual meeting, Raleigh, NC
8. Coyne M, Liu Y, **Zhang X**, Nie LH (2016). Compact DD Generator Based In Vivo Neutron Activation Analysis (IVNAA) System to Determine Sodium and Calcium Concentrations in Human Bone. Abstract published and project presented at the 61st HPS annual meeting, Spokane, WA
9. **X X Zhang**, M R D Rodrigues, T Borello-Lewin, C L Rodrigues, G M Ukita, L R B Benevides, J L M Duarte and L B Horodynski-Matsushigue (2015) Coulomb-nuclear interference in the inelastic scattering of ^{6}Li on ^{76}Ge *J. Phys.*: Conf. Ser. 630 012025